# REACTIVELY COMPATIBILIZED STARCH-BASED RENEWABLE POLYMER BLENDS

by

**Candice L. DeLeo**

B.S., B.A, University of Rhode Island, 2004

Submitted to the Graduate Faculty of

Swanson School of Engineering in partial fulfillment

of the requirements for the degree of

Doctor of Philosophy

University of Pittsburgh

2010

UNIVERSITY OF PITTSBURGH

SWANSON SCHOOL OF ENGINEERING

This dissertation was presented

by

Candice L. DeLeo

It was defended on

July 13, 2010

and approved by

Robert Enick, Professor, Department of Chemical and Petroleum Engineering

Steven Little, Assistant Professor, Department of Chemical and Petroleum Engineering

Ian Nettleship, Associate Professor, Department of Mechanical Engineering and Materials Science

Brian Young, Assistant Professor, Department of Plastics Engineering Technology (Penn State Erie, The Behrend College)

Dissertation Director: Sachin S. Velankar, Associate Professor, Department of Chemical and Petroleum Engineering

**REACTIVELY COMPATIBILIZED STARCH-BASED RENEWABLE POLYMER BLENDS**

Candice L. DeLeo, PhD

University of Pittsburgh, 2010

Starch-based polymeric materials offer a renewable, economical alternative to existing petroleum based, non-renewable or costly biodegradable polymeric materials. We present the development and characterization of two phase blends of plasticized starch (PLS) and polypropylene (PP) compatibilized via an interfacial chemical reaction.

Starch is an abundant, naturally occurring polysaccharide that is obtained from various plant sources. Having three hydroxyl groups per glucose monomer unit, starch is an inherently multifunctional polymer. When starch is blended with another polymer, such functionally can be used to reactively compatibilize the two phase system. We first examine the effects of multifunctional reactive compatibilization in model immiscible polymer blends and compare them to compatibilization using diblock copolymers. We study the rheological and morphological effects of the crosslinked interface and investigate the effects of varying the reactive compatibilizer concentration and the homopolymer loading.

We next develop a processing methodology and conduct a systematic characterization study of PLS and PP blends. Based on the result of our model blend study, multifunctional reactive blending was employed using maleated polypropylene (MAPP). The maleic anhydride functional groups are able to react with hydroxyl functional starch, creating a compatibilized system. The addition of layered silicate to the PLS/PP blends was employed to mitigate the decline in mechanical properties as starch content increased.

At sufficiently high plasticized starch loadings, the maleated polypropylene domains acted as physical crosslinking sites. The processing, blending, compatibilization and characterization of plasticized starch resulted in a material with properties apt for several elastomeric applications, such as rubber feet for electronic devices. The challenges of using plasticized starch as an elastomer are also discussed.

Lastly, we present a comparative life cycle assessment of plasticized starch and polypropylene. The system boundary of this assessment is defined to be "cradle to gate" in which we analyze the system from raw material extraction to the final production of a polymer pellet.

## TABLE OF CONTENTS

## LIST OF TABLES

## LIST OF FIGURES

## PREFACE

I would like to express my deep gratitude to my advisor Dr. Sachin Velankar for his support, advice and patience. Working under his supervision has been a rewarding learning experience, and I am very thankful to him for the knowledge he has imparted to me. I also thank my committee members, Dr. Enick, Dr. Little and Dr. Nettleship and Prof. Young for their guidance.

I thank the former members of my group: Dr. Jeffery Martin, Dr. Prachi Thareja, Dr. Hsin-Ling Cheng for their help, guidance and encouragement. I would also like to thank my undergraduate colleagues (Dolores, Katie, James, Dan and William) who worked closely with me in various projects. I would especially like to thank James Goetz for his contribution to the work on starch based elastomers described in Chapter 6.0.

I am grateful for the opportunity to collaborate with plastics expert Prof. Brian Young of Penn State Erie, The Behrend College and also for the use of their state of the art facilities. I am indebted to and Dra. Maria do Carmo Gonçalves of the State University of Campinas for her guidance and patience and for the opportunity to conduct research at such a distinguished university. I am grateful for many fruitful discussions with Dr. Toby Chapman in the Department of Chemistry at Pitt during the whole course of my graduate studies. I also thank Dr. Lei Hong and the Webber group in the Department of Chemistry for the use of their DMA the members of Center of Biological Imaging (CBI) for allowing us to access their state of the art microscopy facilities.

I would thank to thank Dr. Bob Parker for his kindness during the application process and for informing me about the Mascaro Center for Sustainable Innovation and the IGERT fellowship. That said, none of the research presented in this thesis would have been possible without funding from the IGERT grant and Mascaro Center. I am grateful for all the help and support I received from Gena Kovalick, Dr. Melissa Bilec and Kim Wisnewski, especially in preparation for the research rotation in Brazil. I also thank all of the staff in the Department of Chemical Engineering.

Finally, I never would have accomplished all of this without the unconditional support of my family and fiancé. Their love and encouragement has been an undying source of motivation. I particularly would like to thank my sister, brother in law and niece for countless dinners and much needed comic relief and my fiancé for his love and patience in traveling to see each other every two weeks over the last three years.

# 1.0 INTRODUCTION

The applications for polymeric materials are vast, ranging from plastic bottles to automotive parts to elastomeric medical devices. Since their inception, the majority of commodity polymeric materials, such as packaging and bottles, have been derived from non-renewable petroleum sources. However, the integration of naturally occurring materials, such as starch, into commodity plastics has been increasing in recent years [1]. The inclusion of such materials allows products traditionally produced from non-renewable and environmentally persistent petroleum-based materials, to be produced from materials made from renewable resources which may also provide a degree of degradability to the final product. Starch, in particular, has been used since the 1970s as a filler in plastics [2] and has recently been plasticized and extruded with traditional plastics [3], used as a baked foam for thin walled applications [4], and used as packaging foams [5]. Dry granular starch and baked starch, which is pressed and molded, have limited processability and can be used in only a limited range of applications. Plasticized starch, however, is more versatile and can be blended with various polymeric materials for numerous applications.

As the properties of any polymer blend are determined by its component properties, the volume ratio of components in the blend, and the compatibility of the blend components, starch blends may be tailored to exhibit certain properties. Blending starch with polyolefins produces immiscible blends requiring the addition of a compatibilizer to improve interfacial adhesion and

such blends may exhibit polyolefin-like properties. Also, starch may be blended with more miscible polymers, such as biodegradable polyesters to result in a completely biodegradable material. However, blending with biodegradable polyesters can be costly, while polyolefins such as polystyrene and polyethylene are inexpensive. Furthermore, fully biodegradable materials are not always necessary for many applications where partial biodegradability may be adequate. For example, creating a partially biodegradable garbage bag with a high content of starch would result in a product that could allow for any biodegradable contents to escape from the bag and be exposed to oxygen or microbes. Additionally, there are environmental trade-offs involved in replacing non-renewable materials with renewable materials. Such tradeoffs can be minimized by blending together renewable and non-renewable materials. Therefore, it is worthwhile to explore the properties and applications of polyolefin/starch blends.

The overall goal of this proposal is to explore ways to incorporate a high loading of starch into existing products, viz. create materials that are almost entirely comprised of a renewable material and are highly degradable in landfills. There is a broad interest in controlling polymer blend morphology via compatibilization. This is of great importance when blending starch with polyolefins to create stable blends and overcome the poor mechanical properties that are inherent to starch.

This thesis is divided into two parts. In addition to the background information presented in Chapter 2.0, the first half of the thesis, Chapters 3.0 and 4.0, discusses the morphology and rheology of model immiscible polymer blends that have been compatibilized in situ via an interfacial chemical reaction using multifunctional polymer components. The resulting crosslinked interface provides a robust compatibilizer. The knowledge gained from the model system is then transferred to a "non-model" polymer blend system: starch and polypropylene.

Starch is inherently multifunctional, having three hydroxyl groups on each monomer unit which can be exploited to compatibilize starch with another polymer. The compatibilization and characterization of starch and polypropylene blends comprises the second portion of the dissertation and is presented in Chapters 5.0 and 6.0. The common trend throughout Chapters 3.0 through 6.0 is examining the fundamental characteristics of reactive compatibilization in model blends and applying that method of compatibilization in non-model, renewable polymer blends. An assessment of the environmental impacts of renewable, starch-based materials is presented in Chapter 7.0. Finally, future research directions are discussed in Chapter 8.0.

# 2.0 BACKGROUND

In Section 2.1, we give an overview of rheology of polymer blends in the presence of compatibilizer. The break up and coalescence of droplets under flow is presented and the relations between a polymer blend's morphology and its rheological properties will be discussed. In Section 2.2, we discuss compatibilization of polymer blends via reactive blending and the interfacial compatibilizer architectures that may form. We then switch the focus to the properties and processing of starch. In Section 2.3, we give background information on the chemical structure and functionality of starch, as well as the effects of the plasticization process. The properties of blends of starch with renewable and non-renewable polymers are also discussed. Finally, in Section 2.4, we introduce Life Cycle Assessment, which is a tool used to analyze the environmental impact of materials and processes.

## 2.1 RHEOLOGY OF IMMISCIBLE POLYMER BLENDS

Rheology is the study of material properties during flow and deformation and is often used to gain information about the viscoelastic properties of materials. Immiscible polymer blends display complex viscoelastic behavior due to the presence of the interface. By increasing and decreasing the interfacial area these materials can store and release energy; consequently they show enhanced elastic properties compared to the component polymers. By applying simple flow fields to such blends, the blend's response can provide clues on the microstructures and the properties of materials under flow. The context of this background information is with respect to non-Newtonian polymer blends.

### 2.1.1 Single drop deformation and breakup

When a single drop is sheared, it becomes deformed and orients itself in the direction of the flow. If the drop is sufficiently elongated, drop breakup can occur. Two forces which affect a droplet under shear flow are the applied viscous force, which deforms the drop, and interfacial tension, which aids in the retraction of the drop back to a spherical shape.

The ratio of viscous stress to the interfacial stress is a dimensionless number called the capillary number Ca, and is governs the conditions under which drop breakup may occur. It is defined as

$$Ca = \frac{viscous\ stress}{interfacial\ stress} = \frac{\sigma}{\alpha/R}$$

where σ is the applied shear stress, R is the radius of drop and α the interfacial tension between the two phases. At sufficiently high shear stresses, for a given polymer blend, droplets break above the critical capillary number (Cacr), or the point at which viscous stress overcomes the interfacial tension.

### 2.1.2 Droplet coalescence

No drop breakup is expected when shearing a polymer blend below the critical capillary number. However, shearing cause drops to collide and possibly coalesce, resulting in an increase in the mean drop size, R. During a collision, the drop interface becomes flatten against another drop and a layer of the matrix fluid remains between them. For coalescence to occur, this layer of fluid must drain or become sufficiently thin enough for van der Waals forces between the drops to cause the rupture of the film and therefore coalescence of the drops.

Compatibilizers can often suppress coalescence. The mechanism of coalescence suppression from the addition of a compatibilizer is not completely understood, however, two explanations are generally accepted to explain it [6, 7]. First, in the case of macromolecular compatibilizers, coalescence suppression is a result of steric hindrance when two compatibilized drops approach each other. In this case, a higher molecular weight compatibilizer will more efficiently suppress coalescence. Secondly, Marangoni stresses (discussed further in Section 2.1.3) attempt to distribute a uniform amount of compatibilizer at the interface when

compatibilizer concentration gradients are present at the interface. As a result, the fluid in the gap between two approaching droplets is immobilized, preventing coalescence [8, 9].

### 2.1.3 Dynamic oscillatory properties

The small amplitude oscillatory frequency sweep experiment, with sufficiently small strain to keep the morphology intact, is used as a tool to extract morphological information from the rheological data. This is carried out by applying a sinusoidal strain (γ) at various frequencies (ω) expressed mathematically as follows:

$$\gamma = \gamma_{0\ \sin(\omega t)} \quad 1$$

The stress response of the sample is also sinusoidal and is out of phase by an angle δ:

$$\sigma = \sigma_0 \sin(\omega t + \delta) = \sigma_0 \cos\delta \sin\omega t + \sigma_0 \sin\delta \cos(\omega t) \quad 2$$

$$\sigma = G' \gamma_o \sin(\omega t) + G'' \gamma_0 \cos(\omega t) \quad 3$$

The oscillatory frequency experiment is conducted at various frequencies and the resulting data offer a method of probing the morphology without disturbing it. The data resulting from such oscillatory experiments include the dynamic moduli G' and G". The storage modulus G' is the in-phase component and is indicative of solid or elastic like behavior, whereas the loss modulus G" is the out-of-phase component and is indicative of the viscous or liquid like nature of the material. The dependence of G' and G" on the oscillatory frequency ω is directly related to drop size of the dispersed phase of the blends and therefore, to the morphology of the blends.

At high frequency of oscillation, the drops deform with the applied flow, but do not retract to a spherical shape since the relaxation, or retraction, occurs slower than the interval of

frequency. At lower frequencies, the drops deform during the applied flow and the longer time scale allows drops to relax due to interfacial tension. This relaxation of drops causes the appearance of a characteristic shoulder in a typical log(G') versus log(ω) plot of a polymer blend, as shown in Figure 2.1, and is an indication of the relaxation of the drops (i.e. the interfacial relaxation), provided that the interfacial relaxation is much larger than the relaxation of the bulk components.

The complex viscosity, also displayed in Figure 2.1, is another rheological property which is dependent on frequency. The magnitude of terminal complex viscosity η*, often referred to as the zero shear viscosity, is defined as:

$$|\eta_0^*| = \lim_{\omega \to 0} \frac{G^*(\omega)}{\omega}$$

where $G^*$is the complex modulus, given by $G^*(\omega) = G' + iG''$.

In the case of compatibilized blends, there are two compatibilizer concentration dependent regimes [10]. Blends with low compatibilizer content (<1.0%) display two relaxation processes, a high frequency relaxation attributable to the deformation and relaxation of drop, as discussed in the previous paragraph, and a low frequency relaxation attributable to interfacial elasticity due to the compatibilizer. In terms of shape relaxation, the high frequency relaxation is dependent upon drop size. Dimensional analysis, along with theory [11], suggests that the characteristic frequency of this process must scale as $\frac{\alpha}{\eta m R}$, where α is the interfacial tension of the two component polymers, R is the mean drop size, and ηm is the viscosity of the matrix phase. As the mean drop size increases, the relaxation of drops will increase, decreasing the frequency at which the shoulder occurs. Therefore a shift of shoulder to a lower or a higher frequency is a very useful method to monitor drop size. The low frequency relaxation, which is independent of drop size, increases with additional compatibilizer and is likely attributable to Marangoni

stresses [10]. In particular, upon deformation the compatibilizer becomes concentrated towards the ends of the drop. This gradient in compatibilizer concentration causes a gradient in interfacial tension. Marangoni stresses work to relax the interfacial tension gradients. In the second "high compatibilizer" regime, the interfacial elasticity from the compatibilizer increases and the time scale of its relaxation increases, shifting the frequency at which it occurs, and the two shoulders merge into one. This behavior has been reported previously [10, 12].

### 2.1.4 Steady shear viscosity and strain recovery

The non-Newtonian behavior of immiscible polymers blends has been reported extensively (see Tucker and Moldenaers [13] for many citations). The presence of dispersed droplets in a polymer blend will increase the viscosity of the blend due to hydrodynamic interactions of the dispersed phase and is dependent on the volume fraction of the blend. Upon shearing, the dispersed drops align with the direction of the flow, giving a viscosity that decreases with increasing stress, known as shear thinning. When shearing is ceased, the deformed droplets relax to a spherical shape, which is driven by interfacial tension and known as elastic recovery. With addition of a diblock copolymer, it has been shown that the steady shear viscosities of compatibilized polymer blends are expected to increase as a result of the viscoelasticity of the interface [14]. It has also been reported that addition of a diblock tends to increase the ultimate recovery after cessation of shear, but also tends to slow down the recovery kinetics [15]. One goal of this research is experimentally determine the rheological and morphological effects of compatibilization using reactive blending with multifunctional reactive polymer, which is described further in the following section.

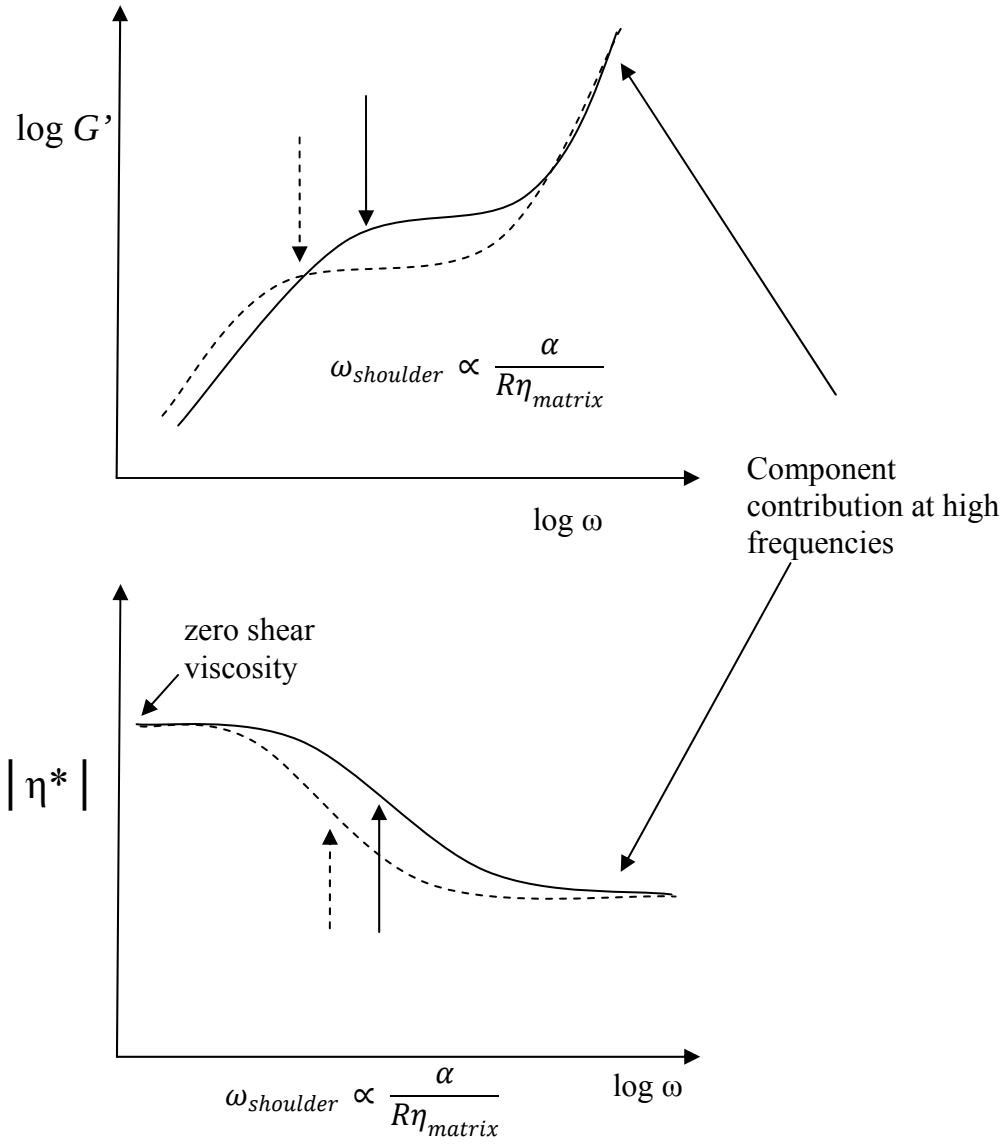


Figure 2.1. Typical plots of (a) Storage modulus (log G') versus angular frequency (log ω); (b) complex viscosity (|η*|) versus angular frequency (log ω) for an immiscible polymer blend. The presence of a shoulder is attributable to deformation and relaxation of drops.

## 2.2 COMPATIBILIZER ARCHITECTURE

When blending any two immiscible polymers, large-scale phase separation is a concern. Compatibilizers are commonly used to promote blending and improve interfacial adhesion, in the solid state, of immiscible homopolymers. Numerous researchers have used premade diblock copolymers in studies of immiscible blends principally because the structure of the compatibilizer is known precisely, and the amount of compatibilizer present in the blend can be controlled exactly. However, industrially it is much more common to generate a compatibilizer by an interfacial chemical reaction between reactive polymers [16]. This method alleviates some of the complications of adding a diblock compatibilizer, such as micelle formation and non-uniform distribution of compatibilizer. Some homopolymers are inherently reactive, e.g. polyamides have primary amine end groups and polyesters have carboxylic acid or alcohol end groups. In other cases, reactive polymers may be added to otherwise inert phases specifically to promote reactive compatibilization in polymer blends. The reactive groups then arrive at the interface by diffusion, usually aided by the flow applied by the blending operation, resulting in compatibilizer formation at the interface. When two reactive polymers are blended together, several blend architectures may form.

The simplest possibility is of linear mono-end-functional chains reacting to form a diblock copolymer (Figure 2.2a). As mentioned, due to the conceptual simplicity of diblock formation, reactively-generated diblocks are popular in laboratory studies of the kinetics and mechanisms of reactive compatibilization [17-21]. However, reactive generation of diblocks is not a common industrial occurrence, although the review by Koning et al. [22] has cited some examples from the patent literature [23-25]. Variations of diblock formation, e.g. three or four

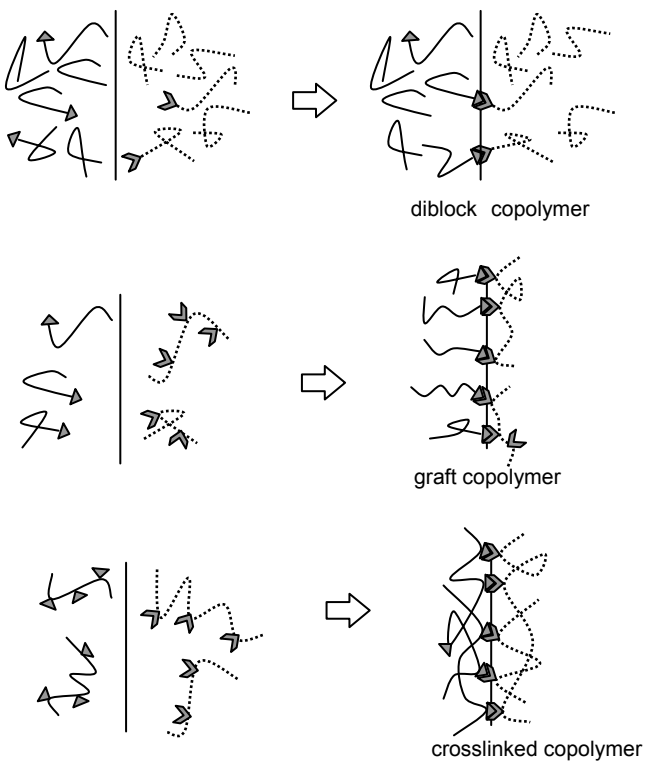


Figure 2.2. Reactive compatibilization leading to various compatibilizer architectures at the interface: (a) Both reactive species are linear, mono-end-functional, resulting in diblock compatibilizers, (b) one reactive species is linear mono-end-functional, whereas the other is a linear multifunctional polymer giving graft architecture, (c) both reactive species are multifunctional, resulting in a crosslinked interface. Note that in addition to the reactive species, unreactive chains may be present in both phases. These are shown explicitly only in (a).

arm stars formed from mono-mid-functional chains, are also possible, but not illustrated in Figure 2.2

The second possibility of reactive compatibilization is that illustrated in Figure 2.2b, where an end-functional chain in one phase reacts with a multifunctional chain in the other to form a graft copolymer at the interface. Numerous reactively generated compatibilizers are graft

copolymers, and for this reason, in some of the literature, "grafting" is virtually synonymous with reactive compatibilization. One heavily-studied example is polyamides, which have primary amine endgroups, reacting with maleated polyolefins (see Section B.5 of Datta and Lohse [26] for numerous citations). This reaction led to the commercialization of Supertough Nylon. Another commonly-studied example is of polyesters, which have acid or hydroxy endgroups, reacting with epoxy-functional polyolefins [27-29]. Graft copolymers can also be formed from reactions such as transesterification [30] or acidolysis [31] that involve pendant groups.

The above two cases of Figure 2.2a and b have the notable feature that at least one of the reactive species was *mono*functional. There are however numerous cases in which both reactive species are multifunctional. In such cases, the compatibilizer is not expected to be a graft copolymer, but instead a crosslinked network as illustrated in Figure 2.2c. Some examples of such reactive compatibilization with two multifunctional species include blends of oxazoline-functional polystyrene and maleated ethylene-propylene [32, 33], blends of acid-functional polymer and polyvinylpyridine (in which the species react by acid-base interactions) [34, 35], polyethylene/polystyrene blends with a Friedel Crafts reaction between the two species [36], and several studies of blends of glycidylmethacrylate-functional polymers with acid-functional polymers [37-40]. Other similar examples can be found in the literature and in the citations of reviews [22, 26, 41].

In short, compatibilization by the interfacial reaction of two *multi*functional species is not uncommon in the literature. Remarkably however, none of the above publications explicitly comment on the possibility that the two multifunctional reactive species can lead to a crosslinked interface. Indeed, in occasional such papers, the compatibilizer is even referred to as a "graft

copolymer" when in fact the multifunctional nature of the reacting species makes a graft copolymer architecture unlikely. Interestingly, even some cases that are generally regarded as graft copolymer compatibilizers may not have a strictly graft architecture. For example with polyamides, some fraction of the chains must have two amine groups, and hence even the polyamide/ maleated polyolefin case cited above may allow some degree of interfacial crosslinking.

Generally, crosslinking the components during processing is discouraged by the possibility that the entire bulk will become crosslinked, rendering the material unprocessable. One goal of this work is to specifically focus on the properties and processability of blends with multifunctional reactive compatibilization that leads to interfacial crosslinking.

## 2.3 STARCH SYSTEMS

Starch is an abundant, naturally occurring polysaccharide that is obtained from various plant sources, such as corn, potato, rice and cassava [42]. Starch is a semi-crystalline polymer comprised of glucose monomer units. As shown in Figure 2.3, its granular form is comprised of linear amylose or branched amylopectin macromolecules with amylose content of ranging from 20-30%. Dry granular starch, by itself, cannot be processed like a plastic; however, it can be heated and blended with several different small polar molecules (water, glycerol) or polar oligomers (polyols), giving a thermoplastic material generally called Thermoplastic Starch or Plasticized Starch (PLS). This process, know as gelatinization, breaks up the granular structure of starch by disrupting hydrogen bonding between adjacent glucose molecules and essentially destroys its crystallinity [43]. PLS has been reported to have been processed by a variety of

processing operations routine in the plastics industry including kneading, extrusion, compression molding and injection molding [44].

### 2.3.1 Effect of plasticizer

The role of a plasticizer that is added to a polymer is twofold. Mechanically, addition of a plasticizer is intended to increase the ductility or elasticity of a material, which often results in a decrease in strength and stiffness. Thermodynamically, plasticization of a polymer decreases its glass transition temperature ($T_g$) corresponding to the increase in chain mobility. PLS has reportedly been plasticized using water, polyols [45-47], water and glycerol combinations [48, 49], alginate [50], and several plasticizers containing amine groups [51, 52]. Despite differences in the plasticizer used, similar mechanical and thermodynamical effects were observed. In particular, as plasticizer content was increased, tensile stress and modulus decreased, elongation and yield at break increased, and $T_g$ decreased.

Prior to plasticization, the crystallinity of starch arises primarily from double helices of amylopectin chains arranged in thin lamellar domains and secondarily from amylose crystallization into single helical structures [53]. Although the ordered structures are disrupted and melted during processing, some residual crystallinity remains depending on processing conditions and plasticizer content [53]. Additionally, processing can induce recrystallization of amylose into single helix structures during cooling [44]. In glycerol plasticized starch, aging of the material after processing occurs by retrogradation, i.e. the reassociation of double helix structures by both amylose and amylopectin chains. This recrystallization, caused by the

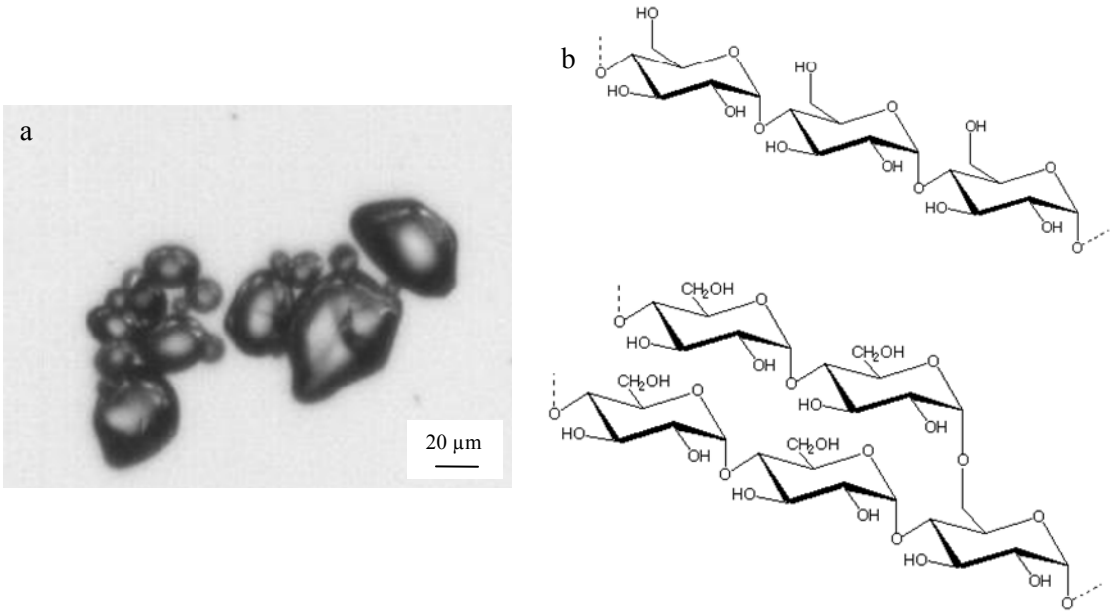


Figure 2.3. (a) Optical image of potato starch granules, glucose monomer units linked together to form (b) linear amylose and (c) highly branched amylopectin.

physical crosslinks in a network of amylose and amylopectin chains, stiffens the material, reduces ductility and eventually promotes cracking. This effect has been interpreted to be a mechanical antiplasticization effect, since over time PLS shows an increase in tensile strength and modulus and a decrease in elongation. Such aging is dependent on relative humidity and aging time [54].

Although processable, PLS generally has quite poor mechanical properties. To address this issue, starch has been chemically modified [55, 56], blended with renewable and non-renewable thermoplastics [3, 57-60], and reinforced with fibrils, whiskers and clays [61-64]. Blends of PLS with other renewable or non-renewable thermoplastics can possess excellent mechanical properties [3, 57, 65-67] and depending on the blend components, PLS blends may

or may not be degradable. A more detailed description of starch blends is discussed in the Section 2.3.2.

### 2.3.2 Properties of starch blends

As stated previously, starch can be blended with non-biodegradable polymers to render the blend partially biodegradable, and with biodegradable polymers to decrease the cost of the material. In cases of blends with petroleum-based polymers, the integration of starch will decrease dependence on non-renewable resources. Accordingly, starch has been reported to have been blended with biodegradable polymers [60, 65] such as aliphatic polyesters [68], polyvinyl alcohol and polyhydroxylalkanoate (PHAs) and non-biodegradable polymers, such as polystyrene (PS) [69] and polypropylene (PP). The majority of research published on starch blends is focused on blending starch with polyethylene (PE). Since it is so widely used in numerous applications such as packaging (i.e. short life span) and mulch films, the raw material used to create PE and the persistence of PE are of concern. Therefore, the integration of PLS with PE is not surprising [3].

Starch contains numerous hydroxyl functional groups (Figure 2.3) making it an ideal candidate for reactive compatibilization since hydroxyl functional polymers may be coupled with polymers containing anhydride or isocyante functional groups [70] via a condensation reaction in which a small molecule (often water) is eliminated during coupling. Maleated polymers, used in the anhydride-hydroxyl reaction, are an excellent choice for blending with starch, since they can be purchased commercially or can be created during processing by grafting maleic anhydride groups onto the polymer backbone. Accordingly, many publications focus on blends of PLS and polyethylene and the use of a maleated polymer has been shown to be an effective compatibilizer

in PLS/PE blends [71]. Ethylene-acrylic acid has also been reported to be an effective compatibilizer in starch systems, but must be used in large loading to obtain improved mechanical properties [3].

PLS and polyolefins blends generally contain low PLS content and can display the good mechanical properties [1, 3, 57, 65-67, 72]. Compatibilized starch blends with both virgin and recycled polyolefins showed improved properties compared with uncompatibilized blends [3, 71, 73]. Particularly, when reactively blending PLS with non-renewable polymers, such as polyolefins, a general trend is observed; blend properties began to deviate sharply from the polyolefin properties as PLS content was increased past 60% [3, 71, 73]. In these cases, high starch loadings resulted in a large decrease in the tensile strength and modulus and in one case [73], an increase in elongation of the blends.

From the perspective of degradability and renewability, increasing PLS content in polymer blends is desirable. However, to our knowledge only one research group has published work focusing on blends containing more than 50% PLS [72] and in PLS/polyolefins blends containing increasing amounts of PLS, a decline in mechanical properties is observed [3, 71-73]. Therefore, the one goal of this research is prepare a starch based material with some degree of biodegradability and good mechanical properties by blending PLS with polypropylene. We intend to reach this goal by preparing blends of plasticized starch and polypropylene, using maleated polypropylene to compatibilize the immiscible blends.

### 2.3.3 Nanocomposites of PLS and layered silicates

Another alternative employed to improve the mechanical properties PLS is to create a nanocomposite with layered silicate clays. Polymer-clay nanocomposites have been researched extensively in the last two decades [74, 75]. Clays, or layered silicates, are popular reinforcing agents due to their low cost, abundance in nature, and their ability to be separated into individual nanometer thick layers for efficient reinforcement. The silicate layers have high aspect ratios, and provide high strength and stiffness at low weight loadings when added to a polymer matrix [75]. Also, compared with traditional composite materials such as glass fiber-reinforced plastics, a significant enhancement of properties is apparent without significant increases to the weight of the material. Clay minerals are composed of nanometer thick layers, commonly consisting of silica and alumina layers. The most commonly studied clays are the family of clays known as the smectite clays. Of the smectite clays, montmorillonite (MMT) is the most common [75]. Smectite clays have a 2:1 layer structure, which consists of one alumina octahedron sheet sandwiched between two silica tetrahedron sheets. Alumina may be replaced with other metals, such as magnesium and, depending on the specific chemistry of the layers, the surface and edges of each layer may bear a negative charge. Stacking of the layers results in a van der Waals interaction in the gap between the layers, referred to as a gallery (See Figure 2.4). Counter-ions, balancing the charge from the clay layer, lie in the gallery between layers. Enhanced properties result from the dispersion of separated nano-layers into a polymer matrix. While the smectite clays are not nano-sized particles, they can be separated into nano-layers by exfoliating or intercalating the clay layers. Exfoliation of layered silicates results in complete separation of each layer, while intercalation is the insertion of polymer molecules into the galleries, which expands the space between the layers, but does not completely separate the layers. Clay is

naturally hydrophilic, and is not readily dispersed into typical hydrophobic polymers without organic modification. Often, it is desirable to swell the interlayer space to reduce layer to layer interactions and allow the polymer to occupy the gallery. Organic surface modification of the clays is generally employed to improve compatibility through the exchange of interlayer counter-ions with ammonium ions. Analogous to a surfactant, the ammonium ions reduce the surface energy and allow the surface of the nano-layer to be wetted by the polymer. The structures of such materials are most often investigated using X-ray diffraction (XRD) and TEM and we will employ both of these methods to characterize our composite materials.

There have been studies that focused on nanoclay used to reinforce plasticized starch [62, 76-78], starch-polyester blends [64, 79, 80] and starch foams [81], but to our knowledge, only one study has reported research related nanoclay composites of starch and polyolefin blends [82]. Because of its hydrophilicity, the unmodified nanoclay Montmorillonite showed the best compatibility with PLS in PLS clay nanocomposites, while organo-modified clays, such as 30B showed better compatibility with hydrophobic polymers [83], which can be further improved with addition of polar functional groups [84]. A review article by Zhao, et. al. reports on the incorporation of layered silicates into plasticized starch via melt processing and cites cases of good compatibility between unmodified smectite layered silicates and PLS.

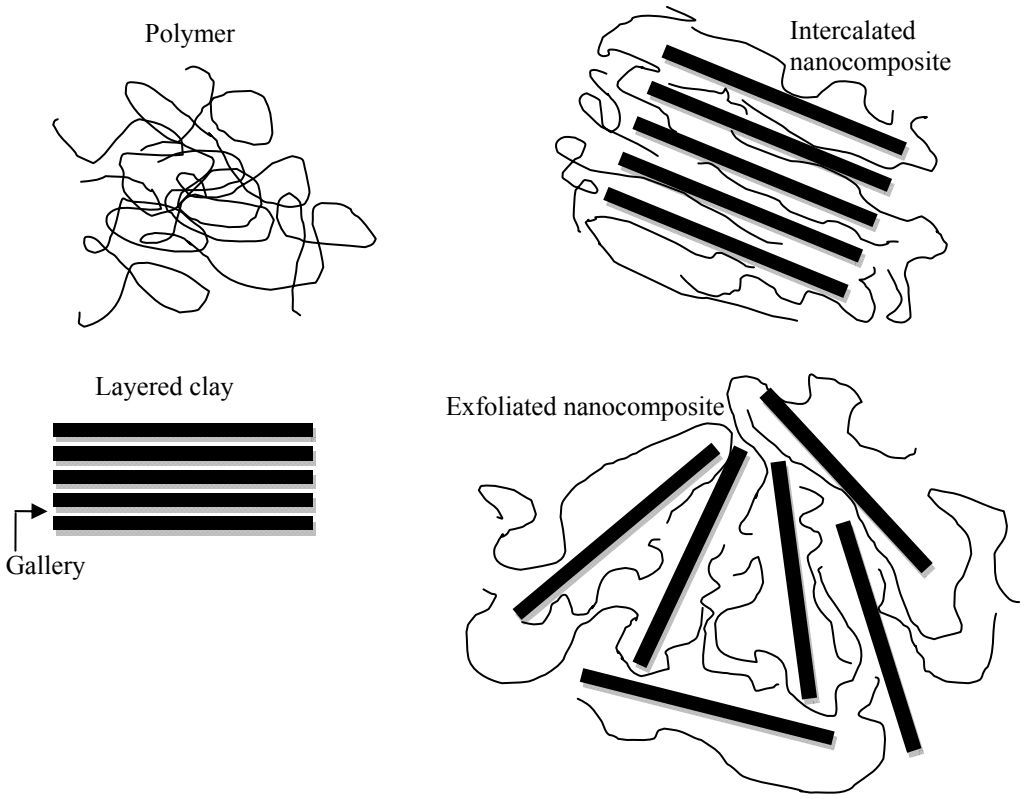


Figure 2.4. Formation of clay based polymer nanocomposites by intercalation and exfoliation, not drawn to scale.

Many studies have also reported enhanced mechanical properties, such as increased tensile strength and modulus, and increases in water resistance [62, 74, 80, 85]. Chen et al. [76] examined the effects of clay type and found that MMT showed greater exfoliation and increased modulus than other smectites, attributable to its high aspect ratio. Clay nanocomposites have also been created from PLS blended with other renewable polymers, both biodegradable and non-biodegradable [64, 82, 86], but blends of PLS and poly-caprolactone (PCL) are the most widely reported. In fact, only one study [82] reported on clay-containing blends of PLS and PP and focused primarily on rheological properties rather than mechanical properties. Furthermore, it has also been shown that the addition of nanoclay to gelatinized starch inhibits starch

retrogradation, or slow recrystallization, and water loss by interactions between the clay and starch and by restricting the motion of plasticizer around the amylose chains [87].

At higher starch loadings in PLS/polyolefin blends, mechanical properties are usually poor [88] since the mechanical properties of the PLS are dominant. Despite the increasing number of studies on starch blends, there is a lack of publications which explore blends containing large fractions of PLS, which is sustainably desirable as a biodegradable renewable blend component. A goal of this research is to mitigate the decline in mechanical properties in the PLS/polypropylene blends as PLS content increases by adding layered silicate clays to create a clay nanocomposite.

## 2.4 LIFE CYCLE ASSESSMENT

As mentioned in Chapter 1.0, there are environmental trade-offs involved in replacing petroleum based materials with renewable materials, such as starch. Unfortunately, no metric exists to assess how "green", or environmentally friendly something is. To fairly compare two materials, products or processes, clear boundaries must be established. Life cycle assessment (LCA) is a tool which critically analyzes a product's life from cradle to grave with the system boundaries set by the person conducting the analysis, which generally include the product's production, use and disposal as shown by Figure 2.5. The LCA process is governed by the International Organization of Standardization (ISO) beginning in 1997 with ISO 14040 [89]. Commonly, the cradle, or beginning of the product's life, is defined at the time when all raw materials are extracted or created and the grave of the product is defined as the end of the product's useful life

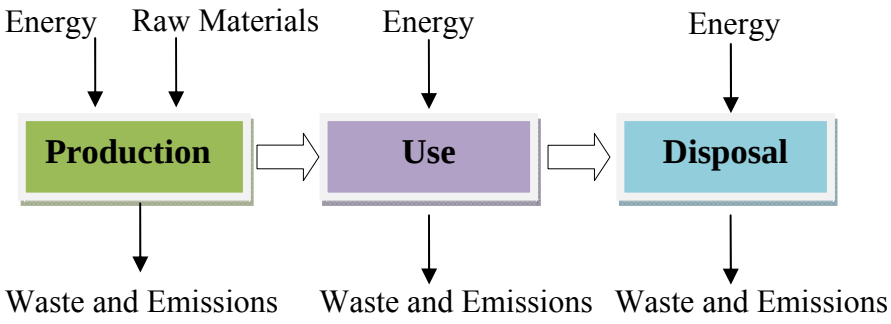


Figure 2.5. An example of system boundaries for a given product or material.

or when the product enters the municipal waste stream. For example, in the case of starch based products, the growing of the plant from which the starch is derived can be defined as the cradle. The purpose of conducting an LCA is to compare similar products and to identify stages in the life cycle which have the most harmful environmental impacts. The environmental impacts of all materials and energy used during a life cycle are analyzed in categories ranging from greenhouse gas emissions and energy consumption to eutrophication and toxicity.

An LCA is the sum of four stages, goal and scope definition, life cycle inventory, impact assessment and interpretation. The goal and scope definition describes the objectives of the LCA and defines a functional unit for the system. A functional unit defines the function of product and allows for fair comparisons of products. The first LCA stage also defines the system boundaries and the environmental impact categories that are to be included in the assessment. The product system within these boundaries is divided into the unit processes of the product. All of the unit processes are connected with input and output flows; such as solar radiation in and greenhouse gas emissions out. In the second stage of an LCA, the life cycle inventory (LCI), these input and output flows are quantified. An LCI is a mass and energy balance of the product system and data is collected for each flow and unit process and an impact is calculated for each

category based on the functional unit. The next stage of the LCA is the life cycle impact assessment (LCIA). During an LCIA, the inventories from the LCI are assigned to larger environmental impact categories which they directly affect. The data contained in these larger environmental categories are characterized and defined relative to the functional unit. Finally, all the results are interpreted, presented in accordance with the goal and scope definition, and used to make decisions in product comparisons and identify where improvement is needed.

### 2.4.1 Life cycle assessment of starch based materials

Biopolymers have received much attention in the last decade as sustainable alternatives to petroleum based polymers [90]. They are after all, made from renewable feedstock and in many cases have some degree of degradability or compostability. Prior to 2007, LCAs favorably compare bio-based polymers with petroleum based polymers [91-94], always citing benefits for bio-based polymers in the areas of energy and global warming potential [95]. For example, Du Pont, Tate and Lyle Bio-Procucts claim that the production of their corn based Bio-propanediol consumes 10% less energy and reduces greenhouse gas emissions by 20% on a per-pound basis, compared to conventional petroleum-based PDO [96]. Cargill Dow, the producers of Polylactic acid (PLA) also claim that the cradle to gate production of PLA uses significantly less fossil fuels than the production of any of it petro based competitors [97]. Both of these claims focus on only one portion of the environmental impact, the fossil fuel use and corresponding greenhouse gas emissions. Energy concerns of the significant importance, but the environmental impacts of nitrogen emissions to the environment are also of value to investigate. The life cycle of any material made from agro-resources must account for farming practices. In fact, the environmental cost of bio based production is high [98]. Environmental trade-offs of bio-based

production have just begun to be considered in comprehensive LCAs [98-101]. The fertilizers and pesticides used to grow the corn, potatoes and soybeans that are the raw materials for many of these bio-based products cause acidification and eutrophication in the rivers and streams in the United States [99]. Such environmental impacts should be included in any comprehensive life cycle assessment of bio-based materials.

# 3.0 MORPHOLOGY AND RHEOLOGY OF COMPATIBILIZED POLYMER BLENDS: DIBLOCK COMPATBILIZERS VS CROSSLINKED REACTIVE COMPATIBILIZERS

Reactive compatibilization is commonly used when blending immiscible homopolymers. The compatibilizers are formed by the interfacial coupling of two types of reactive chains often have a graft copolymer architecture.

As described in Section 2.2, compatibilization by the interfacial reaction of two *multi*functional species is not uncommon in the literature, but the possibility of interfacial crosslinking is rarely, if ever, mentioned and the compatibilizer is often referred to as a graft copolymer. One goal of this research is to specifically focus on blends with multifunctional reactive compatibilization that leads to interfacial crosslinking.

Our experimental approach uses "model" blends: blends of polymers chosen for their experimentally-convenient attributes such as being liquid room-temperature, transparent, inexpensive and readily available. Since the bulk phases of the blends had simple rheological properties, all non-Newtonian behavior can be unambiguously attributed to interfacial phenomena. Model blends compatibilized with diblock copolymers have yielded many insights into the role of the diblock in affecting breakup and coalescence, immobilizing the interface, and causing interfacial viscoelasticity [8, 10, 14, 102-106]. In this chapter, we employ model blends

to examine the effect of multifunctional reactive compatibilizers that crosslink the interface. We compare the rheological and morphological effects of reactive compatibilization to compatibilization via addition of a diblock copolymer. This approach, using a model system, will provide information that has not previously been available.

## 3.1 MATERIALS AND METHODS

Various properties of all materials used are listed in Table 3.I.

The principal components of the blends are polyisoprene (PI, Kuraray) and polydimethylsiloxane (PDMS, Rhodia). The polyisoprene is nearly monodisperse with a high 1,4-cis content, whereas the PDMS is polydisperse. Both polymers were chosen because they are essentially Newtonian liquids at room temperature, thus allowing room temperature blending by hand and experimentation. Two blends are studied in this chapter.

Diblock blend: The first blend, which serves as a reference, uses a nearly-symmetric and monodisperse PI-PDMS diblock copolymer (see Table 3.I) as a compatibilizer. This same compatibilizer was used by Van Hemelrijck *et al.*[104]. The diblock blend contained 1.5 wt% of the diblock copolymer, with the remainder being PDMS and PI in a 30:70 ratio, having an overall viscosity ratio, or the ratio of dispersed phase viscosity to the matrix phase viscosity, of 0.73. The two homopolymers and the diblock copolymer were all weighed into a Petri dish, blended with a spatula by hand for three minutes, and degassed in vacuum prior to experiments.

Reactive blend: The chief concern of this chapter is the second blend, dubbed the "reactive blend" in which a compatibilizer is generated by an interfacial chemical reaction between polyisoprene-graft-maleic anhydride (PIMA) and poly(aminopropylmethylsiloxane-co-

Table 3.I. Model polymer blend materials.

| material | MW (g/mol) | $\eta_{25°C}$ (Pa.s) | composition | supplier |
|---|---|---|---|---|
| PI LIR30 | 29,000[b] | 131 | 100% PI | Kuraray |
| PIMA | 25,000[b] | 1700 | 1.5% MA[b] | Aldrich |
| PDMS | 135,600[a] | 96 | 100% PDMS | Rhodia |
| PDMS* | 5,000[b] | 0.1 | 2-3% $NH_2$[b] | Gelest |
| PI-*b*-PDMS | PI: 26000: PDMS: 27000 | | 48% PI | |

[a] Weight-average molecular weight estimated from known viscosity-MW relationship
[b] Value quoted by supplier.

dimethylsiloxane) (PDMS-$NH_2$). The PIMA has an (isoprene) : (isoprene maleic anhydride) ratio of 98.5:1.5, and a molecular weight of 25 kg/mol; this corresponds to an average of ~ 4.7 anhydride groups per chain. The PDMS-$NH_2$ is quoted as having a molecular weight of 5 kg/mol and 2-3% of aminopropyl groups pendant from the chain; this corresponds to an average of 1.3-1.9 amine groups per chain.

One goal of this thesis is to directly image the reactively-formed copolymer at the interface by confocal microscopy. This necessitates tagging one of the reactive blocks with a fluorophore. For this purpose, we used 4-chloro-7-nitrobenzofurazan (commonly known as NBD chloride). While NBD chloride is itself not fluorescent, upon reacting with an amine, it forms a fluorescent species [107]. In the present case, some of the amine groups of PDMS-$NH_2$ were reacted with NBD chloride in a mutual solvent, dichloromethane, at room temperature. This reaction resulted in fluorescently-tagged, amino-functional PDMS, which is dubbed *PDMS-$NH_2$ where the "*" refers to the fluorescent tagging. For reference purposes, we also reacted the PDMS-$NH_2$ with excess NBD chloride, leading to complete fluorescent tagging (i.e. no unreacted amine groups). This fully-tagged PDMS is dubbed *PDMS. The fluorescence emission spectra of *PDMS-$NH_2$ and *PDMS were recorded. The absorption spectrum of the fluorophore has a maximum at a wavelength of ~460 nm, whereas the peak fluorescence

emission occurs at ~520 nm. The peak fluorescence emission intensity of *PDMS-$NH_2$ was found to be roughly half of that of *PDMS, suggesting that half of the original $NH_2$ groups of PDMS-$NH_2$ were reacted with NBD chloride. Accordingly, *PDMS-$NH_2$ has an average of 0.65-0.95 groups per chain available for reacting with PIMA.

The chief concern of this chapter is to examine the effect of multifunctional reactive compatibilizers. From that point of view, the average functionality of the *PDMS-$NH_2$ appears to be too low to be "multifunctional". Nevertheless, since a distribution of chain lengths and functionalities are expected, at least some of the *PDMS-$NH_2$ chains are expected to have at least two reactive groups. Generally even a small fraction of multifunctional chains is adequate for crosslinking. To confirm that the functionality was adequate for crosslinking, we prepared a blend of PIMA and *PDMS-$NH_2$ in a 1:1 weight ratio. The result was a solid mass that would not dissolve in cyclohexane, which is a good solvent for both PIMA as well as *PDMS-$NH_2$, suggesting that crosslinking did occur. Moreover, as the following section shows, there are profound differences between the behavior of the reactive blend and the diblock blend which are consistent with interfacial crosslinking.

The reactive blend contained 0.75 wt% of the PIMA and 0.75 wt% of the *PDMS-$NH_2$, and the PDMS and PI phases were in a 30:70 ratio. The total compatibilizer loading of 1.5 wt% is identical to that of the diblock blend. Moreover, assuming that the concentration of reactive groups quoted by the manufacturers is correct, and because half of the amine groups are fluorescently tagged, the two reactive species are stoichiometrically-balanced i.e. in the reactive blend, the number of anhydride groups of PIMA are equal to the number of amine groups of *PDMS-$NH_2$.

Methods: Brightfield microscopy was performed using an Olympus CKX41 inverted microscope equipped with a Basler area scan camera. Confocal microscopy was performed using an Olympus FluoView FV1000 inverted confocal microscope using an Ar-Ion laser at an excitation wavelength of 488nm. Low magnification photographs of the samples were taken using a Canon Rebel XT digital camera. Rheological experiments were performed using a TA Instruments AR2000 stress-controlled rheometer with 40mm/1º cone and plate geometry, and the sample temperature of 25ºC was maintained using a Peltier cell.

## 3.2 RESULTS

### 3.2.1 Morphology

Immediately after blending, a drop of each blend was placed between glass slides separated by a thin spacer and examined by optical microscopy. Figure 3.1a shows that the diblock blend exhibits a typical drop matrix morphology composed of round drops of diameter on the order of several microns. The PI, which is the majority phase, is expected to become the continuous phase. This was verified by placing a drop of the blend, and a drop of pure PI, next to each other on a slide. As the two drops spread and touched each other, no interface was evident, confirming that PI is the continuous phase of the diblock blend.

The reactive blend was also found to have a PI-continuous morphology, however, Figure 3.1b shows that the morphology is significantly different: the drops appear to be clustered together. Close observation also suggests that some drops are non-spherical, whereas some

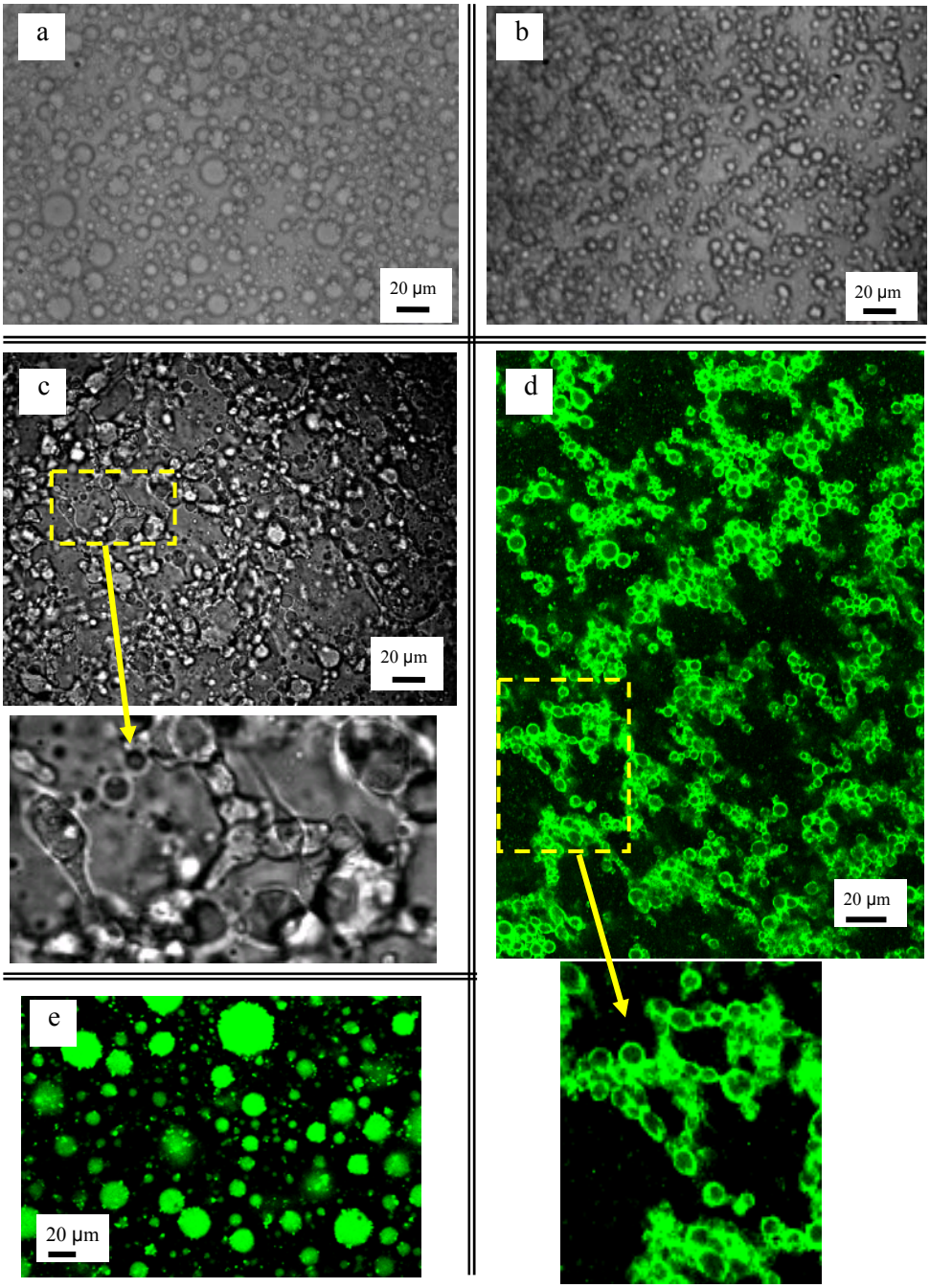


Figure 3.1. Microscopic images of: (a) bright field diblock blend, (b) bright field reactive blend (c) reactive blend after diluting with mineral oil, with the dotted rectangle being shown in magnified form as indicated by the arrow, and (d) confocal image of reactive blend, with the dotted rectangle being shown in magnified form as indicated by the arrow. (e) confocal image of the reactive blend, but without PIMA. Images d and e are colored in the electronic version.

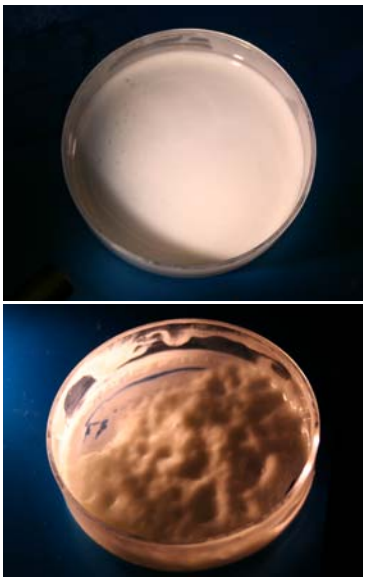

Figure 3.2. Macroscopic image of (a) diblock blend (b) and reactive blend.

appear fused with their neighbors. To observe the drop clusters more clearly, a small sample of the reactive blend was placed on a slide, and covered with a few drops of light mineral oil, which can dissolve the matrix phase PI. After several hours, the matrix phase PI dissolved in the mineral oil causing the blend to spread in a thin layer on the slide, and greatly improving the quality of the image. (Note that the mineral oil also has some solubility in the PDMS and the drops are likely to be somewhat swollen by the oil.) The cluster structure became clearly apparent (Figure 3.1c) in this oil-treated sample, in fact, many drops appear to be connected to form a network. Furthermore, close observation reveals that some of the drops may not have smooth surfaces, as illustrated in the magnified view of a portion of Figure 3.1c. We attribute all three features (non-spherical drops, their non-smooth surface, and the network of drops) to the multifunctional nature of the reactive species. Specifically, we propose that the interface of each drop is a soft solid shell or "skin" of crosslinked compatibilizer. It is this solid-like nature of the

interface that is responsible for the non-spherical drops and the non-smooth interfaces. Furthermore, since the crosslink network forms during the blending process, it is able to connect the drops (formed as large drops break) together into large clusters.

Since the reactive PDMS is fluorescently-tagged, the compatibilizer can be imaged directly by fluorescence microscopy. Figure 3.1 shows a confocal microscope image of the blend. Since this image was taken on an "as-prepared" blend (i.e. without oil treatment of Figure 3.1c), it is a more reliable indicator of the morphology of the blends. The drops in Figure 3.1d appear to be covered by bright shells of compatibilizer, with relatively little fluorescence evident inside the bulk of the drops. In contrast, an image (not shown) of a similar blend without PIMA added to the PI phase shows uniformly-bright drops indicating that the *PDMS-$NH_2$ is evenly distributed throughout the bulk. Thus, the bright shells of Figure 3.1d are evidence that the reactive *PDMS-$NH_2$ is present at the interface, and that such interfacial localization is definitely attributable to the reaction with the anhydride. Furthermore, Figure 3.1d confirms that the drops are clustered together; suggesting that the fluorescent shells covering adjacent drops may be linked into a single crosslinked network. Finally, in agreement with Figure 3.1c, some drops appear to be somewhat non-spherical, although grossly distorted shapes are not evident.

The remainder of this chapter explores the rheology of the reactive blends. Before proceeding with the quantitative investigation of the rheology, it is worth noting a qualitative rheological difference between the reactive and the diblock blends that is evident even from simple visual observation. During blending, numerous air bubbles were entrained within both blends, and these were removed by degassing in vacuum at room temperature. At the end of the degassing process, the diblock blend settled in a uniform, thick layer in the Petri dish (Figure 3.2a). In contrast, after degassing, the reactive blend showed an irregular surface (Figure 3.2b)

with some portions of the sample being much thicker than others. The bumpiness at the surface of the reactive blend in the Petri dish relaxed with time, but even after 20 hours, it still did not flatten out. These visual observations suggest that the reactive blend is highly viscous, or perhaps has a small yield stress – possibilities that are supported by the more quantitative measurements of the following section.

### 3.2.2 Rheology: Dynamic oscillatory properties of as-prepared blends

Strain-sweep measurements were conducted at four different frequencies (100, 10, 1 and 0.1 rad/s) for strains ranging from 0.1% to 10%. Both blends showed linear dynamic mechanical properties under these conditions. All subsequent oscillatory measurements were conducted at 1% strain.

Figure 3.3 compares the dynamic oscillatory frequency sweep behavior of both blends at 1% strain. The behavior of the diblock blend is similar to similar blends studied previously [10, 102, 108, 109]. In particular, the diblock blend shows a higher G' and a higher $|\eta^*|$ as compared to the pure components at low frequencies. These higher G' and $|\eta^*|$ are manifested as a prominent shoulder in G' and $|\eta^*|$ indicating that the diblock blend has additional relaxation processes that are absent in the components. These additional relaxations have been attributed to the shape-relaxation of drops of the blend [11, 110, 111], and to the interfacial viscoelasticity of the compatibilizer [10, 112-114]. At low frequencies, the diblock blend has a G' that is nearly proportional to the square of the frequency, and the $|\eta^*|$ shows a plateau – both characteristics of the terminal behavior of a viscoelastic liquid.

Turning to the reactive blend, the high-frequency oscillatory properties of this blend appear to be similar to those of the diblock blend. However, at low frequencies, the reactive

blend shows gel-like (rather than liquid-like) behavior: the G' shows a plateauing tendency, whereas the complex viscosity increases with no sign of leveling off to some well-defined terminal value. These two observations, which suggest that the blend has an extremely high terminal viscosity (or a yield stress), are a quantitative explanation for why the degassed blend did not relax in the Petri dish in Figure 3.2b.

The properties of the diblock blend under quiescent conditions did not change with time over the timescale of the oscillatory test; repeated oscillatory measurements gave identical results. In contrast, repeated oscillatory tests on the reactive blend showed significant changes in the rheological properties with time even under quiescent conditions. For example, Figure 3.3 shows that the G' and the $|\eta^*|$ of the reactive blend in the low frequency region increased sharply after just one frequency sweep lasting about 100 minutes (curves a), with further small increases over three additional frequency sweeps lasting an additional 5 hours (curves b,c,d). The reason for these changes is not clear; it may be that the deformation experienced by the sample during loading relaxes over a long timescale, and the corresponding changes in morphology enhance the gel-like behavior.

A common concern when dealing with multifunctional reactive systems is the possibility that the entire bulk may become crosslinked, rendering the material virtually unprocessible, similar to a thermoset [115]. In the present case, only 1.5% of the entire system has reactive functionality, furthermore, the crosslinking is confined to the interface. Accordingly, crosslinking of the entire bulk seems unlikely. Nevertheless, since the dynamic oscillatory properties indicate gel-like behavior, the issue of processibility must be considered in more detail. We therefore address two issues in the following two sections: (1) rheological behavior upon startup of steady shearing which is an indicator of flow-induced breakdown of the gel-like

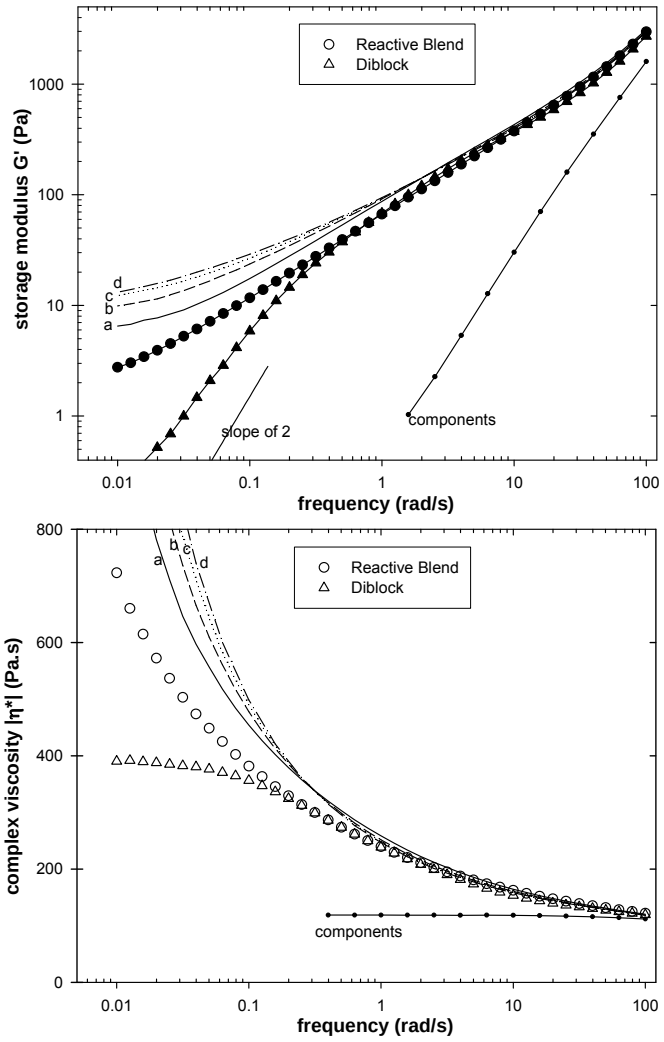


Figure 3.3. Dynamic oscillatory properties of the diblock blend and reactive blend as-loaded into the rheometer. The lines labeled a-d are four successive frequency sweeps for the reactive blend. The data labeled "components" are a volume-weighted average of the bulk PI and PDMS.

behavior, and (2) rheological behavior (especially viscosity) under steady shearing, which is the most basic indicator of processibility.

### 3.2.3 Rheology: Startup of Shearing

The shear history used to investigate structural breakdown is illustrated in Figure 3.4a. It consisted of a series of successively longer shearing steps (creep steps) ranging from 20 seconds to 15 minutes, all at a fixed stress of 100 Pa (chosen arbitrarily). The strain recovery upon cessation of shear, i.e. the recovery at the end of each creep step, was monitored.

For the diblock blend, in each creep step, the viscosity (formally denoted $\eta_c^+$) shows a weak overshoot (Figure 3.4b), with the steady shear viscosity being reached in less than 10 s. Upon cessation of shear (Figure 3.4d), the recovery is completed in about 10 s. All creep steps show identical behavior, and all recovery steps also show identical behavior, both of which indicate that shearing at 100 Pa causes no morphological changes in this sample. Typically, two morphological changes are possible: flow-induced drop breakup, or flow-induced coalescence. Flow-induced coalescence is not expected in the present case because the PI-b-PDMS diblock copolymer is known to suppress coalescence of PDMS drops in PI [104]. Drop breakup is not expected either because the hand-blending process involves high stresses (likely much higher than 100 Pa), and hence the drop size of the as-prepared blend is already expected to be smaller than the critical drop size at 100 Pa. Since neither coalescence nor breakup are expected, consistent behavior of the sample during or after each 100 Pa shearing step is not surprising.

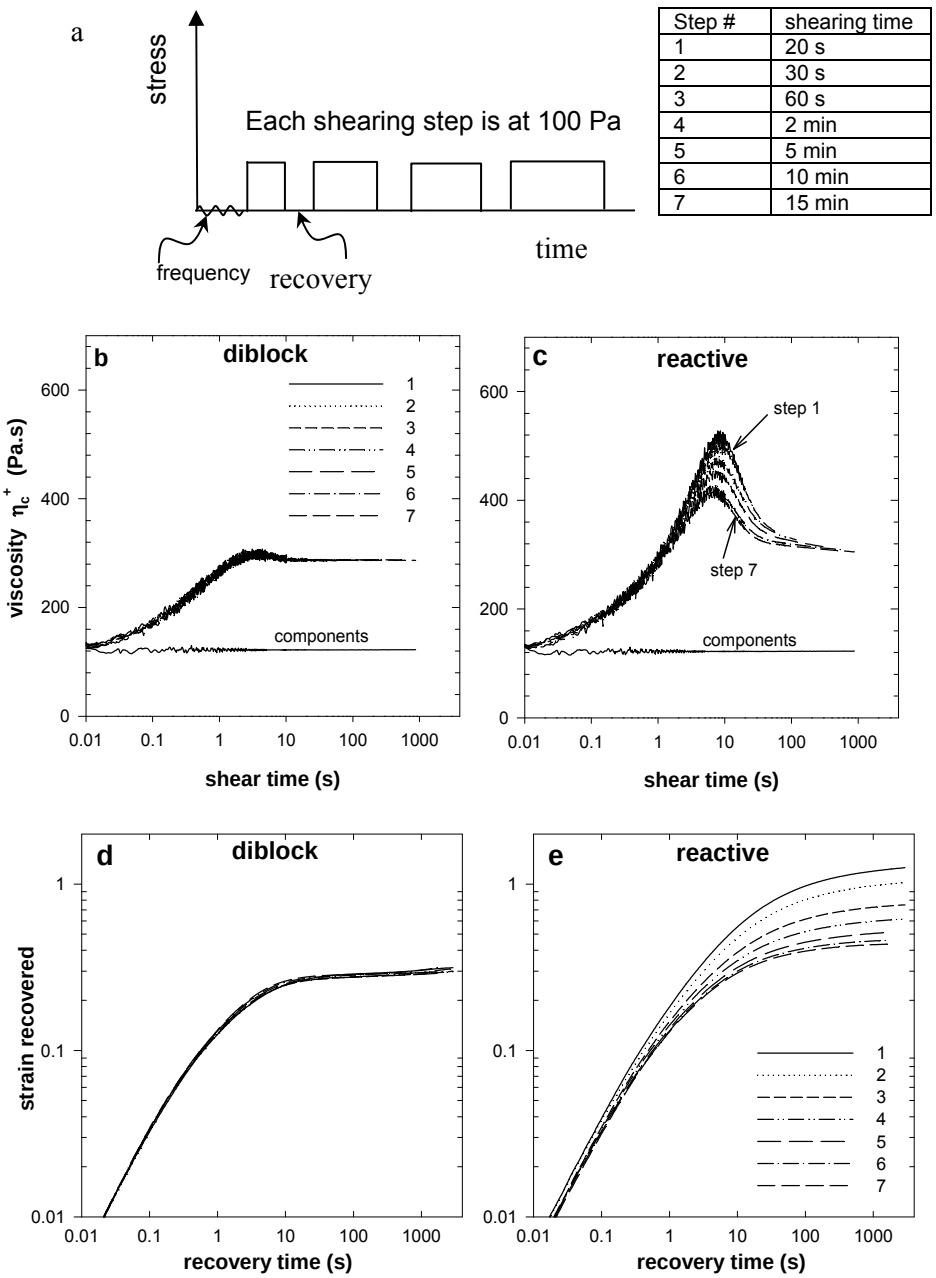


| Step # | shearing time |
|---|---|
| 1 | 20 s |
| 2 | 30 s |
| 3 | 60 s |
| 4 | 2 min |
| 5 | 5 min |
| 6 | 10 min |
| 7 | 15 min |

Figure 3.4. (a) Shear history. The table shows the shearing time in each step. (b,c) viscosity during each shearing step listed in the legend. (d,e) recovery upon cessation of shear after each shearing step listed in the legend. In (c), the highest peak is shown by step 1, and each successive step shows a weaker peak. The data labeled "components" in b and c are volume-weighted averages of the bulk PI and PDMS.

Next we will consider the behavior of the reactive blend. The most important qualitative change evident from the creep steps is a large overshoot in the viscosity $\eta_c^+$ of the sample (Figure 3.4c) at short shearing times. The magnitude of the overshoot is largest during the first shearing step and decreases in subsequent steps, yet it is noteworthy that the overshoot persists even after shearing for several hundred seconds (corresponding to several hundred strain units). The recovery behavior of the reactive blend (Figure 3.4e) also differs qualitatively and quantitatively from the diblock blend. Firstly, the recovery kinetics are much slower; an unambiguous plateauing of the strain vs. time data (indicating the ultimate recovery of the sample) is not reached even after 1000 s, especially in the early shearing steps. Secondly, the magnitude of the ultimate recovery is much larger than for the diblock blend. This becomes clearer when the ultimate recovery is plotted as a function of the total strain experienced by the sample (see Figure 3.5); for the early steps, the ultimate recovery of the reactive blend is more than double that of the diblock blend.

### 3.2.4 Rheology: Steady shear characteristics

At the conclusion of the rheological test of the previous section, the samples were subjected to the shear history of Figure 3.6a. The sample was sheared at 400 Pa for 2000 strain units, then the subsequent recovery upon cessation of shear was monitored, followed by an oscillatory frequency sweep at 1% strain. This sequence (shear for 2000 strain units, recovery, and oscillatory) was repeated at five successively lower stresses of 400, 200, 100, 50 and 25 Pa.

The rheological behavior of the diblock blend (Figure 3.6b, d, f) resembles data on similar samples measured previously. Note that Figure 3.6f shows only one set of data for the

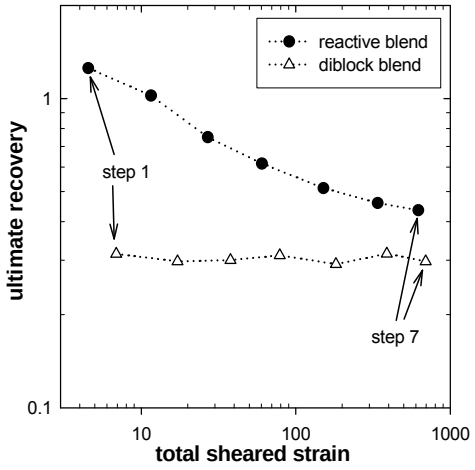


Figure 3.5. Ultimate recovery, $\gamma_{\infty}$, as a function of total sheared strain for both blends. The recovery vs. time data for the reactive had not fully leveled off, thus, the actual $\gamma_{\infty}$ for the reactive blend is slightly higher than shown here.

diblock, viz. the G' and the $|\eta^*|$ recorded after shearing at the 400 Pa stress level. Data after shearing at lower stress levels (not shown) are almost identical to this curve, furthermore, the "as-loaded" data for the diblock (Figure 3.3) are also identical to this curve. All the observed trends can be interpreted by simply recognizing that since coalescence is suppressed, shearing at successively lower stresses does not affect the drop size. Accordingly, (1) the oscillatory properties, which are expected to depend only on drop size, are unaffected by shearing at various stresses, (2) the transient time during startup of creep (Figure 3.6b) which is expected to scale with (drop size)/stress increases with decreasing stress, (3) and the magnitude of the ultimate recovery (Figure 3.6d), which is expected to scale with stress/(drop size), decreases with decreasing stress, (4) decreasing stress without changing the drop size reduces the capillary number, thus explaining the observed shear thinning (Figure 3.6b).

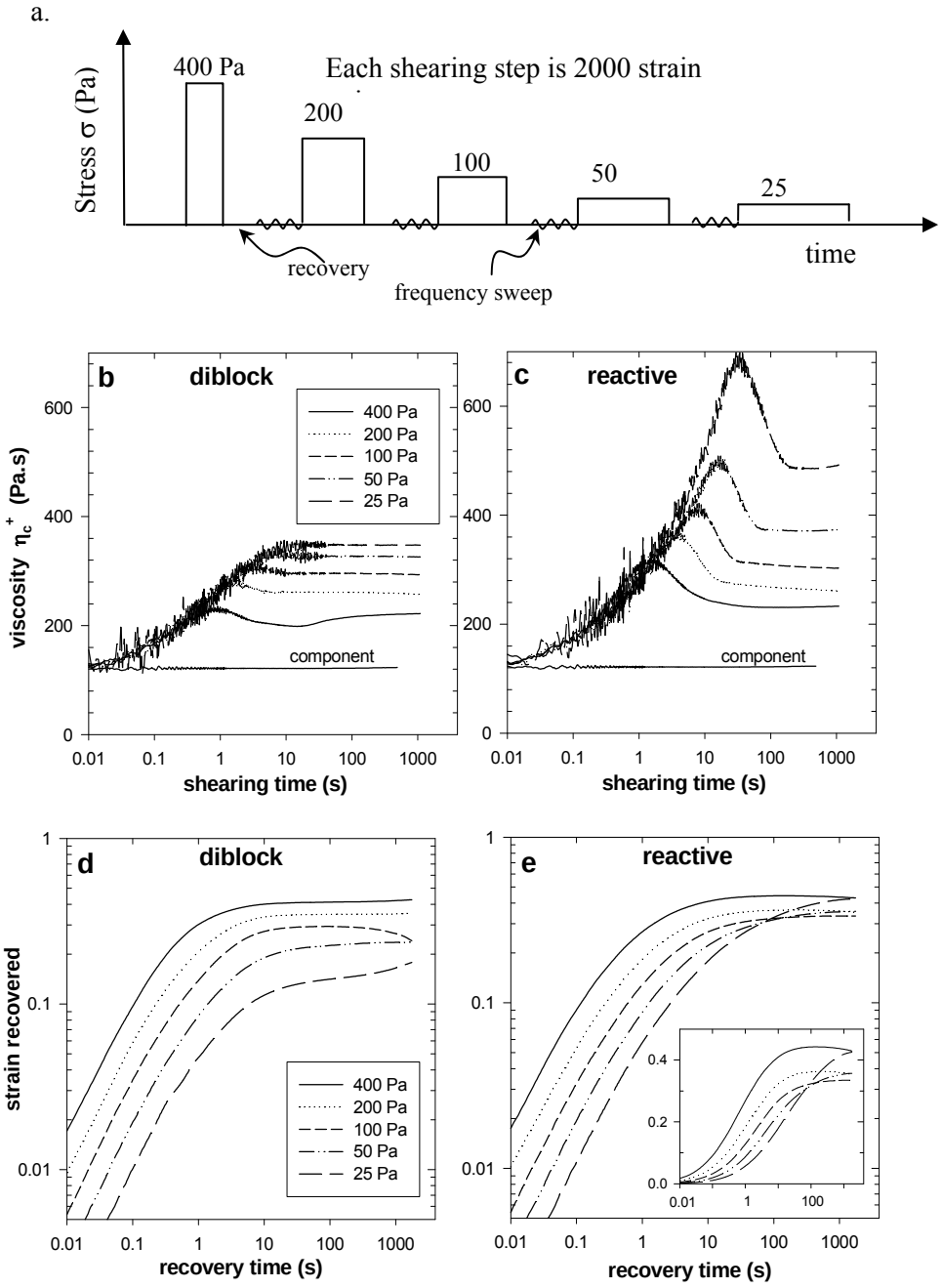
a.
400 Pa
Each shearing step is 2000 strain
200
100
50
25
Stress σ (Pa)
time
recovery
frequency sweep
b
diblock
400 Pa
200 Pa
100 Pa
50 Pa
25 Pa
component
viscosity $\eta_c^+$ (Pa.s)
shearing time (s)
c
reactive
component
shearing time (s)
d
diblock
strain recovered
recovery time (s)
e
reactive
recovery time (s)

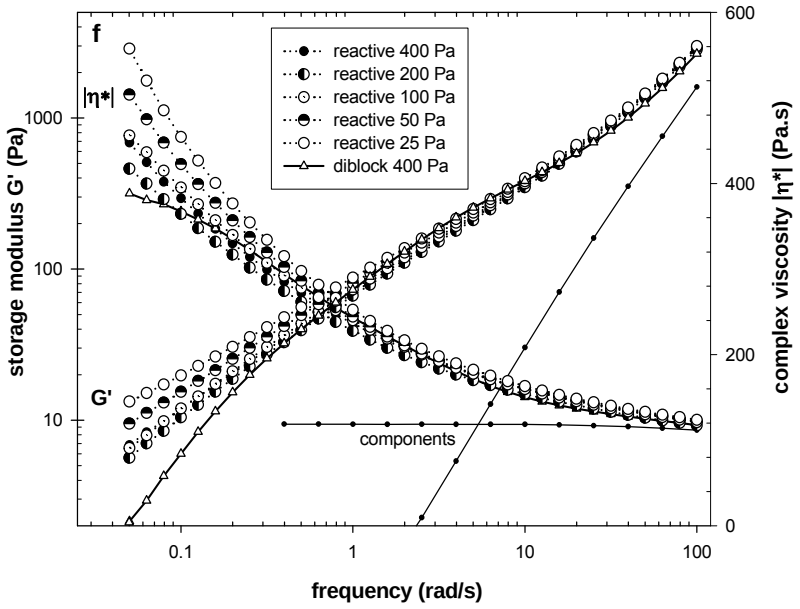


Figure 3.6. (a) Shear history. Note that the samples experienced the shear history of Figure 3.4 a prior to this experiment. (b, d) Data for diblock blend. (c, e) Data for reactive blend. (b,c) startup of creep at the various stresses listed in the legend, (d,e) recovery upon cessation of shear following the various stress listed in the legend. The inset in e shows the same data on a linear y-scale. (f) oscillatory behavior of both blends subsequent to shearing at the stresses listed in the legend. Diblock data are shown only at 400 Pa since data at all lower stresses nearly superpose upon the 400 Pa curves. The data labeled "components" in b, c, and f are volume-weighted averages of the bulk PI and PDMS.

The rheological behavior of the reactive blend in the same experiment shows several differences. Similar to the data of Figure 3.4c, the viscosity $\eta_c^+$ of the reactive blend (Figure 3.6c) during the creep steps shows a peak before reducing again to a steady shear value. The peak magnitude as well as the steady shear viscosity both increase with decreasing stress. The recovery behavior of the reactive blend (Figure 3.6e) is qualitatively similar to that of the diblock blend at high stress levels. However, at the lowest two stress levels, the ultimate recovery increases again. This is more clearly evident in the inset to Figure 3.6e; the linear y-scale highlights the sharp increase in ultimate recovery after the 25 Pa shearing step. Finally, Figure 3.6f shows the evolution of the dynamic moduli after shearing the sample. It is clear that shearing does not destroy the gel-like behavior; indeed, at the lowest two stress levels, shearing significantly enhances the gel-like behavior as evidenced from the larger magnitude of the G' and the larger upturn in $|\eta^*|$ at low frequencies.

Figure 3.7 plots some of the key features of Figure 3.6 quantitatively. The location of the maximum in the $\eta_c^+$ vs time data is seen to scale nearly inversely with the stress (Figure 3.7a). The peak magnitude increases with decreasing stress (Figure 3.7b), but no simple relationship between the peak magnitude and the stress is apparent from the data. We have also examined two related quantities: the interfacial contribution to the peak magnitude (defined as (peak magnitude) – (volume-averaged viscosity of the components)), and the excess viscosity (defined as (peak magnitude) – (steady shear viscosity)). Neither of these quantities show any simple dependence on stress. Figure 3.7c compares the steady shear viscosities of the two blends. The viscosity of the two blends is comparable at high stress, but below 100 Pa, the reactive blend has a sharply higher viscosity, with no sign of leveling off to a zero-shear plateau.

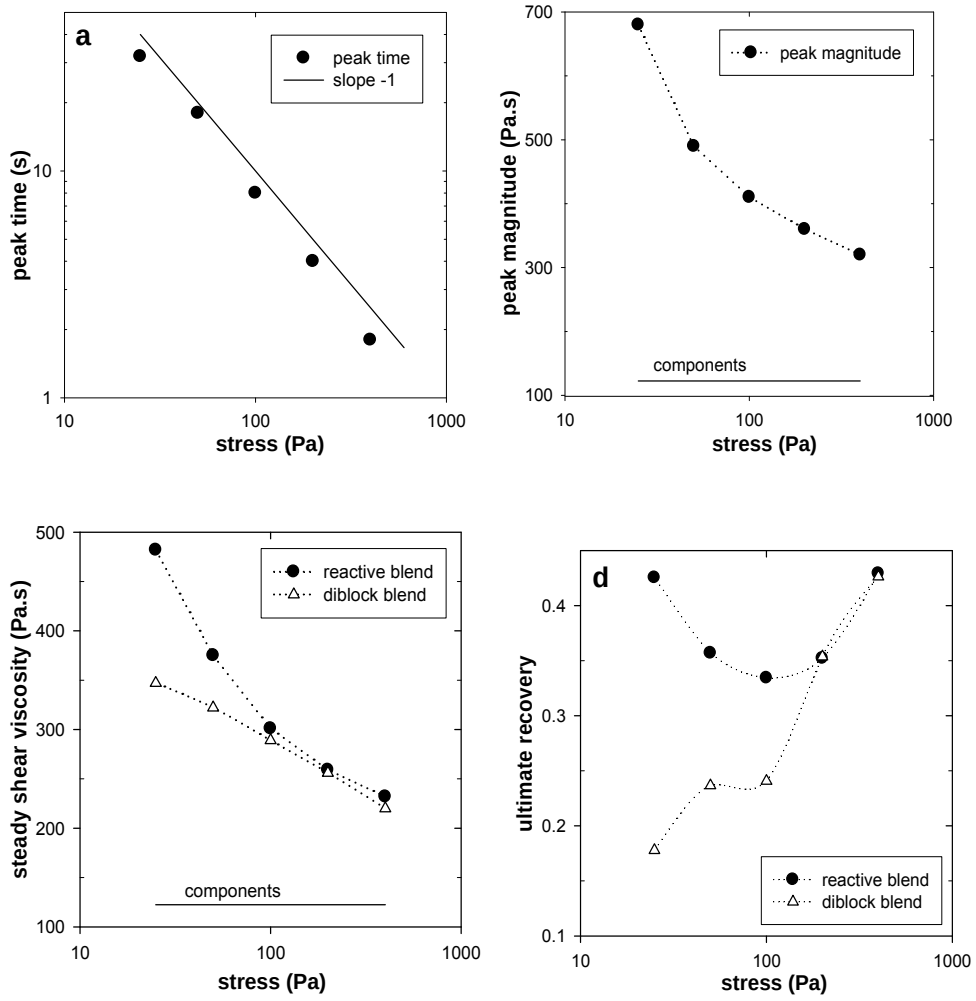


Figure 3.7. (a) Position and (b) magnitude of the viscosity overshoot of the reactive blend shown in Figure 3.6e. (c) Steady shear viscosity recorded at long shearing times in Figure 3.6b and e. (d) Ultimate recovery from Figure 3.6c and f. The line labeled "components" in b and c is a volume-weighted average of the bulk PI and PDMS.

Finally, the ultimate recovery for the two blends is compared in Figure 3.7d. As with the viscosity, the ultimate recovery is very similar for the two blends at high stresses, however, upon decreasing stress, the reactive blend shows a sharp increase in recovery.

## 3.3 SUMMARY AND DISCUSSION

We first review the chief observations about the reactive blend: (1) Optical and confocal microscopy reveal three unusual features about the reactive blend: that some drops are non-spherical, that they are connected together in clusters, and that some drops have interfaces that do not appear smooth. Confocal microscopy also shows fluorescent shells around the drops, confirming that the reaction between *PDMS-NH2 and PIMA has occurred. (2) Rheologically, the reactive blend shows gel-like behavior at low frequencies in dynamic oscillatory experiments. With decreasing stress, the steady shear viscosity and strain recovery after cessation of shear increase sharply. Finally, the creep behavior shows a large peak in the viscosity at short shearing times, especially at low stress. (3) The gel-like behavior in dynamic oscillatory experiments and the peak in viscosity in creep experiments both persist even after shearing the sample for several hundred strain units.

To our knowledge, similar features have been noted previously in only one reactive blend. Sailer and Handge [116] examined the morphology and rheology of blends of polyamide and maleated styrene-acrylonitrile (SAN) with of ~20 maleic anhydride groups per chain. They noted similar drop clusters, and a large increase in elastic recovery of the reactively-compatibilized blends. They have attributed these observations to “elastic interactions between grafted shells”, but the mechanism for the elastic interactions is not clear. We propose that a

crosslinked network was formed that spanned across multiple drops; as mentioned in the Section 2.2, some polyamide chains must have two amine groups, and hence interfacial crosslinking is possible.

Two issues bear further discussion. The first is the structural origin of the gel-like oscillatory behavior (Figure 3.3 and Figure 3.6f) and the peak in the viscosity at short shearing times (Figure 3.4c and Figure 3.6c). The fact that the gel-like behavior and the viscosity overshoot persist and even grow stronger upon shearing suggest that it is a physical network (rather than a network of chemical crosslinks) that is responsible for these rheological features. We hypothesize that the physical network is comprised of large drop clusters, and that under low stress shearing, the clusters can grow to a relatively large size and hence cause enhanced gel-like behavior and larger ultimate recovery. One may also expect clusters to grow under quiescent conditions, and this provides the following possible mechanism to explain the viscosity overshoot upon startup of shear of Figure 3.6c: each creep step is preceded by a half hour strain recovery step and a ~1 hour oscillatory step. If clusters grow under these nearly-quiescent conditions, the subsequent breakdown of these clusters may be responsible for the viscosity overshoots. To test this, we directly examined whether the viscosity overshoot grows with "rest time" after cessation of shearing. The reactive blend was subjected to the shear sequence of Figure 3.8a, where the blend was sheared repeatedly at 100 Pa for 500 strain units, with an increasing rest time between successive shearing steps. Indeed Figure 3.8b and c show that the viscosity overshoot increases steadily with rest time. These data support the idea that the viscosity overshoots are caused by physical changes in the blend structure during quiescent conditions. Whether these physical changes do indeed correspond to droplet clustering as hypothesized above is presently being tested by direct visualization. What is the mechanism for

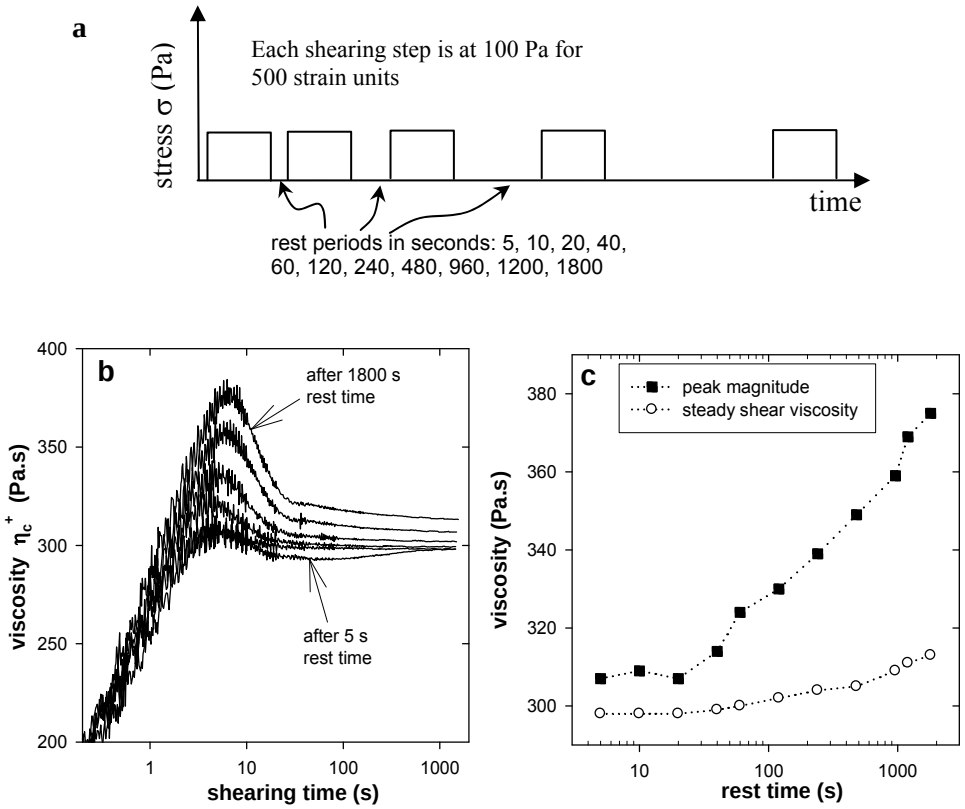


Figure 3.8. (a) Shear protocol for testing effect of rest period on viscosity overshoot. (b) startup of creep at 100 Pa. Rest time increases monotonically from the lowest curve to the highest. Only some selected steps are shown for clarity. (c) Magnitude of viscosity overshoot as a function of rest period. Closed squares are the peak viscosity; open circles are the viscosity at the end of the step (i.e. at 500 strain units). The vertical distance between the two symbols is the viscosity overshoot.

the droplets to form clusters? We speculate that clusters occur because the drops attract each other due to van der Waals forces. These would ordinarily lead to coalescence, however in this case, the crosslinked skin is able to prevent coalescence, and hence the drops stick to each other forming clusters.

The second issue concerns processability. As mentioned in Section 3.2.2, when dealing with crosslinkable materials, a common concern is whether the system remains processable. Figure 3.7 allays this concern: at high stress levels, the viscosity as well as the creep recovery of the reactive blend is similar to that of the diblock blend. It is only at stresses lower than 100 Pa that the reactive blend rheology departs qualitatively from the diblock blend. Thus we tentatively conclude that using multifunctional compatibilizers to crosslink interfaces does not adversely affect the processibility of the blends.

## 3.4 CONCLUSIONS

We have examined the effect of reactive compatibilization using two multifunctional species in model blends of PI and PDMS. The blends consisted of PDMS and PI in a 30:70 ratio, along with a total of 1.5 % of multifunctional reactive PI and PDMS for compatibilization. Optical microscopy shows significant differences between the morphology of the reactive blend and a reference blend compatibilized by a diblock copolymer. The diblock blend shows a "normal" droplet-matrix morphology. In contrast, the reactive blend was characterized by non-spherical drops, drop clustering, and some non-smooth drop surfaces. We believe that the multifunctional reactive compatibilizer forms a crosslinked "skin" on the surface of the drops. Such an interface is a soft solid which cannot be characterized by an interfacial tension. It is the solid-like nature

of the interface that permits non-spherical drop shapes to persist. The crosslinked network spans across several drops causing them to cluster together.

The rheological properties of the diblock blend resemble those of similar systems studied previously, and are consistent with the previous observation that the diblock compatibilizer suppresses coalescence. In contrast, the reactive blend shows many unusual rheological features including a high viscosity and high creep recovery at low stress, overshoots in viscosity in creep experiments, and gel-like oscillatory behavior. Nevertheless, at high stress levels, the rheological properties of the reactive blend are nearly identical to those of the diblock blend, i.e. multifunctional reactive compatibilization, at least at 1.5% of compatibilizer, does not significantly affect the processibility.

Finally we note that a crosslinked interfacial "skin" – and in particular, the fact that the interface behaves as if it does not have interfacial tension – offers new opportunities for controlling the morphology of immiscible polymer blends.

# 4.0 EFFECTS OF COMPATIBILIZER CONCENTRATION AND HOMOPOLYMER WEIGHT FRACTION ON MODEL IMMISCIBLE BLENDS WITH INTERFACIAL CROSSLINKING

The previous chapter reported a comprehensive comparison of compatibilization using diblock copolymers vs. compatibilization by generating a chemical reaction at the interface using multifunctional polymers. In this chapter, using the same model system of PI/PDMS blends, we explore the effects of reactively formed compatibilizer concentration. The differences in PI continuous and PDMS continuous blends were also examined at various reactive compatibilizer loadings. The unusual features noted in the previous chapter, including drop clusters and non-spherical drops in PI continuous blends increased with compatibilizer content, while PDMS continuous blends display a typical droplet-matrix morphology in which droplets do not appear to stick together. Contrary to the gel-like behavior, enhanced viscosity, and strong viscosity overshoots in creep experiments observed in PI continuous blends, the oscillatory experiments showed liquid like behavior for the PDMS continuous blends and enhanced viscosity and viscosity overshoots were lacking. The drop clustering in PI continuous blends and the absence of it in PDMS continuous blends is likely the result of compatibilizer architecture and steric hindrance due to homopolymer chain length and is the likely cause for the asymmetries between the blends.

## 4.1 MATERIALS AND METHODS

Various properties of all materials used are listed in Table 3.I and are the same as used in the previous chapter with one important difference: The functionality of the PDMS-$NH_2$ increased from 2-3 mol % to 6-7 mol % corresponding to an *increase* to 3.9 functional groups per chain. The principal components of the blends are polyisoprene (PI), polydimethylsiloxane (PDMS), polyisoprene-graft-maleic anhydride (PIMA) and poly(aminopropylmethylsiloxane-co-dimethylsiloxane) (PDMS-$NH_2$). PDMS-$NH_2$ is fluorescently tagged using NBD-Chloride as described in Section 3.1 and is dubbed *PDMS-$NH_2$.

The effects of compatibilizer concentration were investigated using blends which contained varying amounts of reactive species in blends which were either PDMS continuous or PI continuous. The dispersed phase was always 30% by weight. Blends containing total compatibilizer loadings of 0.1, 0.4, 0.6, 0.75, 1.5 and 3.0 wt% were prepared for PI continuous blends and 0.1, 0.6 and 3.0 wt% for PDMS continuous blends. Moreover, assuming that the concentration of reactive groups quoted by the manufacturers is correct, and because one quarter of the amine groups are fluorescently tagged, the number of amine groups of PDMS-$NH_2$ are approximately three times the number of available anhydride groups of the PIMA. The reactivity was calculated using a stoichiometric balance and ensures sufficient functionality for crosslinking. Samples will be designated by $Sx$-$w_{comp}$ where x is the weight fraction of PDMS on a compatibilizer-free basis, and $w_{comp}$ is the overall weight % of compatibilizer. For example, a 1 gram sample of S30-3.0 contains 0.2955 g PDMS, 0.66895 g PI, and 0.015 g each of PIMA

Table 4.I. Model blend component properties.

| material | MW (g/mol) | $\eta_{25°C}$ (Pa.s) | composition | supplier |
|---|---|---|---|---|
| PI LIR30 | 29000[b] | 131 | 100% PI | Kuraray |
| PIMA | 25000[b] | 1700 | 1.5% MA[b] | Aldrich |
| PDMS | 135,600[a] | 96 | 100% PDMS | Rhodia |
| PDMS* | 5000[b] | 0.1 | 6-7% $NH_2$[b] | Gelest |
| PI-*b*-PDMS | PI: 26000: PDMS: 27000 | | 48% PI | |

[a] Weight-average molecular weight estimated from known viscosity-MW relationship
[b] Value quoted by supplier

and *PDMS-$NH_2$. All blends were mixed by hand using a spatula and degassed prior to experiments and all experimental methods are the same as those in Chapter 3.0.

## 4.2 RESULTS AND DISCUSSION

### 4.2.1 Effect of compatibilizer concentration on morphology

This chapter, as well as Chapter 3.0, relies on an interfacial chemical reaction between PIMA and *PDMS-$NH_2$. Labeling one of the reactive species (in the present case PDMS-$NH_2$) with a fluorescent moiety offers an opportunity to verify the reaction visually (Figure 4.1). In the absence of PIMA (and therefore no possibility of interfacial coupling) the dispersed reactive PDMS forms droplets in the PI matrix (Figure 4.1a) confirming that no chemical reaction takes place. The drops appear as bright fluorescent green spheres, as the *PDMS-$NH_2$ is evenly mixed

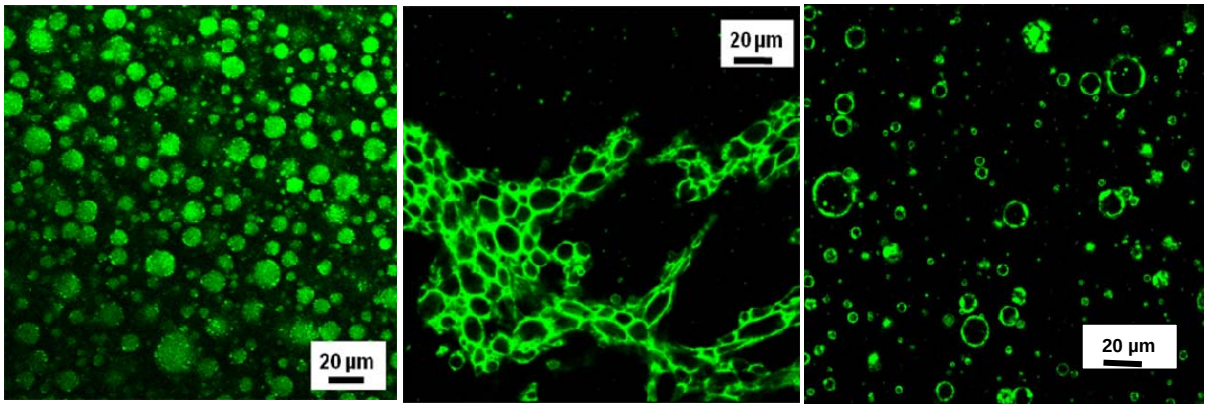


Figure 4.1. The fluorescent images of (a) uncompatibilized S30-0 and (b) S30-1.5 and (c) S70-3.0 clearly show the reactive fluorescent species has moved to the interface.

within the non-reactive PDMS causing the fluorescence to be distributed throughout the drop. Upon the addition of small amounts of compatibilizer to S30 (Figure 4.1b), the drop size begins to decrease and drops begin to cluster or stick together. The fluorescence is now localized at the interface and the drops are observed as bright green shells, suggesting that the amine/maleic anhydride chemical reaction has taken place. Moreover the droplet shape becomes increasingly non-spherical with increasing compatibilizer concentration. This observed interfacial "skin", which is formed by the interfacial chemical reaction, forms a network of PDMS drops. Similarly, in the PDMS continuous blend, S70-3.0 (Figure 4.1c), the enhanced fluorescence at the interface as compared to the bulk confirms that the chemical reaction has indeed occurred. However, there is significant difference in the PI and PDMS continuous samples—the droplets do not appear to stick together or form a network structure in the PDMS continuous sample (Figure 4.1c). This will be discussed in greater detail later in this chapter.

Varying reactive compatibilizer concentrations, ranging from 0.1% to 3% of the total weight, were added to S30 blends. All blends of this composition were found to have PI as the

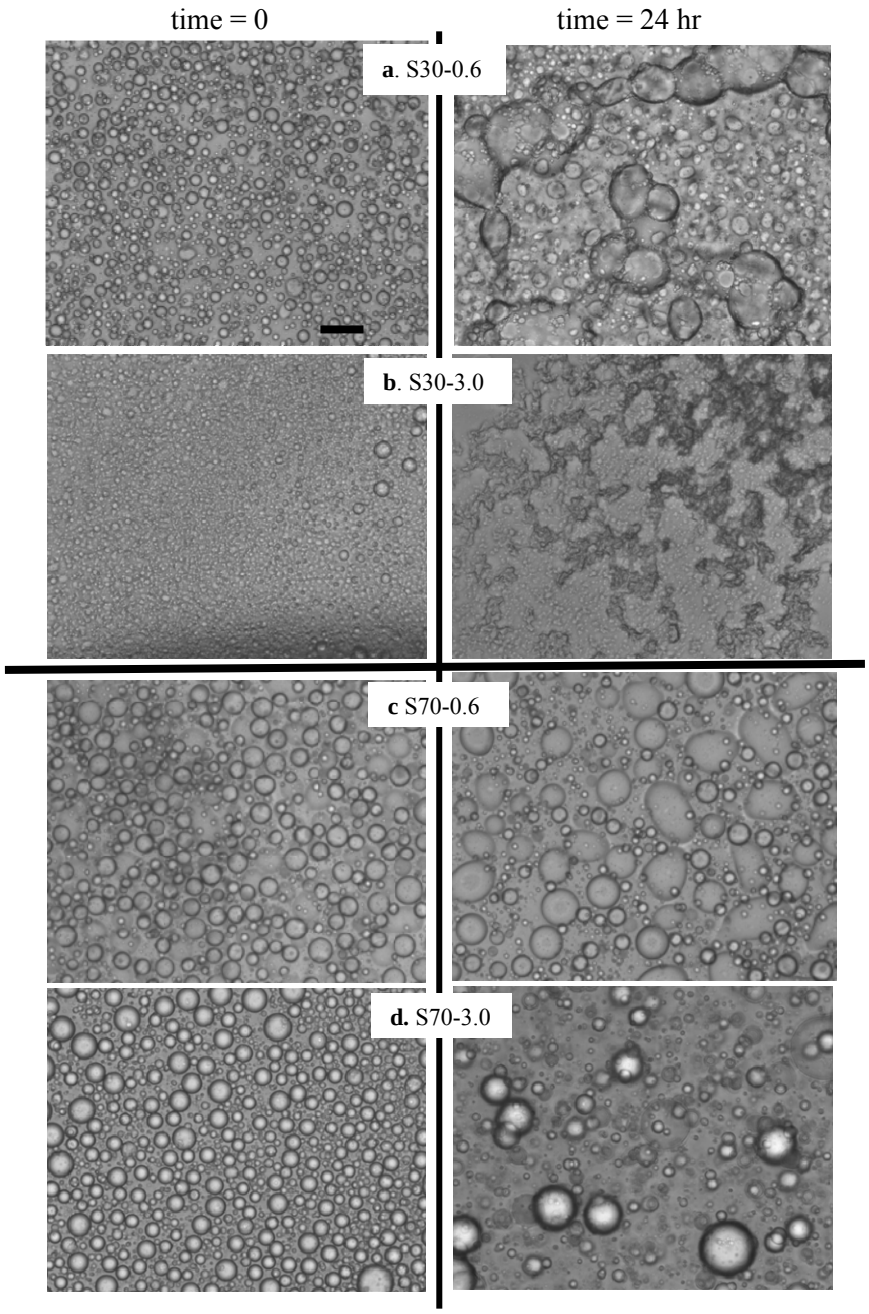


Figure 4.2. Visualization of microstructure immediately after mixing (t=0) and after 24 hours at quiescent conditions. Droplet clusters increase with increasing reactive compatibilizer as shown by bright field microscopy by (a) S30-0.6 and (b) S30-3.0. The morphologies of (c) S70-0.6 and (d) S70-3.0 are not significantly affected by compatibilizer concentration. The scale bar shown in (a) represents 20 μm and applies to all images.

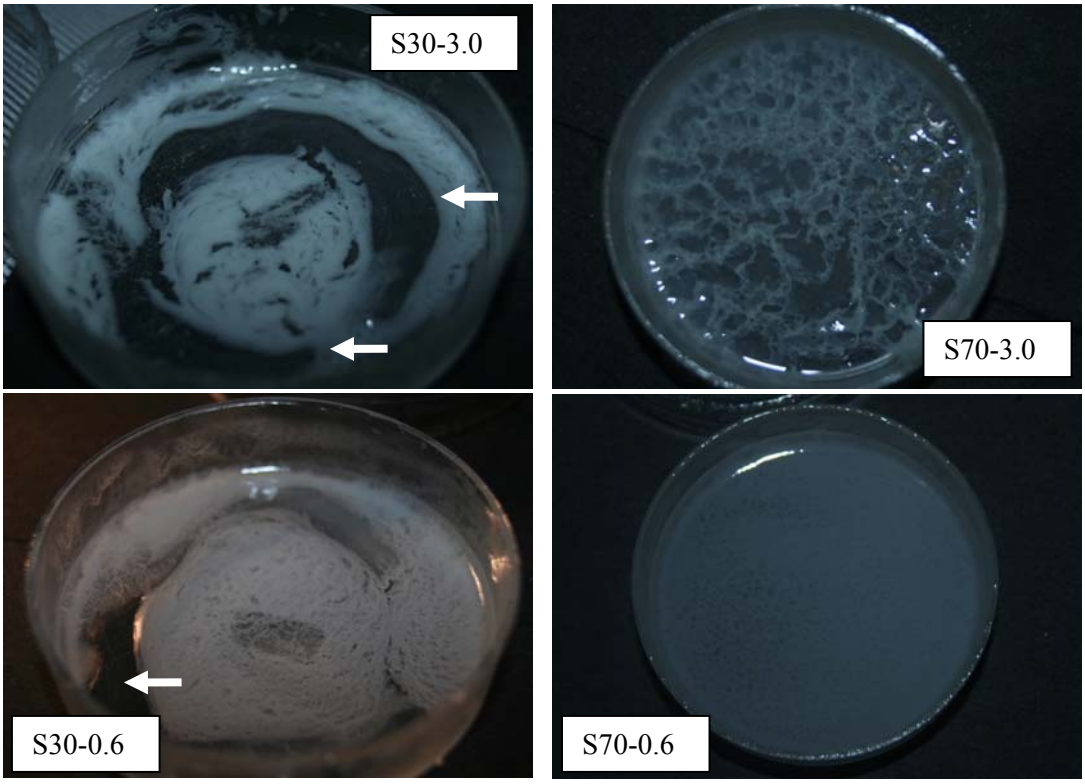


Figure 4.3. Macroscopic images of S30 and S70 blends after several months of quiescent conditions.

continuous phase. Microscopic images are presented for S30-0.6, S30-3.0 (Figure 4.2a,b). The morphologies of the blends were examined using a bright field microscope promptly after blending. The freshly blended samples were then allowed to sit under quiescent conditions for 24 hours and bright field microscopy was repeated. Immediately after blending S30-0.6 and S30-3.0, small PDMS drops were observed. Over 24 hours under quiescent conditions, the samples changed morphology significantly. At 0.6% compatibilizer loading, there appears to be significant increase in drop size due to coalescence, and the larger drops, many of which are non-spherical, appear to be fused together. In contrast, at 3.0% compatibilizer loading, there appears to be no significant change in the primary drop size, however, there is extensive aggregation of the drops. These effects are attributable [117] to the interfacial chemical reaction which forms a

interfacial “skin” covering the drops. This skin permits non spherical drop shapes, as well as drop clustering without coalescence.

The microstructures of S70-0.6 and S70-3.0 are presented in Figure 4.2c,d. Upon mixing and after 24 hours of quiescent conditions, a typical droplet-matrix morphology is evident, although the drop size appears larger than in the corresponding S30 samples. Upon standing under quiescent conditions for 24 hours, there are notable differences between the S30 samples: all drops appear spherical, and clustering is not evident. (The non-spherical shapes in Figure 4.2c are not drops suspended in the bulk, instead they are drops that settled onto the glass slide and spread). Several drops appear to grow in size but other drops do not coalesce, suggesting that coalescence is slow, occurring over a time scale of days.

If these samples are allowed to sit under quiescent conditions for longer periods, the difference between the PDMS-continuous samples (e.g. S70-3.0) and the PI-continuous samples (e.g. S30-3.0) becomes evident even to the naked eye. The samples shown in Figure 4.3 have been under quiescent conditions for several months. The S70-3 sample has undergone large-scale phase separation (the clear regions resulted from numerous coalescence events). The S70-0.6 has phase-separated to a smaller extent, but mm-scale coalesced regions are evident. The remaining regions, which are bright white, have a much smaller-scale two-phase structure. In contrast, the S30 samples undergo much less phase separation with most of the regions of the petridish appearing bright white (indicating a phase separation on lengthscale smaller than ~50 microns). Even more importantly, there are regions of the Petri dish (indicated by the white arrows) that are not covered by the sample indicating that these samples have a yield stress that prevents the sample from uniformly flowing over the bottom of the petridish. A similar

observation was made in Chapter 3.0. In contrast, the S70 samples do not show such a bare region, but instead cover the bottom uniformly.

In summary, visualization results confirm that the interfacial reaction is occurring in both the S30 as well as the S70 blends as evidenced by the bright interfacial regions in the confocal images. They also show that the effects of the reactively-generated compatibilizer are highly asymmetric, both structurally (S70 blends show large round drops that can coalesce, S30 blends show drops that stick and can take on non-spherical shapes) as well as rheologically (S30 blends show a yield stress, whereas S70 blends do not). This asymmetry will also be apparent in the rheological experiments of the next section.

### 4.2.2 Dynamic oscillatory properties

#### 4.2.2.1 Gel-like behavior at high compatibilizer loading

Strain-sweep measurements were conducted at four different frequencies (100, 10, 1 and 0.1 rad/s) for strains ranging from 0.1% to 10%. All blends showed linear viscoelastic behavior under these conditions. All subsequent oscillatory measurements were conducted at 1% strain. The complete shear history of the rheological experiment is detailed in Figure 4.4.

Figure 4.5 shows the oscillatory frequency sweeps of the as-prepared samples, i.e. the samples were tested immediately after degassing with no pre-shearing other than that experienced during sample loading. For clarity, only the S30-0.1, S30-0.6 and S30-3.0 blends are shown. The oscillatory behavior for the remaining blends closely resembled that of the three blends shown, in particular, S30-0 and S30-0.4 were similar S30-0.1; S30-0.75 was similar S30-0.6; and S30-1.5 was similar S30-3.0. The behavior at low compatibilizer levels (0.4% and

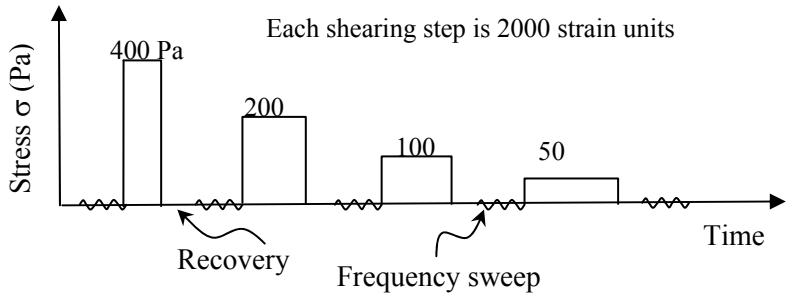


Figure 4.4. Shear history of the rheology experiment.

lower) is consistent with previously-reported behavior in similar systems. In particular, the G' and the $|\eta^*|$ show a pronounced shoulder at lower frequencies that has been attributed to interfacial relaxation processes such as relaxation of the drop shape. Furthermore, at the lowest accessible frequencies, the G' scales with nearly the square of the frequency, and $|\eta^*|$ nearly levels off, both of which are indicative of liquid-like behavior.

With increasing compatibilizer loading, the following changes occur: the shoulder in G' becomes less prominent, the slope of the log(G') vs. log(frequency) increasingly deviates from a slope of two at low frequencies, and the $|\eta^*|$ shows a trend of increasing with decreasing frequency. Such 'gel-like' behavior was already noted in the previous chapter using similar materials, and is attributed to the aggregation (without coalescence) of drops as evident in Figure 4.1b. Here it is apparent that the gel-like behavior is not obvious at or below 0.4 wt% loading, but is highly pronounced at compatibilizer loadings exceeding 1.5 wt%.

The as-loaded oscillatory properties for the S70-3.0 compatibilizer are presented in Figure 4.6, along with the S70-0.6 and S70-0.1. At low compatibilizer loading the results resemble those of Figure 4.5: the interfacial relaxation process is clearly evident, and the terminal region indicates liquid-like behavior. However, at higher compatibilizer loadings, it is

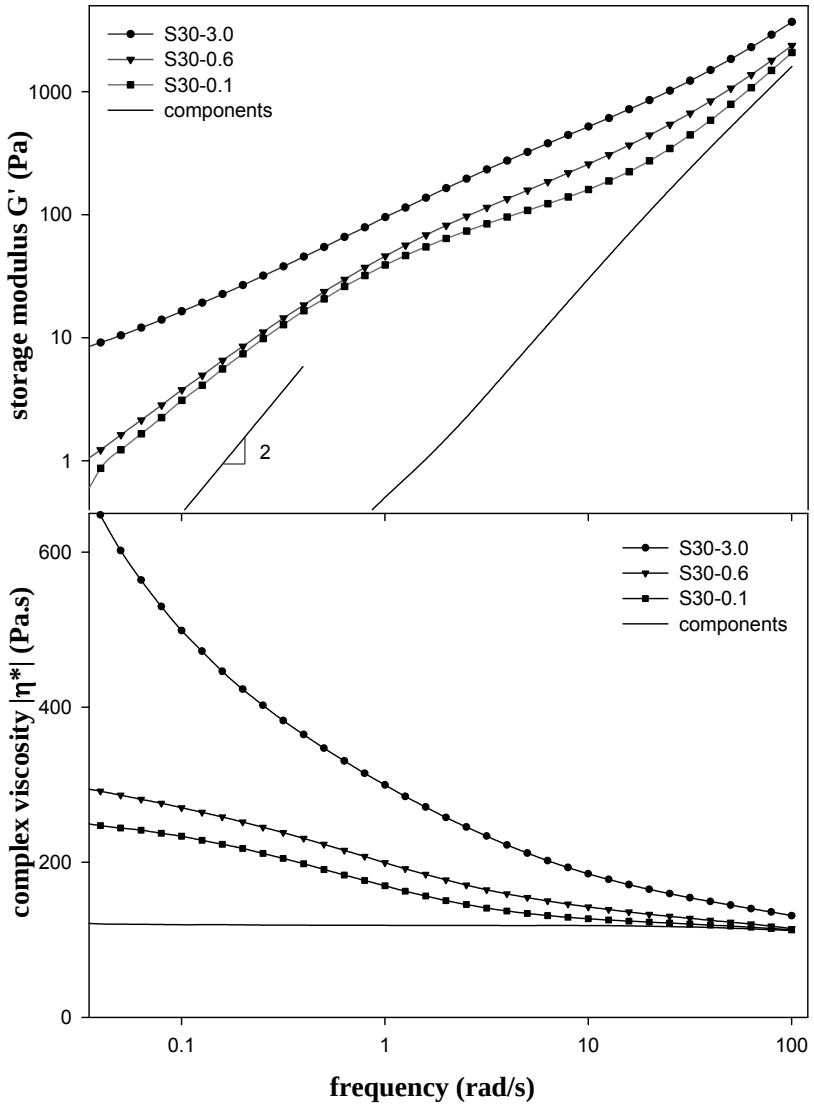


Figure 4.5. As-loaded oscillatory for varying compatibilizer concentrations in PI continuous blends.

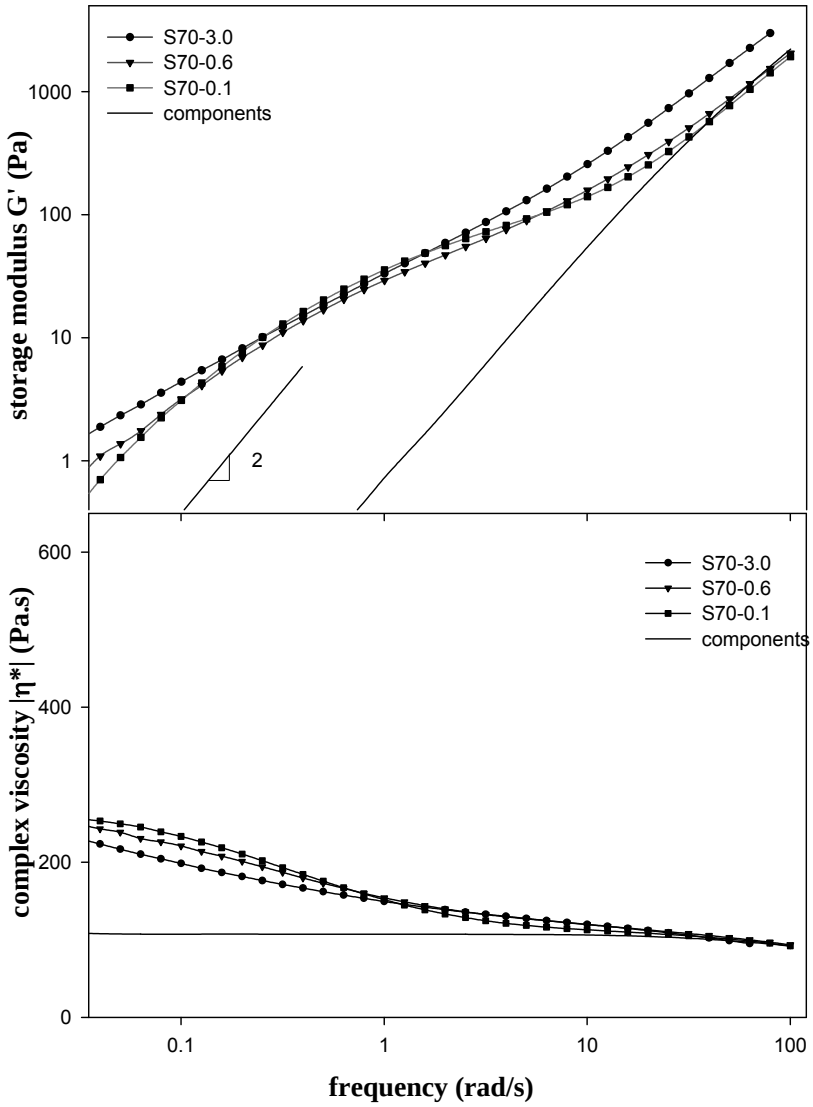


Figure 4.6. As-loaded oscillatory for varying compatibilizer concentrations in PDMS continuous blends.

immediately clear that the gel-like behavior is less prominent in the S70-3.0, compared to S30-3.0. The oscillatory behavior of S70-3.0 appears more liquid like and has a much smaller complex viscosity than the S30-3.0. In effect, at the same compatibilizer loading (3%), the rheological properties are qualitatively different depending on which phase is continuous. Such asymmetries are peculiar but not unique [12] and will be discussed further in Section 4.2.3.

#### 4.2.2.2 Gel-like behavior at low compatibilizer loading

Our previous article compared a reactive compatibilizer with a diblock compatibilizer at a single – and fairly high – compatibilizer loading. It is useful to make same comparison at low compatibilizer loadings, because diblock compatibilizers are known to show qualitatively different behavior when the diblock loading is very low. Specifically, as the amount of diblock compatibilizer decreases to below roughly 0.5-1%, the single relaxation process discussed in the previous paragraph splits into two: a higher frequency relaxation attributable to the deformation and relaxation of drops ("shape relaxation"), and a new slower relaxation that has been attributed to interfacial viscoelasticity, most importantly to dilational elasticity of the interface (see end of this section). The slow relaxation has been found to be nearly independent of drop size. With decreasing compatibilizer content, the slow relaxation moves to even lower frequencies until it is no longer observable in the accessible frequency range. With increasing compatibilizer content, the slow relaxation moves to higher frequencies until it merges with the shape relaxation and is no longer separately visible. Further details of this slow relaxation have been discussed in several articles [10, 114, 118]. To summarize, blends compatibilized with low loadings of diblock copolymer can show two distinct relaxations, and it is of interest to examine whether the reactively-compatibilized blend shows two relaxations as well at low compatibilizer loading.

Accordingly, we examined the blends with 0.1% compatibilizer in greater detail: the experiments with S30-0.1 and S70-0.1 were repeated, with the frequency sweep accessing lower frequencies. Figure 4.7 compares these data against corresponding blends compatibilized with 0.1% diblock copolymer. This same diblock was used as the basis of comparison in Chapter 3.0 [117] and also by Van Hemelrijck et al.[104]. The diblock-containing blend was prepared in the same manner as the reactively compatibilized blends. It is clear from this figure that while the diblock-containing blends clearly show two shoulders in the relaxation spectrum, the reactively-compatibilized blends do not.

This observation can be explained readily. Diblock compatibilizers lower the interfacial tension between immiscible homopolymers, and any dilation of the interface will raise the interfacial tension above the equilibrium value – an effect called dilational elasticity. If the interface is deformed non-uniformly (as is the case when drops are subjected to oscillatory shear), interfacial tension gradients result. It is the relaxation of interfacial tension gradients (via the spreading pressure of the diblock) that causes the slow relaxation. A crosslinked interface on the other hand is solid-like and lacks mobility; concepts such as interfacial tension and spreading pressure do not readily apply to such solid-like interfaces. Thus, such an interface lacks dilational elasticity and a slow relaxation is not observed.

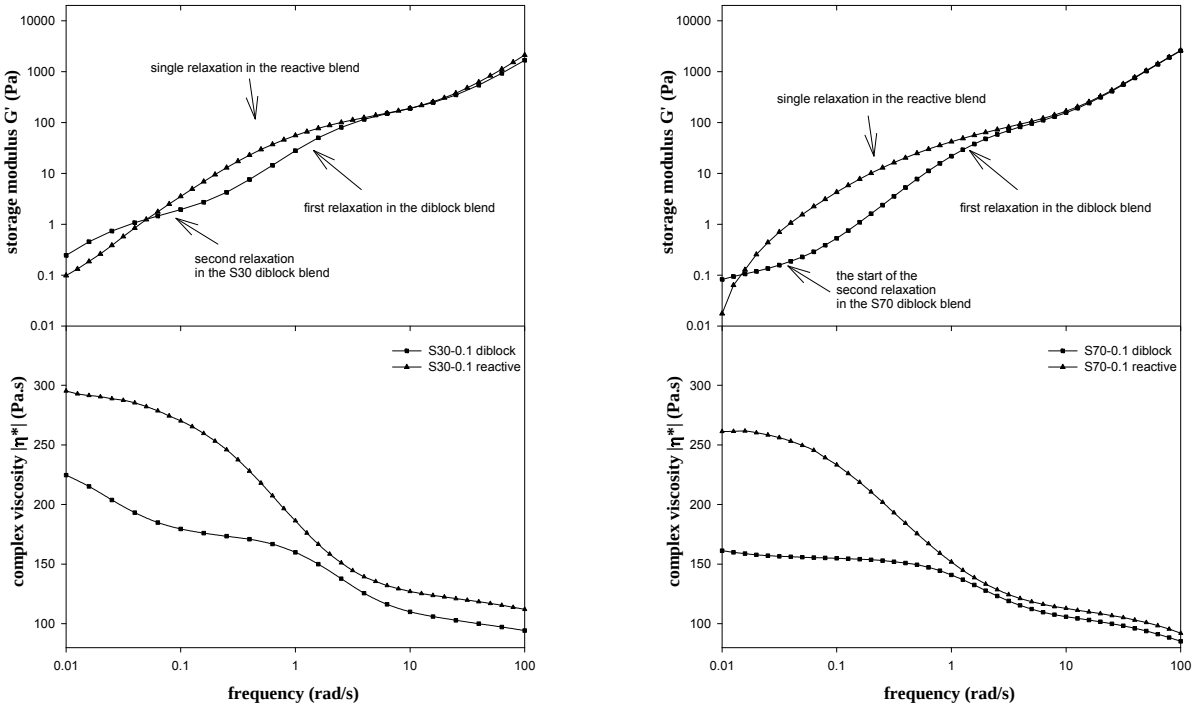


Figure 4.7. Diblock (squares) vs. reactive blending (triangles); no second shoulder is apparent in G' or $|\eta^*|$ the reactive blends of S30 and S70.

### 4.2.3 Steady shear characteristics

#### 4.2.3.1 Effect of lowering stress: Coalescence suppression

Directly after the initial oscillatory measurements, the samples were subjected to the shear history of Figure 4.4. The samples were sheared at 400 Pa for 2000 strain units, then the subsequent recovery upon cessation of shear was monitored, followed by an oscillatory frequency sweep at 1% strain. This sequence (shear for 2000 strain units, recovery, and oscillatory) was repeated at successively lower stresses of 200, 100, and 50 Pa.

One important role of compatibilizer in droplet-matrix blends is coalescence suppression [14]. If coalescence is effectively suppressed, a finer morphology can result because the small

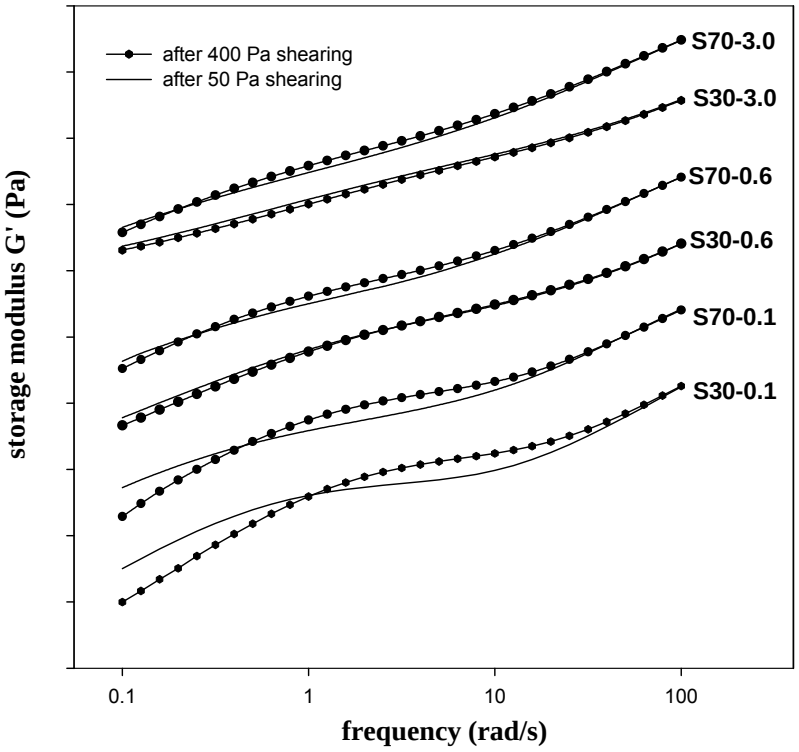


Figure 4.8. Dynamic oscillatory properties after the 400 Pa shearing (symbols) and the 50 Pa shearing (no symbols). Data sets are scaled by a factor of ten with respect to the previous data set.

drops created during the most intense portion of the blending procedure do not recoalesce in the less intense portions. The mechanism of coalescence suppression from the addition of a compatibilizer is not completely understood, however, two explanations are generally accepted to explain it [6, 7]. First, coalescence suppression is a result of steric hindrance when two compatibilized drops approach each other. In this case, a higher molecular weight block will more efficiently suppress coalescence. Secondly, Marangoni stresses attempt to distribute the compatibilizer uniformly at the interface. As a result, when two drops approach each other, their

interfaces become immobilized, greatly inhibiting the fluid in the gap from draining out and hence preventing coalescence [8, 9].

As stated in the previous section, the additional relaxation process evident in the dynamic oscillatory data is attributable to interfacial processes. In compatibilizer free blends, the only interfacial process is shape-relaxation of the drops, and the timescale of this process (i.e. the reciprocal of the frequency of the shoulder in G') scales with the drop size. Accordingly, the changes in drop size can be followed quantitatively by changes in the shoulder of G'. The situation is more complex for compatibilized blends, and other interfacial processes can also play a role, nevertheless, the changes in the dynamic oscillatory properties are still qualitatively related to changes in drop size.

Figure 4.8 presents the oscillatory data recorded after shearing at 400 Pa and at 50 Pa for S30 and S70 samples containing various amounts of reactive compatibilizer. The data for the two intermediate shearing steps (200 Pa and 100 Pa) fall between these lines in all cases. At 0.1% compatibilizer loading (as well as in the uncompatibilized sample, not shown), the interfacial relaxation process shifted to lower frequencies upon shearing the sample at lower stress. The clearest indication of the shift is that the G' at the two stresses now cross each other; in effect upon shearing at low stress, G' increases at the lowest frequency, but decreases at intermediate frequencies. This slowing down of the interfacial relaxation is clearly evident in both the S30-0.and S70-0.1 samples, and indicates a growth in drop size due to coalescence. At 0.6% and 3% compatibilizer loadings however, the behavior of the S30 and the S70 samples diverges. In the S70 samples, a small slowing down of the interfacial relaxation process is still evident, although it is not nearly as prominent as at 0.1% compatibilizer loading. In contrast, in the S30 samples, the slowing down is not evident (a crossover is not evident in the accessible

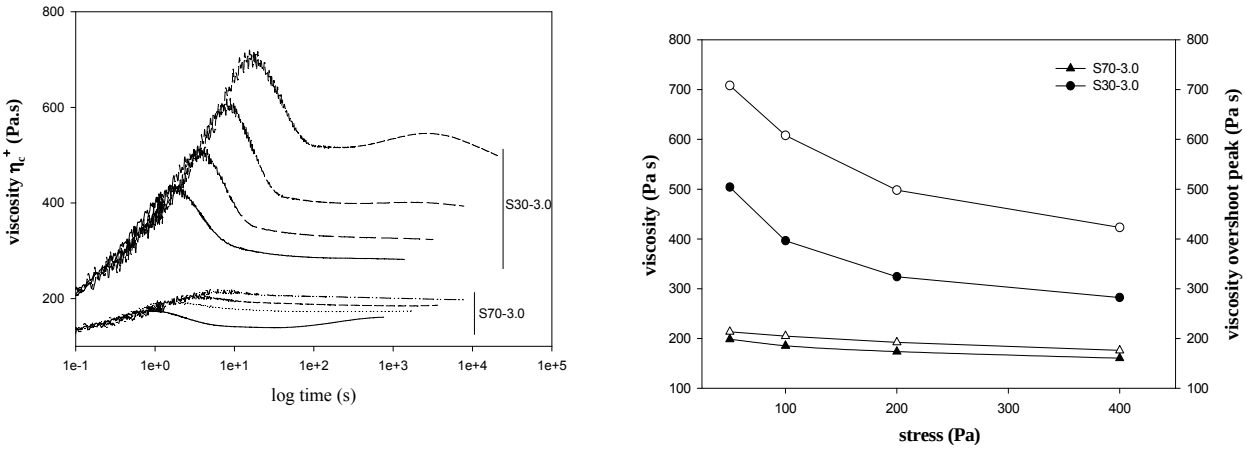


Figure 4.9. (a) Steady shear viscosity after successive stepdowns in stress of S30-3.0 and S70-3.0. Both blends show shear thinning behavior and viscosity overshoots during the start-up of shearing. (b) Steady shear viscosity (closed symbols) and viscosity overshoot peak magnitude as a function of stress (open symbols) of S30-3.0 and S70-3.0.

frequency range). In summary, the oscillatory data after cessation of flow suggest that flow-induced coalescence is nearly suppressed in the S30 blends at compatibilizer levels exceeding 0.6%. In contrast, flow-induced coalescence is still possible in the S70 blends. This asymmetry of flow-induced coalescence appears to mirror the observation of quiescent coalescence from optical microscopy Section 4.2.1.

#### 4.2.3.2 Creep behavior and steady shear viscosity

With addition of any compatibilizer, all the steady shear viscosities of polymer blends are expected to increase as a result of the viscoelasticity of the interface [14]. In Figure 4.5, the marked increase in the complex viscosity, especially at low frequency, suggests that there exists some compatibilization limit beyond which the material would become unprocessable. To

examine the processibility of the blends, we examine the creep behavior of blends at various stress levels (Figure 4.9).

Figure 4.9a shows the creep behavior of S30-3.0 and S70-3.0 at various stress levels. It is immediately apparent that the S30-3.0 blends show a large overshoot in the viscosity at short times whereas S70-3.0 shows a weak peak or no peak. In the previous chapter, a similar viscosity overshoot was seen for a similar S30 blend, and we showed that the overshoot is attributable to the aggregation of drops into clusters (as seen in Figure 4.1). Earlier in this chapter, we showed that drops of the S70 blends do not aggregate (they can only coalesce). Thus the lack of a viscosity overshoot is consistent with the lack of aggregation.

Figure 4.9b plots the steady shear viscosity reached at long times at the various stress levels. The fact that S30 and S70 blends retain a modest viscosity under steady shear indicates that they remain processible, i.e. as a practical matter, as long as crosslinking is restricted to the interface, processibility is retained.

Finally, we have also conducted limited experiments on S50-3.0 (data not shown) which has a far higher steady shear viscosity (as well as a far higher G' and $|\eta^*|$ at low frequency). The morphology of S50-3.0 was not a simple droplet-matrix morphology and displayed very large droplet clusters. In summary, the compatibilizer effects on the rheological properties depend severely on the morphology: in blends with compositions closer to 50/50 and with extensive drop aggregation, processibility may be compromised.

## 4.3 SUMMARY AND DISCUSSION

We first summarize the chief observations. Previously, we had examined blends with a crosslinked reactive compatibilizer at a single compatibilizer loading (1.5%), and at a single composition (30% PDMS in 70% PI). The focus of that chapter was comparing the crosslinked compatibilizer against a diblock. In this chapter, we examined blends of two different compositions (30% PDMS in 70% PI and 30% PI in 70% PDMS) and varied the compatibilizer loading.

The results of varying the compatibilizer loading are broadly as expected: at low compatibilizer loadings the behavior of the blend approaches that of the uncompatibilized blend. Even at the lowest compatibilizer loading, the linear viscoelastic properties showed a single interfacial relaxation (as compared to two relaxations for a diblock-containing blend). This indicates that the crosslinked compatibilizer, which forms a soft solid-like interface, cannot be described by a spreading pressure.

The results of varying the composition however were unexpected in that at least three asymmetries were noted: 1) In S30 blends, the PDMS drops can stick to each other. If the drops do coalesce, they can form non-spherical drops. In contrast, in S70 blends, the PI drops do not stick: they can coalesce, and the coalesced drops are spherical. 2) In regards to the dynamic oscillatory data, liquid like behavior is observed in the S70 blends, while gel-like behavior, manifested by an increase in G' at low frequencies, was observed in the S30 blends. 3) The steady shear viscosity of the S70 blend, as well as the magnitude of the viscosity overshoots, was significantly lower than the PI continuous blend.

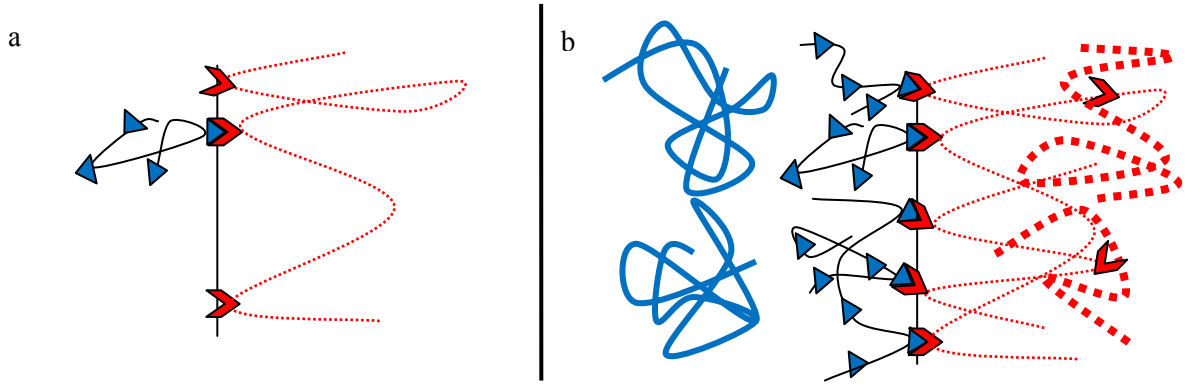


Figure 4.10. Interfacial crosslinked compatibilizer representing (a) a single reaction between on PDMS and one PI polymer chaing and (b) the PDMS (solid lines) PI (dotted lines) system in which PI can interpenetrate PIMA and PDMS cannot interpenetrate PDMS-$NH_2$ creating a wet brush – dry brush interface. The non-reactive homopolymers are shown by the bold lines.

What explains this asymmetric behavior? On a macroscopic level, the viscosity mismatch between the PI (130 Pa·s) and the PDMS (96 Pa·s) creates some asymmetry, yet, it appears to be too small to explain the above differences. On a molecular level however, the architecture of the interfacially-formed compatibilizer is not symmetric. The architecture of the compatibilizer is determined mainly by the structure of the reactive chains, and by the mixing process. Table 4.II lists some of the important molecular parameters on each side of the interface. Based on these numbers, and assuming that the all the monomers react; we may schematically draw the structure of the interface illustrated in Figure 4.10. From Figure 4.10, we can see that each reactive species may form loops between two reacted functional groups (we ignore the tails because they do not change the arguments below). The key features of this structure are: (1) the PI-side of the interface has much longer loops than the PDMS-side suggesting a thicker steric layer bound to the interface on the PI side, (2) on the PI side, the homopolymers MW is about 4 times that of the loop molecular weight, whereas on the PDMS

side, the homopolymer MW is over 100 times that of the loop MW, i.e. while both sides may be regarded as dry brushes, the PDMS side is especially so.

Such asymmetry may be expected to affect coalescence behavior. Specifically, in cases when a block copolymer suppresses coalescence, the key mechanism is believed to be steric hindrance of the block. It has been observed that the effectiveness in suppressing coalescence increases with the length of the block, presumably because a longer and more swollen block can suppress coalescence more effectively. The numbers in Table 4.II suggest that coalescence should be suppressed more effectively in the S30 blends (PDMS drops in PI) than in S70 blends (PI drops in PDMS). This is indeed observed experimentally, i.e. the asymmetry in coalescence suppression may be explained based on the asymmetry in the loop length.

Explaining the asymmetry in sticking behavior is more challenging. At first glance, sticking appears to result from two phenomena: (1) Drops attract each other under quiescent conditions (due to Van der Waals forces), but (2) cannot coalesce because they are covered with a crosslinked skin. Therefore they stick to each other. This is similar to aggregation of solid particles dispersed in a polymer matrix, except that the drops can deform, and hence can stick more strongly. This is also analogous to the strong adhesion between low-modulus solids as explained by the JKR theory. This explanation can readily clarify the sticking of PDMS drops in the S30-3.0 blend. It can even explain the coalescence behavior of the S30-0.6 blend: in that case we speculate that the crosslinked skin is not sufficiently robust and it ruptures permitting coalescence. However – unlike a diblock – a crosslinked compatibilizer cannot desorb from the interface, accordingly the resulting drops are non-spherical perhaps with a wrinkled skin (Figure 4.1). However this explanation cannot explain why PI drops in PDMS *do not* stick to each other.

Table 4.II. Physical characteristics of blend components.

| | PI side | PDMS side |
|---|---|---|
| Homopolymer MW $M_H$ (g/mol) | 29000[b] | 135,600[a] |
| Reactive species MW (g/mol) | 25000[b] | 5000[b] |
| reactive content of the reactive species on weight basis (mmol/g) | 0.22 | 0.88 |
| Reactive groups per reactive chain | 5.5 | 4.4 |
| Number of groups per chain that are expected to react[d] | 5.5 | 1.1 |
| MW of block (loop or tail) between reacted groups $M_B$ (g/mol) [c] | 4390 | 2500 |
| Number of monomers in each block (loop or tail)[c] | 50 | 30 |
| Ratio $M_H/M_B$ | 6.6 | 54 |

[a] Weight-average molecular weight estimated from known viscosity-MW relationship
[b] Value quoted by supplier
[c] Mean number based on stoichiometric calculations
[d] The two reactive species present in an equal weight ratio. However, the PDMS-$NH_2$ has 4 times as many reactive groups per gram than PIMA. Therefore all MA groups are expected to react, whereas an average of 25% of NH2 groups are expected to react.

Specifically, if the S70 blend has a nearly identical crosslinked interface on the drops, why does it rupture so readily? After rupturing, why do the coalesced drops to regain spherical shape? We are unable to address these questions.

An alternate possibility is that that the architecture of the compatibilizer is not the same in the S70 and the S30 blends, and more specifically, the S30 blends have a more solid-like interface than the S70 blends. Once again, the reasons why this may be so are not clear.

Asymmetries in the rheological properties of polymer blends containing a diblock copolymer have previously been reported [12, 104]. In both previous studies, the asymmetries were directly attributable to the suppression of coalescence when one polymeric component was continuous and the lack of coalescence suppression when that same component was the

dispersed phase. Therefore, the rheological properties which depend on drop size where affected and the theories proposed to explain these differences were based on the mechanisms which control coalescence suppression, namely steric hindrance of the copolymer. In the present case, we have observed coalescence suppression in both PI continuous and PDMS continuous systems, as detailed in Section 4.2.3 and cannot attribute any asymmetrical behavior to changes in drop size. Despite this, differences in the morphology of the PI continuous and the PDMS continuous blends – the sticking of droplets in the PI continuous blends - may still provide a basis for the asymmetric behavior.

The mechanism for the sticking of PDMS drops or the reasoning for PI drops not sticking may provide an explanation for all of the noted differences, since the sticking of the PDMS droplets may be responsible for the resulting rheological differences. Several mechanisms, or combinations of mechanisms, may be responsible for the droplets sticking (or not sticking) together, such as steric hindrance, hydrodynamic interactions or chemical reactions. We were unable to readily test the drop sticking mechanism and therefore have no conclusive explanation for it. However, to propose a possible explanation the asymmetric effects of the polymer blends, we begin with a discussion about architecture of the compatibilizer when it forms at the interface.

The two reactive species are multifunctional and react to create an interfacial crosslinked copolymer. The architecture of the compatibilizer formed at the interface is determined mainly by the structure of the reactive chains. From Figure 4.10a, we can see that each reactive species forms loops between two reacted functional groups. These loops and the ends of the reactive polymer chains (or sections of the polymer chain with unreacted functional groups) create the structure of our compatibilizer on both sides of the interphase. PDMS-$NH_2$ has a molecular

weight of approximately 5 kg/mol with about 4 reactive groups per chain, with an average of 15 monomer units between functional groups. PIMA, on the other hand, has a molecular weight of about 25 kg/mol and 4-5 reactive groups per chain. By comparison, the PDMS-$NH_2$ has short polymer chains with frequent functional groups, while PIMA has longer chains with less frequent reactive groups. From this we can assume that, given an interfacial chemical reaction, the length of the 'loops', i.e. the chain distance between functional groups, of PIMA are about four times the length of the PDMS-$NH_2$ loops. This observation may lend support to the argument that the longer PIMA loops attached to one droplet may be able to "reach" nearby drops and react with them, thereby creating a network of drops when PI is the continuous phase, while the PDMS loops are too short to react in a PDMS continuous system. However, we also need to consider the effects of steric hindrance and therefore consider the state of the reactive species on each side of the interface.

To clarify the effect of molecular mass on surface segregation in compatibilized polymer blends, two regimes have been previously proposed: a dry brush regime and a wet brush regime [119]. These regimes depend on the lengths of the homopolymer and copolymer and the ability of the homopolymer to interpenetrate the copolymer. When the homopolymer chain length is much larger than the copolymer chain (or loop) length, the homopolymer is unable to penetrate the copolymer, creating a dry brush. When the chain length of the homopolymer is smaller than the length of the copolymer chain (or loop) length, the homopolymer is able to penetrate the copolymer, creating a wet brush. In the present case, the molecular weights of PI and PDMS are 29 kg/mol and 135 kg/mol, respectively, which creates a blend in which the PIMA loops are near the size of the PI chains and the PDMS-$NH_2$ loops are drastically smaller than the PDMS chains. In the PI-in-PDMS blends, in which no drops sticking are observed, the long homopolymer

chains, the copolymer chains (or loops) are not able to be penetrated, creating a dry brush. A consequence of the dry brush is that the drops are not able to closely approach each other to a distance suitable for sticking. A wet brush is formed when PI is the continuous phase as the chains of the PI matrix are short enough to penetrate the PIMA and steric hindrance does not keep the drops apart. In summary, we speculate that the differences in the chain lengths of the homopolymers compared with the reactive polymer species, in addition to the functionality of the reactive species, may contribute to the asymmetries observed in the morphologies and rheological properties of the blends.

## 4.4 CONCLUSIONS

We have examined the effects of reactive compatibilizer concentration and homopolymer component concentration in model blends of PI and PDMS using two multifunctional reactive species which create a crosslinked interface. Increasing reactive compatibilizer loading in PI continuous (S30) blends was found to increase formation of drop clusters and increase the "gel-like" behavior and viscosity of the blend. Contrarily, blends of PI dispersed in PDMS (S70) showed no droplet clusters or "gel-like" oscillatory behavior. Flow-induced coalescence was suppressed at compatibilizer loadings greater that 0.4% of the total weight in S30 blends and in S70 blends with at least 0.6% compatibilizer. Coalescence did occur in all blends under quiescent conditions.

We speculate that the formation of drop clusters is responsible for the gel-like oscillatory behavior, large increases in steady shear viscosity, and the large viscosity overshoots in S30 blends. The decrease in these properties in S70 blends is attributed to the fact that droplets do

not appear to stick or cluster together in S70 blends. The morphological differences in S70 vs. S30 blends are due to compatibilizer asymmetry, homopolymer chain length and steric hindrance.

# 5.0 REACTIVE COMPATIBILIZATION IN STARCH BASED SYSTEMS

In this chapter, we transfer the knowledge gained from the model system of PDMS and PI discussed in Chapters 3.0 and 4.0 to a "non-model" system, i.e. composed of conventional commercial thermoplastics. The concept of reactive compatibilization using multifunctional reactive polymers is applied here to an immiscible polymer blends based on plasticized starch. In Section 2.3.2, we discussed properties of starch and its blends with polyolefins. In short, starch is a biodegradable, semi-crystalline polymer consisting of linear amylose chains and branched amylopectin chains, both of which have a glucose monomer unit [120]. Granular starch must be plasticized in order to create a processable material called plasticized starch (PLS). The properties of PLS are quite poor and it is therefore often blended with polyolefins to improve its mechanical properties. However at high starch contents, which are desirable from a sustainability point of view, a particular trend was observed: as PLS content increased a strong decline in mechanical properties was observed. An alternative approach to improving the mechanical properties of PLS is to blend it with layered silicates to create PLS-clay nanocomposites [62, 76-78].

This research examines the effect of clay added to two-phase blends of PLS and a polyolefin (polypropylene). Polypropylene (PP) was chosen to be blended with PLS based on its superior hydrophobicity and mechanical properties. Specifically we hypothesize that the clay can improve the mechanical properties of the PLS phase and therefore mitigate the decline in

properties as PLS content increases. Thus, PLS/PP blends may be realized that retain good mechanical properties in spite of a high PLS content.

## 5.1 EXPERIMENTAL

### 5.1.1 Materials

Cassava starch was supplied by Copagra (Nova Londrina, Paraná, Brazil) and injection grade polypropylene was supplied by Quattor (Brazil) and has a density of 0.905g/cm$^3$ and MFI (2.16 kg, 190°C) of 11 g/10min. Maleated polypropylene (MAPP) was supplied by ExxonMobil (USA) ($\rho$=0.9g/cm$^3$ and MFI (1.2 kg, 190°C) 125 g/10min) and had a maleic anhydride content of 0.5 to 1.0% as quoted by the manufacturer. MAPP is used as a coupling agent to increase compatibility between the PLS and PP phases [121, 122]. Glycerol was obtained from LabSynth Products (Diadema, São Paulo, Brazil).

Two nanoclays were used in this research: one with an expected affinity for the PLS phase and the other with an expected affinity for the PP phase. The first is natural sodium montmorillonite (MMT), which is hydrophilic, and expected to be compatible with PLS [62]. The second, used as a control, is Cloisite 30B (30B), which is MMT that has been organically modified with methyl, tallow, bis-2-hydroxyethyl, quaternary ammonium salts. The organic modifier is known to intercalate into the clay galleries, thus greatly increasing the affinity of the clay for hydrophobic polymers. In particular, Cloisite 30B can be well-dispersed (i.e. exfoliated) into PP, particularly in the presence of a coupling agent containing polar groups, such as maleic

anhydride [123, 124]. MMT and 30B were obtained from Southern Clay Products (Texas, USA).

### 5.1.2 Preparation and processing of materials

Modified and unmodified clays were dried for 24 hours at 70°C and then added to glycerol (5% of the total weight of PLS) and allowed to sit for 8 hours. Wide-angle x-ray diffraction suggests that the glycerol swells the clay and intercalates into the galleries between the clay platelets (see below). To plasticize the starch, the glycerol/clay mixture was then added to dry cassava starch, mixed by hand for 20 minutes and allowed to sit overnight to allow the glycerol mixture to diffuse into the starch granules. The clay free samples were prepared in the same manner but without the addition of clay to the glycerol. The ratio of glycerol to starch was always 40% glycerol by weight. Sample compositions are listed in Table 5.I.

The composites were processed in an intermeshing co-rotating twin-screw extruder (Coperion Werner-Pfleiderer, model ZSK-26 Mc, $L/D = 44$, $D = 24$ mm) with a side-feeder. The starch and glycerol were passed twice through the extruder at 150°C to make PLS and the extrudate was pelletized. PP and MAPP were mixed by hand and passed through the extruder via the main feeder, while PLS was added in the side feeder. The PP:MAPP ratio was 75:25 and the PP and MAPP blend is referred to as the "PP phase" henceforth in this chapter. The temperature profile used was 180°C for the first three zones of the extruder and 165°C in the remaining zones which extend from the side feeder to die. The PLS was added in the side feeder at lower temperatures to decrease its residence time in the extruder.

Table 5.I. PLS/PP blends sample compositions.

| | Starch wt% | Glycerol wt% | PP wt% | MAPP wt% | PP/MAPP vol% | MMT | 30B |
|---|---|---|---|---|---|---|---|
| PLS50 | 30.0% | 20.0% | 37.5% | 12.5% | 61.0% | | |
| PLS70 | 42.0% | 28.0% | 22.5% | 7.5% | 40.0% | | |
| PLS80 | 48.0% | 32.0% | 15.0% | 5.0% | 28.0% | | |
| PLS90 | 54.0% | 36.0% | 7.5% | 2.5% | 15.0% | | |
| PLS100 | 60.0% | 40.0% | 0.0% | 0.0% | 0.0% | | |
| | | | | | | | |
| PLS50MMT | 27.5% | 17.5% | 37.5% | 12.5% | | 5.0% | |
| PLS70MMT | 39.5% | 25.5% | 22.5% | 7.5% | | 5.0% | |
| PLS80MMT | 45.5% | 29.5% | 15.0% | 5.0% | | 5.0% | |
| PLS90MMT | 51.5% | 33.5% | 7.5% | 2.5% | | 5.0% | |
| PLS100MMT | 57.5% | 37.5% | 0.0% | 0.0% | | 5.0% | |
| | | | | | | | |
| PLS5030B | 27.5% | 17.5% | 37.5% | 12.5% | | | 5.0% |
| PLS7030B | 39.5% | 25.5% | 22.5% | 7.5% | | | 5.0% |
| PLS8030B | 45.5% | 29.5% | 15.0% | 5.0% | | | 5.0% |
| PLS9030B | 51.5% | 33.5% | 7.5% | 2.5% | | | 5.0% |
| PLS10030B | 57.5% | 37.5% | 0.0% | 0.0% | | | 5.0% |

### 5.1.3 X-ray diffraction

The crystalline structures of the samples were examined using a Shimadzu XRD7000 X-ray Diffractometer (São Paulo, Brazil). The samples were exposed to the X-ray beam with the X-ray generator running at 40 kV and 30 mA. Scattered radiation was detected at ambient temperature in the angular region of 5-50° at a rate of 2°/min using a Cu beam ($\lambda$=1.54nm). The $d_{001}$ spacing was determined by substituting the 2$\vartheta$ scattering peak in to the Bragg's equation.

### 5.1.4 Morphology

The morphology of the nanocomposites was examined in a Carl Zeiss CEM 902 transmission electron microscope (Oberkochen, Germany). The microscope was operated at an acceleration voltage of 80 kV and was equipped with a Castaing-Henry energy filter spectrometer within the column. Ultrathin sections, approximately 40 nm thick, were cut perpendicular to the film plane at −120 °C, in a Leica EM FC6 cryo-ultramicrotome. Next, the thinned, polished microtome samples were examined using a JEOL JSM-6340F field emission scanning electron microscope (FESEM), operating at an accelerating voltage of 3 kV. Finally, various extruded samples, with and without nanoclay, were immersed in liquid nitrogen for at least 10 minutes and fractured. The fractured surfaces were sputter coated and observed using a JEOL JSM-6360 LV scanning electron microscope (Middleton, WI) at an acceleration voltage of 5-10 kV.

### 5.1.5 Tensile testing

The extruded materials were pelletized. Samples containing 80% PLS or more were soft and tacky and could not be injection molded. Therefore, these samples were calendared using a MH-Equipamentos double roll mill model MH-150C (Guarulhos, Brazil) at temperatures of 120-150°C and heat pressed into films at 160°C. The films were then cut into dumbbell shaped tensile specimens according to ASTM D-412 [79]. The prepared materials containing less than 80% PLS were injection molded into dog-bone shaped tensile specimens according to ASTM D-638 [125] using an Arburg Allrounder injection molding machine model 221M 250-55 (Lossburg, Germany). The following temperature was kept along the barrel zones: 165, 165, 165, 170, and 175°C. The mold temperature was kept at 40°C. For all samples, tensile properties were characterized using an EMIC DL2000 universal testing machine (São José dos Pinhais, Brazil) with a load of 5000 N for injection molded tensile specimens and 500 N for film specimens. Test speeds of 50 mm/min were used for both specimen types. All specimens were conditioned for at least 72 h at 23°C and 44% relative humidity before testing. Typical specimen dimensions, as well as the test conditions were chosen according to standards ASTM D-638 and D-412. At least eight specimens of the same sample were tested.

### 5.1.6 DMA

The dynamic mechanical analysis (DMA) of the extruded blends was performed in a TA Q800 DMA (New Castle, Delaware (USA)). Pellets of the extruded blend specimens were compression molded into films and were subjected to sinusoidal deformation in tension mode analysis at a frequency of 16 Hz, strain amplitude of 0.01% and temperature rate of 5°C/min in

the temperature range from −100°C to 200°C, or until the sample broke. Typical sample dimensions were 0.65 mm x 10 mm x 5.3 mm.

### 5.1.7 Viscosity measurements

Rheological experiments were performed using a TA Instruments AR2000 stress-controlled rheometer with 25mm parallel plate geometry, and the sample temperature of 165ºC. Oscillatory measurements were conducted at 1% strain.

## 5.2 RESULTS AND DISCUSSION

Clays are most effective as reinforcement when the clay layers are able to exfoliate [62, 76, 77]. The most important factors to consider in achieving exfoliation are the ability of the polymer matrix to intercalate the clay layers, and the possibility of promoting favorable interactions between the polymer and the silicate layers. In the present case, we have chosen the unmodified, hydrophilic sodium montmorillonite for its compatibility with starch and the organically modified Cloisite 30B as a control, as it is compatible with hydrophobic polymers, especially in the presence of polar groups, such as maleic anhydride [123, 124].

The XRD patterns showed the scattering peaks for dried MMT and 30B were $2\vartheta$=8.2 and 4.8, respectively (Figure 5.1). The presence of a scattering peak is indicative of a layered structure, and the location of the peak is roughly inversely proportional to the interlayer distance, i.e. a small theta corresponds to a large interlayer distance. These values correspond to $d_{001}$

values of 1.07nm and 1.83nm, respectively and agree well with the literature [126]. The larger $d_{001}$ value for 30B arises from the organic modification. Upon swelling in glycerol, the interlayer distance increased for the both MMT ($d_{001}$= 1.81nm) and 30B ($d_{001}$= 2.32 nm), as shown by the shift of the peak to lower theta values. This suggests that glycerol intercalates into the galleries of both clays. Some level of exfoliation cannot be ruled out. Upon extrusion of the glycerol-swollen clays with starch to obtain PLS100-MMT and PLS100-30B the peak position remains essentially unchanged. In summary, from the XRD experiments we can conclude that glycerol intercalates both MMT and 30B clays, and melt extrusion with PLS does not exfoliate the clay any further than glycerol. These data do not provide a complete picture of the location or quality of dispersion of the clay, and hence we further explore the morphology using transmission electron microscopy (TEM).

The TEM images of PLS50-MMT and PLS50-30B are shown in Figure 5.2. These two samples were chosen for discussion because they clearly show both the two phase morphology of the blends, as well as the location of the clay. The dark regions in Figure 5.2 correspond to the polypropylene matrix phase and the gray regions correspond to the dispersed PLS phase. Due to beam sensitivity, portions of the PLS phase were destroyed by the electron beam and appear bright white. The images in Figure 5.2 show that, in both MMT as well as 30B, there is good dispersion of clay (no large aggregates) and indeed, the PLS-rich regions of the MMT-containing sample show intercalated and possibly exfoliated clay platelets. The chief difference between the two samples is the location of the clay: in PLS50-MMT, the clay appears to be primarily in the PLS phase, whereas in the PLS50-30B sample, the clay appears to have migrated to the interface, presumably because its surface hydrophobicity gives it greater affinity for the PP

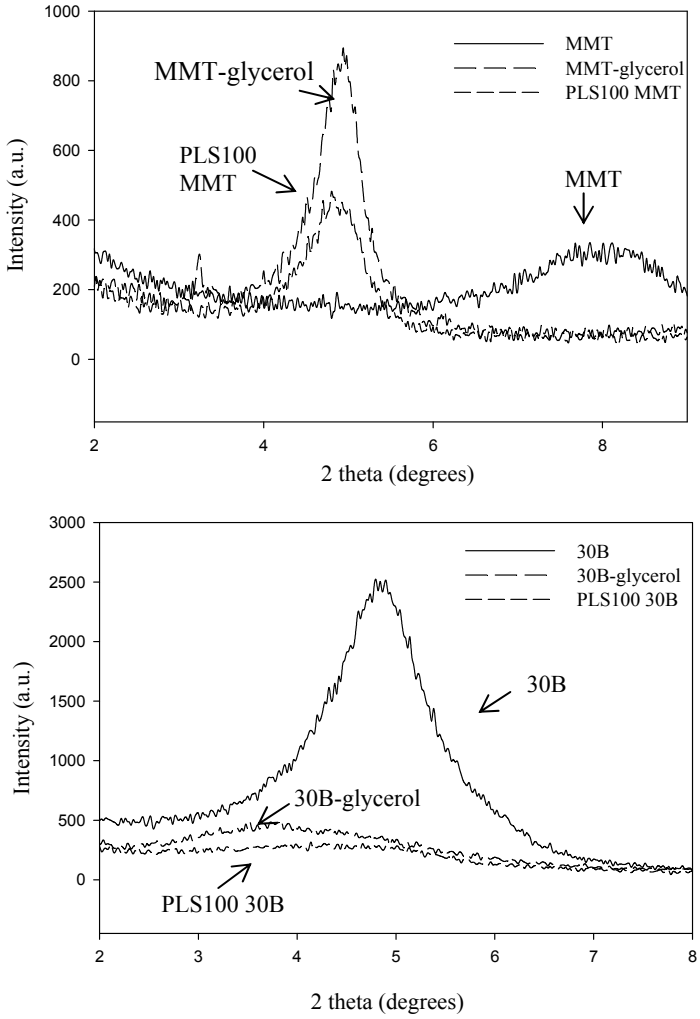


Figure 5.1. The XRD patterns showed the scattering peaks for MMT (top) and 30B (bottom).

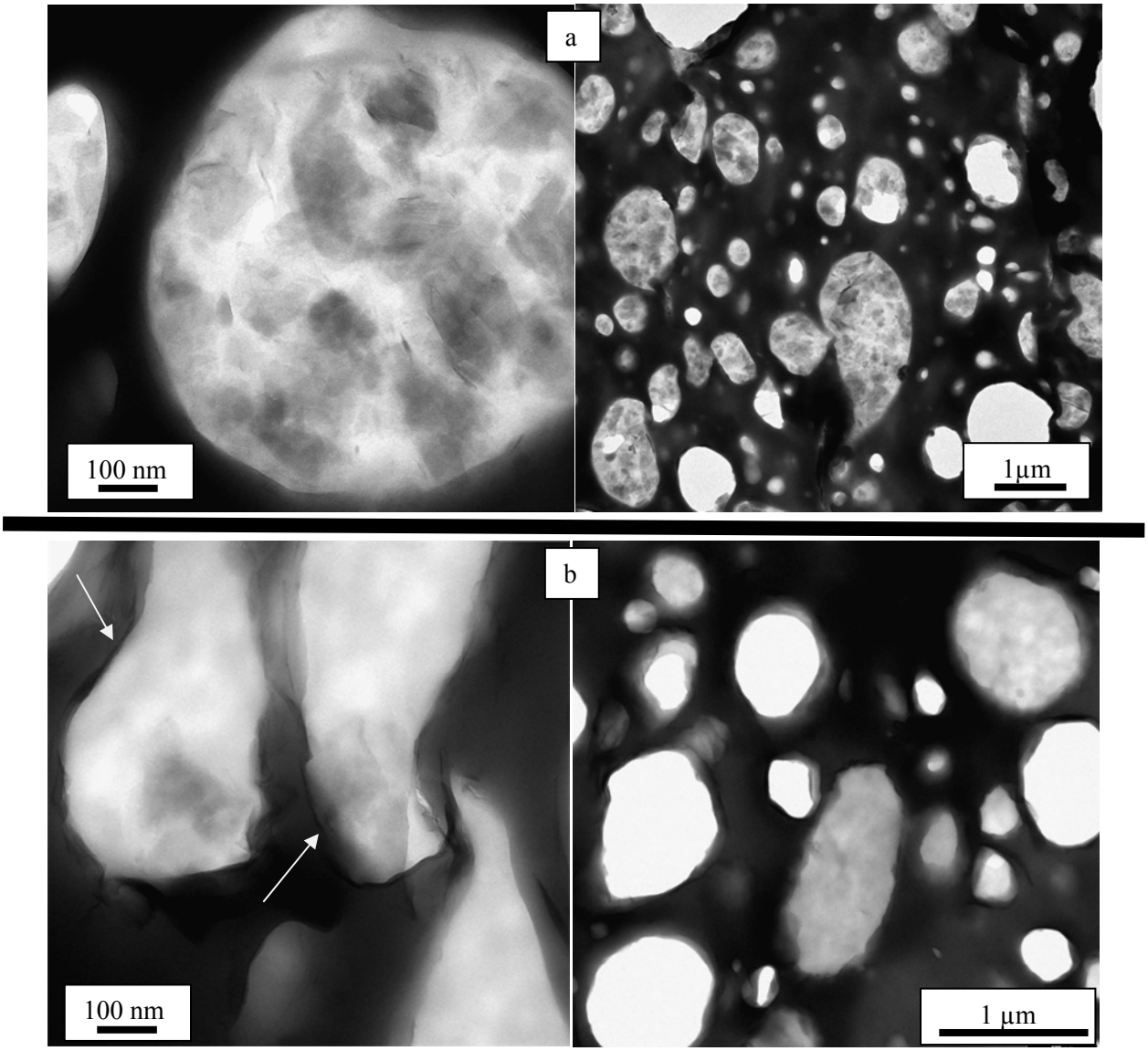


Figure 5.2. TEM (a) PLS50-MMT platelet and (b) PLS50-30B showing interface distortion from the clay.

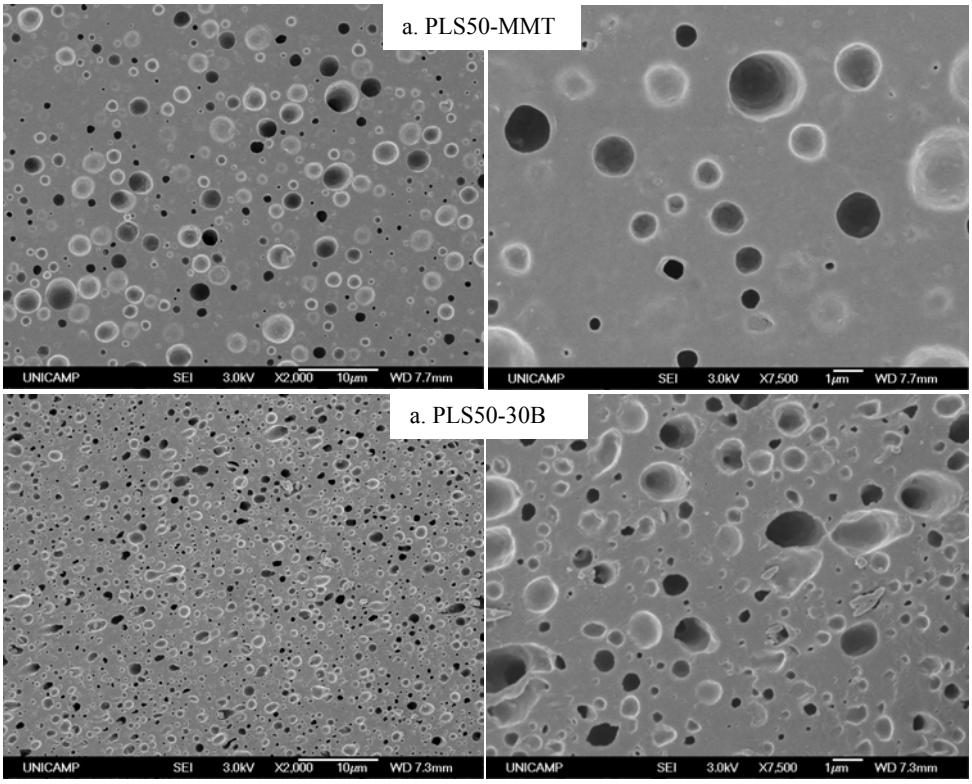


Figure 5.3. Field emission scanning electron micrographs for (a.) PLS50-MMT and (b.) PLS50-30B.

phase. Furthermore, the migration of 30B has distorted the interface of the PLS50-30B sample, creating a jagged interface in the areas where the clay is found. The localization of the MMT in the PLS is not surprising: MMT is known to have poor affinity for low-polarity polymers such as polypropylene, and indeed this is the reason why organically-modified clays are essential for making nanocomposites from most synthetic polymers. The case of Cloisite 30B is more complex: it has favorable interactions with the PLS phase (due to the possibility of hydrogen bonding with starch or glycerol), but it also has favorable interactions with the PP phase (the organic modification with a tallow-based surfactant makes it more compatible with PP, and it can also hydrogen-bond with the anhydride groups from the maleated PP). We speculate that the interfacial localization of some of the clay is due to its favorable interactions with both the phases. It is noteworthy that similar interfacial localization of the clays has been reported in a

variety of immiscible polymer blends, and several such examples have been cited in references [127, 128].

In the low magnification TEM images, it is apparent that the PLS domain size is slightly larger in PLS50-MMT (~ 1 micron in diameter) than PLS50-30B (< 1 micron in diameter). The differences in domain sizes (as well as the jagged interface in PLS50-30B) are further confirmed in FESEM images (Figure 5.3) and are likely attributable to the differences in the clays' affinities towards the two phases. The role of organically modified layered silicate in the breakup and coalescence of droplets in immiscible polymer blends has been published by *Hong et al.*[129] . The authors showed that at sufficient clay concentrations, the clay was found to go into the phase with which it had a higher affinity. Specifically, Hong et al. showed that in polybutylene terephthalate/polyethylene (PBT/PE) blends, the organoclay was observed to have more affinity for the PBT phase. Thus when the drop phase was PBT, the domain size increased with increasing concentrations of organoclay. According to the authors, this was because the clay in the drop phase made the drop less deformable and thus harder to break up. In contrast, the presence of clay in the matrix changed the blend's rheological properties such that coalescence was decreased. The authors compared the interfacial tension of clay laden blends with blends containing no clay, which confirmed that the slowed coalescence was indeed a result of the clay. The suppression of coalescence due to the presence of layered silicates at the polymer blend interface has been reported by other authors [130, 131]. Here, we surmise that the MMT, found primarily in the PLS phase, increases the PLS domain size as the clay may prevent breakup. Furthermore, the interfacial location of 30B may aid in the suppression of the coalescence of the PLS phase in PLS50-30B, leading to a smaller domain size.

Figure 5.4 shows the mechanical properties of the samples obtained from tensile testing. In the absence of clay, with increasing PLS content, the modulus and strength of the materials reduce significantly and the ultimate elongation increases. As mentioned in the Section 2.3.2, this was expected from the previous research in this area [3, 71-73]. Addition of either nanoclay increases the strength and modulus at all compositions, and the effects are especially large at high PLS content. Equally importantly, this improvement occurs with only a modest decrease in ultimate elongation, i.e. the clays are able to reinforce the PLS/PP blends without making them brittle. Indeed the marked improvement in mechanical properties from the addition of clay was apparent even before the tensile experiments were performed: The mechanical properties of the PLS100 samples were so poor (i.e. tacky and soft) that the tensile specimens failed during handling and loading in the EMIC tensile tester. The addition of either clay improved the properties such that the 100% PLS samples were easily handled. As a result, data for PLS100 without clay are not presented in Figure 5.4.

The effect of clays is not uniform at all compositions. The addition of clay at 50% PLS content does not significantly enhance the modulus or tensile strength. However, as the PLS content is increased to 70 and 80%, the modulus and tensile strength are both increased by the addition of MMT and 30B. The most significant increase was seen in PLS70-MMT, which showed increases of 1200% and 800% in the modulus and tensile strength, respectively. The reasons for this will be discussed below. At the highest (comparable) PLS loading of 90% the modulus and tensile strength are both increased by at least 50%. In summary, these results support the chief hypothesis that the addition of nanoclay to PLS/PP blends will mitigate the decline in mechanical properties at high PLS content increases.

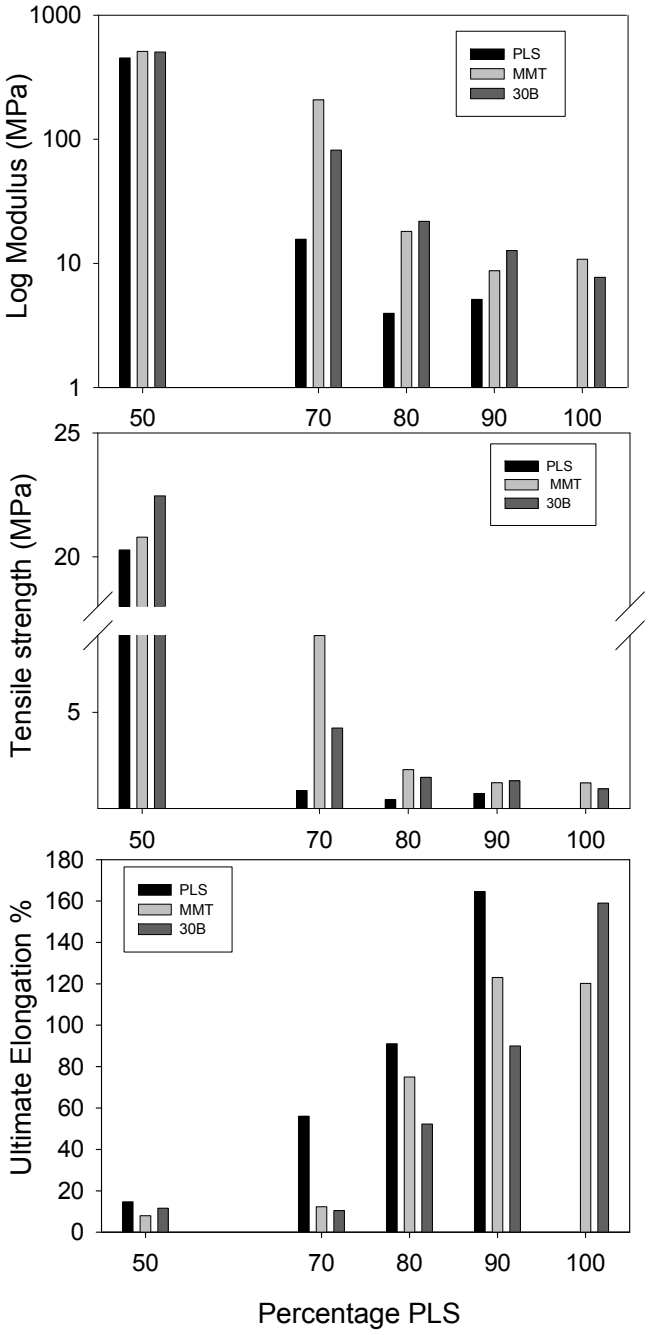


Figure 5.4. Tensile properties of plasticized starch and polypropylene blends (note the y-axis for modulus is a log scale).

Comparing the two different clays, there appear to be no systematic differences in the magnitude of the reinforcement in the MMT-containing samples vs. the Cloisite 30B-containing samples. This is somewhat surprising for two reasons. The first is that the TEM micrographs indicate that the MMT is located in the PLS phase, whereas Cloisite 30B clay is located partly in the PLS phase, and partly at the interface. The second is that while the weight loading of the clay is the same (5 wt %) in all samples, Cloisite 30B has roughly 30 wt% organic modifier. Thus, effective volume fraction of the reinforcing agent (i.e. the silicate platelets) is about 30% lower in the Cloisite 30B. Yet, neither the difference in the location of the clay, nor the ~30% difference in the clay loading seems to affect the tensile properties significantly. Although this insensitivity to organic modification of the clay is surprising, it is supported by recent publications: A recent study reported that 30B and MMT are both good choices for reinforcing plasticized corn starch [132]. A review by Averous et. al. also reported good dispersion when incorporating Cloisite 30B into plasticized starch, which in turn results in the improvement of mechanical properties [133].

Thermomechanical data of the samples is shown in Figure 5.5. The glassy modulus and glass transition temperature were essentially unaffected by the addition of clay. Upon the addition of clay, the storage modulus increases above the glass transition temperature, with the largest increase observed in the samples containing 70% PLS. Strongly polar polymers, especially with hydrogen bonding have slightly higher glassy moduli [134], and accordingly, the samples containing higher concentrations of PLS, which is more polar than PP, show the highest moduli in the glassy region (-100°C). Moreover, the effect of clay was negligible in the glassy region. The $T_g$ of all samples (as judged by the peak in tan δ), was near -25°C and was unaffected by the addition of clay. In all samples, the modulus increased with increasing PP

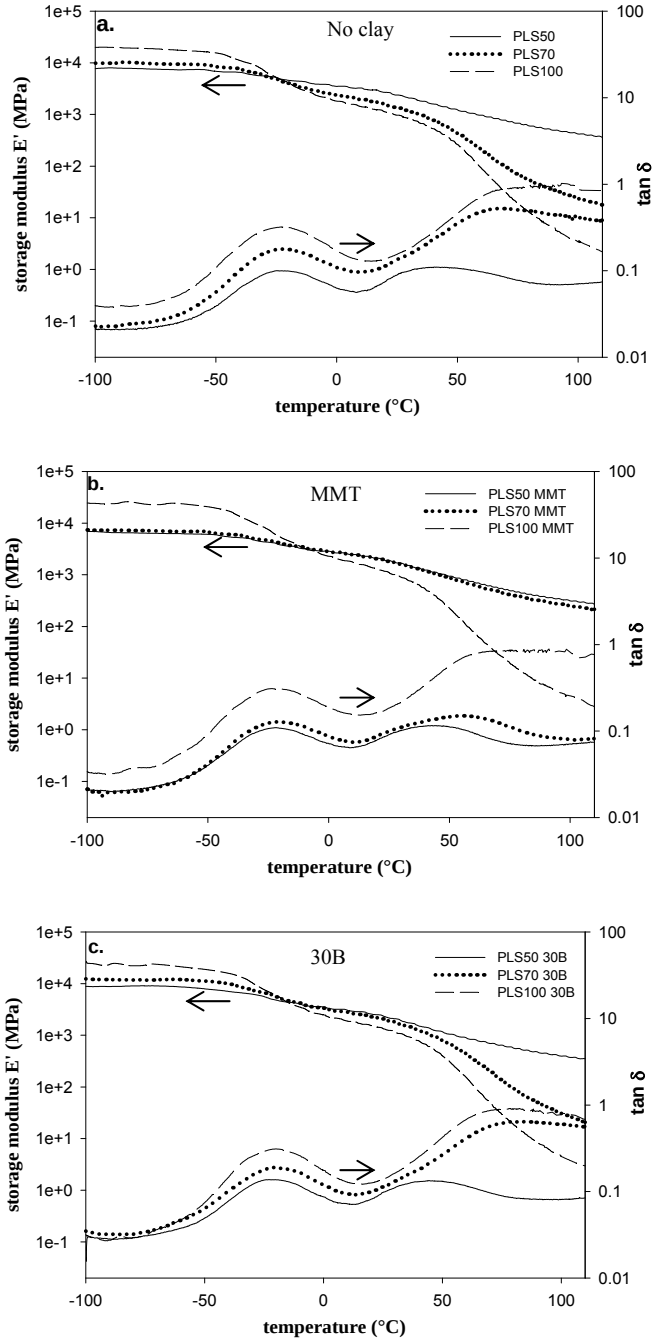


Figure 5.5. DMA of (a) plasticized starch and polypropylene blends, (b) PLS/PP blends with MMT and (c) PLS/PP blends with 30B.

content in the temperature range from the glass transition temperature to 100°C. In the PLS70-MMT sample, the addition of clay resulted in a large increase in the storage modulus as temperature is increased, presumably due to the stiffening of the material due to the restriction of chain mobility by the nanoclays. The same was observed for the PLS80- MMT sample. In contrast, the addition of 30B does not increase in the plateau modulus at high temperature significantly.

Finally we discuss the mechanism for the improved mechanical properties with addition of clay. In homopolymer nanocomposites, the change in mechanical properties occurs because the clay acts as a reinforcing agent. In the present case of *two-phase* nanocomposites, there is potentially a second, more subtle reason, viz. the mechanical properties also depend on the two-phase morphology, and if the clay changes the two-phase structure, then the mechanical properties will be affected as well. For example, if the clays induce a change in phase continuity (changing from a dispersed PP phase to a continuous PP phase), a dramatic change in mechanical properties may be expected. Such changes in morphology are most readily examined by scanning electron microscopy (SEM). The SEM of PLS50, PLS70 and PLS80 with and without clay is presented in Figure 5.6a-c and shows the two-phase structure of the composite materials. The PLS50 samples have smooth PLS domains and porous, rougher PP domains, with the PLS domains as the dispersed phase. The reason for the pores in the PP domains is not clear. At 50% PLS, the addition of clay does not have a significant effect on the large scale domain size, shape, or phase continuity. At 70% PLS however, the clays have a significant effect on the morphology (Figure 5.6b). The clay-free PLS70 sample has the PLS as the continuous phase, and has roundish PP domains with smooth borders. In contrast, both PLS70-MMT and PLS70-30B

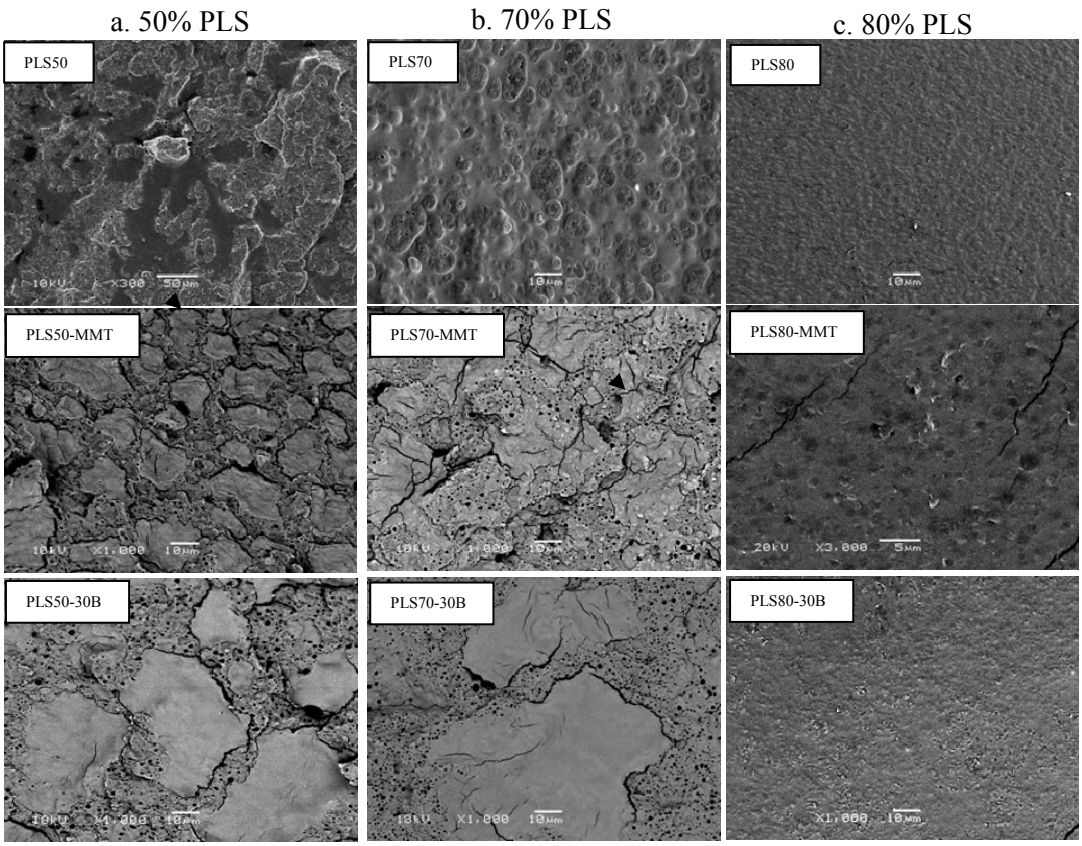


Figure 5.6. SEM of PLS50, PLS70 and PLS80 blends containing (a) no clay, (b) MMT and (c) 30B. Some images were taken in electron backscattering mode, which causes some cracking of the sample. The scale bar in the PLS50 and PLS80-MMT images are varied.

samples contain larger PP domains which do not seem to be completely separate domains, but appear continuous throughout the sample. Upon further increase in the PLS content to 80%, the clay appears to have little effect on the morphology and all 80% PLS samples appear to be PLS continuous (Figure 5.6c).

The issue of phase continuity can be further examined by solvent exposure using dimethylsulfoxide (DMSO) which is a good solvent for PLS. Clay-free samples with 70% or 80% PLS were swollen significantly and separated into small fragments, while PLS90 and

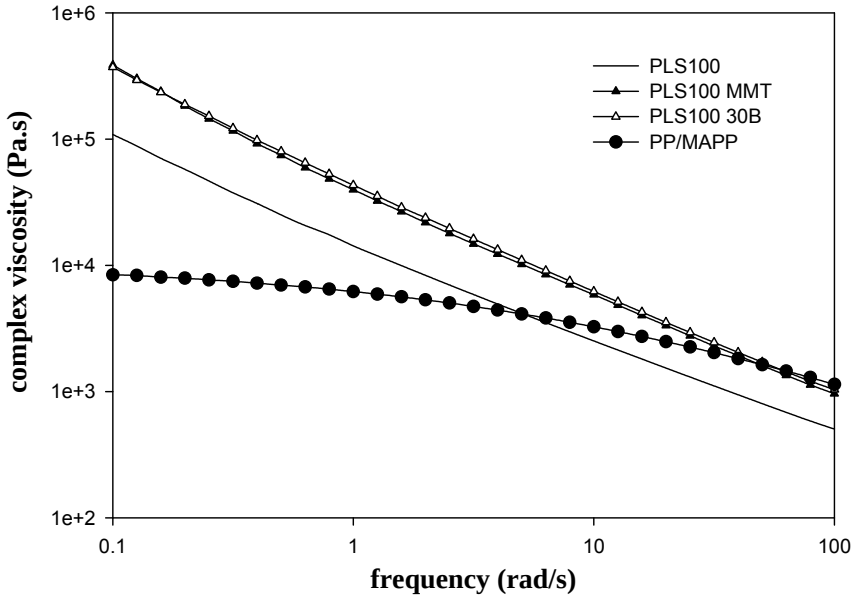


Figure 5.7. Complex viscosity of PLS with and without the addition of clay compared to the complex viscosity of the PP phase, measured at 1% strain. The low frequency complex viscosity can be viewed as zero shear viscosity.

PLS100 completely disintegrated upon immersion in DMSO. In contrast, PLS70-MMT and PLS70-30B both remained intact in DMSO further validating the change in phase continuity. PLS80-MMT and PLS80-30B became slightly swollen by DMSO but no separation of the samples was observed. Clay-containing samples with 90% or 100% PLS disintegrated altogether.

In summary, in most of the samples, the change in mechanical properties is attributable mainly to the reinforcing effect of clays. However, at 70% PLS (and perhaps at 80% PLS) the change in morphology caused by the addition of clay may also contribute to the large change in mechanical properties.

We surmise that the large change in morphology occurs in the 70% PLS sample because at this weight loading, the *volume* fraction of PP in the blend is near 40%. The clay-free sample has PLS as the continuous phase, but due to the relatively high volume fraction of PP, the morphology is susceptible to phase inversion. The viscosity of PLS is approximately an order of magnitude greater than that of the PP phase. With addition of either clay, the zero shear viscosity of PLS100 was increased by a factor of nearly 4 (see Figure 5.7). This suggests that the clay reinforced PLS phase would have an increased resistance to deformation and breakup, resulting in larger domains the in the PLS/PP blend. Moreover, this increase in viscosity may shift the composition at which the PLS/PP blends can phase invert. Similarly, Galgali et. al. found that layered silicates can form network structures within a polymer matrix, increasing the viscosity of the matrix and its ability to resist deformation [135]. The effects of clay on the morphology of the sample are apparent in the samples containing 70% PLS, in which the increased viscosity due to the addition of clay was able to affect the continuity of the blends since the volume fraction was nearest to 50%. The 50% and 80% samples, both having volume fractions far from 50%, were not largely affected by the change in the PLS viscosity and have only subtle morphological differences.

## 5.3 CONCLUSIONS

In summary, the properties of clay nanocomposites based on plasticized starch and polypropylene were investigated. X-ray diffraction and TEM revealed that both unmodified and modified clays were well-dispersed in the polymer matrix with no large aggregates of clay platelets. The unmodified MMT was primarily located in the PLS phase due to its affinity and

hydrogen bonding with PLS. The organically modified 30B was both dispersed in the PLS phase as well as located at the interface between PLS and PP, which is likely attributable to affinity with hydrophobic PP and hydrogen boding with the polar maleic groups of the MAPP. The addition of clay resulted in hybrid materials with improved tensile modulus and strength in relation to PLS/PP blends alone, as observed from the DMA and tensile testing results. The improvements are greatest at high PLS content suggesting that addition of clay is a possible route to realizing starch-based plastics that have a high renewable and biodegradable content, but still possess good mechanical properties. Such improvements are the result of the addition of clay as a reinforcing component and also from the effect of clay on the morphology of the blends.

Finally, throughout this chapter, the discussion has focused on reinforcing PLS/PP blends with clay. However it is also useful to reconsider the results as blending PP with PLS/clay nanocomposites. From that point of view, a significant increase in mechanical properties of PLS nanocomposites required approximately 20-30% polypropylene. Since other polymers may be used in place of PP, this perspective expands the paths available to creating starch-based plastics.

# 6.0 STARCH BASED RENEWABLE ELASTOMERS

## 6.1 INTRODUCTION

There has been enormous progress in polymeric materials obtained from renewable resources to provide a more sustainable pathway to meet our current commercial needs [136]. Virtually all these developments, including those discussed in Chapter 5.0, have been in the thermoplastics family, and may be considered as renewable alternatives to materials such as polyolefins, polyvinyl chloride or polyester terepthalate. There have been no comparable developments in the last few years in the elastomer family. Currently, natural rubber is the only commercially-available renewable polymer with elastomeric properties. Poly-4-hydroxybutyrate (P4HB), a renewable polymer synthesized through bacterial fermentation, is known to be elastomeric, but is used exclusively in medical devices, and is not available for routine elastomeric applications [137-140]. Applications such as shoe soles, gaskets, shock absorbers, etc. would benefit from the development of elastomers from renewable resources. Here we evaluate the possibility of developing renewable elastomers based on starch.

The key characteristics of elastomeric materials include a low glass transition temperature, generally below 0°C and a large strain at break. In addition, such materials need the ability to recover large amounts of strain and have a constant modulus over a wide range of temperatures.

Past publications on the thermomechanical properties of glycerol-plasticized PLS suggests that the properties of PLS may be well-suited for elastomeric applications. Specifically, at sufficient glycerol content (>25%), the glass transition temperature ($T_g$) of PLS is well below room temperature, which is of crucial importance to elastomers [45, 49, 141-143]. Due to its low $T_g$, such PLS is a soft, tacky material at room temperature and hence cannot be directly used as an elastomer. Natural rubber behaves similarly, and in that case, useful products can only be made upon crosslinking, either chemical crosslinking, e.g. in vulcanized rubber, or physical crosslinking, e.g. styrene-butadiene-styrene (SBS) copolymer elastomers. Analogously, it may be possible to crosslink PLS, while still retaining its elastomeric properties. Although there is much published research on crosslinking native starch for food applications [144, 145], the use of crosslinked starch as an elastomeric material has not been previously reported. We will explore the possibility of crosslinking PLS with maleated polypropylene (MAPP) to create an elastomeric material with a microphase-separated morphology where MAPP domains behave as physical crosslinks for the rubbery continuous phase PLS.

## 6.2 EXPERIMENTAL

### 6.2.1 Materials

Potato starch was obtained from Honeyville Food Products (California, USA) and is approximately 79% amylopectin and 21% amylose. Glycerol, used as plasticizer, was obtained from TheChemistryStore.com (Pompano Beach, FL). Reagent grade dimethyl sulfoxide (DMSO) was obtained from Mallincrodkt Baker (Phillisburgh, NJ). Maleated polypropylene

(MAPP) was obtained from ExxonMobil (Houston, TX) and has a maleic anhydride content of 0.5-1% by weight, corresponding to approximately 16 reactive anhydride groups per chain (according to the manufacturer's estimated molecular weight). The anhydride groups of the MAPP can react with the hydroxyl groups of the starch as will be discussed later in this chapter.

### 6.2.2 Plasticization and processing

All blends had a starch: glycerol weight ratio of 60:40. Three blends were made with MAPP contents of 0%, 5% and 15% by weight. Samples are designated as Sx where x is the weight percent of the starch/glycerol phase in the blend (and hence 100 - x is the weight percent of MAPP). Details of the blend compositions are given in Table 6.I.

The processing of all blends was conducted in collaboration with Pennsylvania State University's Plastics Engineering Professor Brian Young and undergraduate student James Goetz. The three blends were prepared as follows. The starch and glycerol were first mixed together in a 60:40 weight ratio using a table top dough mixer at 350 RPM for 30 minutes and allowed to sit overnight to ensure the diffusion of glycerol into the starch granules. The starch-glycerol mixture was then extruded using a single screw extruder (SSE) to obtain PLS, and the extruded strands of PLS were then cut into pellets. Mixtures of PLS pellets and MAPP pellets in the appropriate ratios were then extruded to obtain the blends of the compositions listed in Table 6.I. These extrudates were pelletized and extruded twice more to promote adequate blending of MAPP and PLS (since single-screw extruders are known to be relatively poor for dispersive blending), and to ensure the chemical reaction between the alcohol and anhydride groups. The S100 blend was also extruded two additional times to ensure that all blends have the same

Table 6.I. Starch based elastomers sample compositions.

| Sample | Starch | Glycerol | MAPP | MAPP[a] |
|---|---|---|---|---|
| S100 | 60% wt | 40% wt | 0% wt | 0% vol |
| S95 | 57% wt | 38% wt | 5% wt | 7.5% vol |
| S85 | 51% wt | 34% wt | 15% wt | 21.5% vol |

[a] Calculated assuming the following densities: MAPP = 0.9 g/cm$^3$ ; glycerol = 1.26 g/cm$^3$ and starch = 1.53 g/cm$^3$, and assuming linear mixing rule for density.

thermomechanical history. For all samples, a Brabender single screw extruder (0.75 inch diameter) was used at a temperature of 150˚C, and a rotational speed of 45 RPM. The three blends were injection molded into tensile bars using a DeMag injection molding machine for mechanical testing. All samples were stored at room temperature in sealed plastic bags.

### 6.2.3 Characterization

Scanning electron microscopy (SEM) was performed on cryofractured samples using a Philips XL-30 field emission scanning electron microscope at an acceleration voltage of 10kV. The samples were briefly immersed in water to remove the glycerol close to the surface (which may evaporate in the high vacuum of the SEM), and then fractured under liquid nitrogen. Samples were sputter coated with platinum prior to imaging.

Thermomechanical measurements were conducted using a TA Instruments Dynamic Mechanical Analyzer (DMA) Q800 in tensile mode. Prior to measurement, samples were heat pressed into ~1 mm thick films and cut into 5.3 mm wide strips. Dynamic mechanical temperature sweep measurements were conducted at a frequency of 1 Hz, amplitude of 1 μm (which corresponds to a strain of ~ 0.0074%) and a temperature ramp rate of 3°C/min from -120°C to 100°C or until the sample broke.

Calorimetric measurements were conducted using a TA Instruments DSC 2920 Modulated Differential Scanning Calorimeter, at heating or cooling rates of 10°C/min.

Tensile tests were performed at a rate of 0.2 in/min on an Instron 4400R tensile tester using a 200 lb load cell.

### 6.2.4 Results and discussion

Due to the immiscibility of MAPP and PLS, the morphology of MAPP/PLS blends is expected to be composed of MAPP domains dispersed in the majority PLS matrix. Under the blending conditions, the anhydride groups are expected to react with the hydroxyl groups of starch to form ester linkages (Figure 6.1a). The main hypothesis of this chapter is that because of starch-anhydride reactions, the MAPP domains can serve as physical crosslinking sites for PLS, and that such physically-crosslinked PLS/MAPP blends will show good elastomeric properties. It should be noted that the term "physical crosslinking" does not necessarily imply reversible chemical associations as it does in materials such as ionomers or multiblock polyurethanes. The term is used only to draw the analogy to block copolymer elastomers such as styrene-butadiene-styrene in which the glassy polystyrene domains serve as physical crosslinks for the elastomeric polybutadiene [146].

It is important to note that the MAPP domains can serve as effective crosslinks only if the hydroxyl groups on the starch chains react with the anhydride groups on MAPP; if the reaction does not occur, the MAPP domains will merely act as rigid fillers. While the anhydride is expected to react with hydroxyl groups under our extrusion conditions, in the present case, not all such reactions are between MAPP and starch. Specifically, since the glycerol used as plasticizer is itself a triol, it competes for the same anhydride groups (Figure 6.1b). At the 60:40

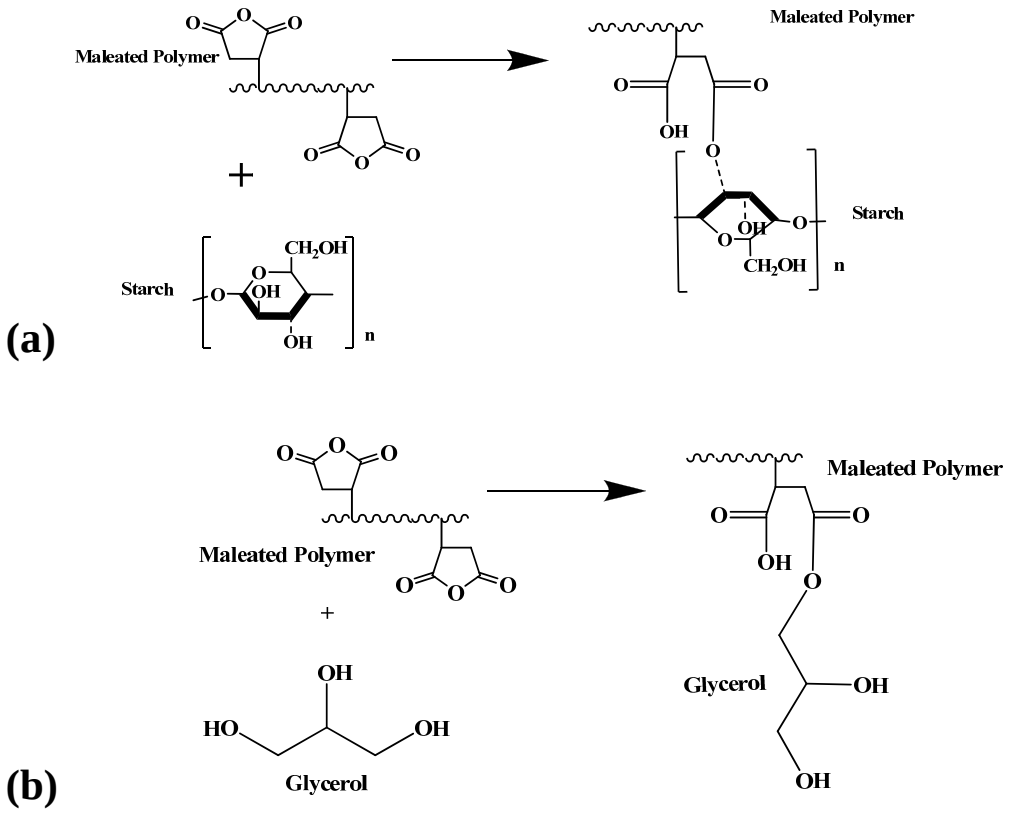


Figure 6.1. (a) Reaction of the MAPP and starch that results in crosslinking. (b) Competitive reaction between MAPP and glycerol.

starch:glycerol ratio used here, there are 1.3 glycerol-hydroxy groups for every starch-hydroxy group. If it is assumed that the starch hydroxy groups and the glycerol hydroxy groups are equally reactive, only an estimated 43% of the anhydride groups that react are expected to react with starch. Moreover, the anhydride may also react with residual levels of water, further reducing the number of anhydride groups that can react with starch. Accordingly it is crucial to confirm that the starch reacts with MAPP. Spectroscopic techniques such as FTIR are of only limited use since they cannot distinguish between MAPP-glycerol vs. MAPP-starch reactions. Therefore we used solubility tests and adhesion tests to verify the starch/MAPP reaction.

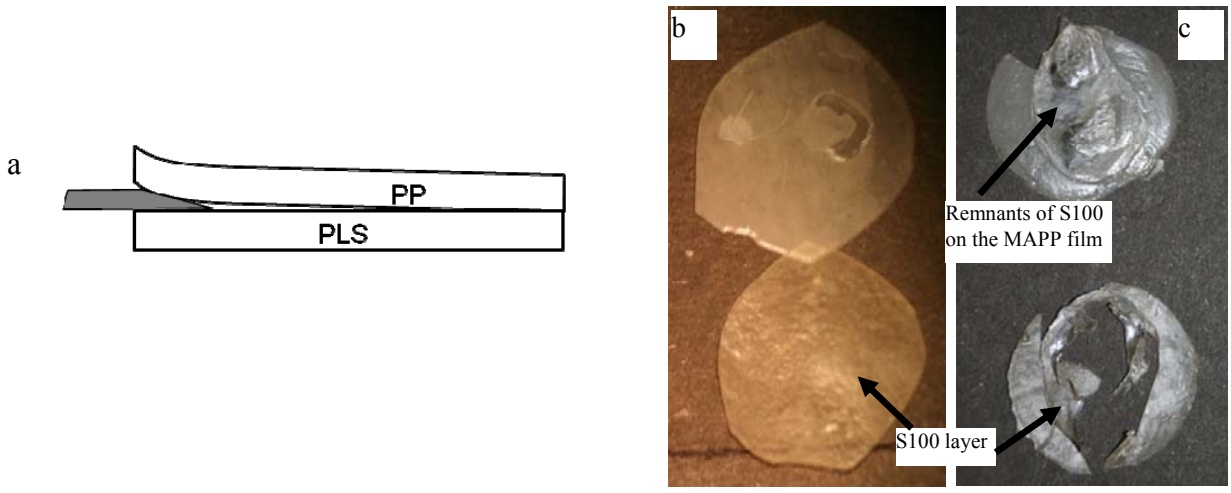


Figure 6.2. Schematics of the crack propagation experiment used to calculate interfacial fracture toughness (a). (b) S100 and non-reactive polypropylene, completely delaminated. (c) S100 and MAPP, after an attempt to completely separate the bilayer.

One simple test of the reaction is to test whether the MAPP/PLS blends are soluble in dimethyl sulfoxide (DMSO) which is a good solvent for PLS, but is unable to dissolve MAPP. Pellets of each blend were placed between two Teflon coated aluminum sheets and hot-pressed to form films. The films were placed in 10 ml of DMSO and gently shaken by hand upon immersion in the solvent. In less than 15 minutes, S100 completely dissolved in the DMSO, yielding a clear solution. In contrast, the S95 blend first became swollen, and then over a one hour period broke into smaller fragments giving the solvent a cloudy, opaque appearance. This suggests that the physical crosslinking of S95 is not complete, although small regions may be locally crosslinked. Finally, the S85% sample remained intact even after 20 hours, and did not show significant swelling or breakup, signifying that physical crosslinking is complete. These results strongly suggest that the MAPP can react with the starch under the extrusion conditions, and that the MAPP/PLS blend with 15% MAPP behaves as if it is physically crosslinked.

The second test is to examine the adhesion between PLS and MAPP; any reaction between MAPP and starch would sharply increase the adhesive strength [147]. A crack propagation test was performed on pressed films of the samples. This test is a modified double cantilever beam experiment and is the same as that used by Cole and Macosko [148] to obtain the interfacial fracture toughness. Films of S100, MAPP, and non-reactive polypropylene (i.e. not maleated) were heat pressed using 0.5 mm thick spacers to control the film thickness. Using these films, two bilayers laminates were made; one of S100 and MAPP, and the other of S100 and the non-reactive PP. If there is any interfacial reaction between the maleated polypropylene and starch, the interfacial fracture toughness of the PLS/MAPP bilayer will be larger than the bilayer containing non-reactive polypropylene. The bilayer samples were place in a vacuum oven at about 180°C for 30 min and then a razor blade was inserted at the interface (Figure 6.2a). After several hours, the crack length ahead of the razor blade was measured and the fracture toughness was calculated according to:

$$G = \frac{3\Delta^2 E_1 E_2 h_1^2 h_2^2 \left(C_1 E_2 h_2^3 + C_2 E_1 h_1^3\right)}{8a^4 \left(C_1^3 E_2 h_2^3 + C_2^3 E_1 h_1^3\right)} \tag{1}$$

where:

$$C_i = 1 + 0.64\left(\frac{h_i}{a}\right)$$

$\Delta$ = wedge thickness

E= elastic modulus

h = layer thickness

a = crack length ahead of wedge

Upon application of the razor blade, the PP/S100 bilayer completely delaminated (Figure 6.2b), and hence the fracture toughness could not be measured; as expected, this pair of materials

has poor adhesion. For the MAPP/S100 bilayer laminate, the crack length ahead of the razor blade was measured and the resulting fracture toughness was calculated to be 2.45 ± 0.66 J/m$^2$. After the completion of the fracture toughness test, an attempt was made to force the MAPP and S100 layers apart. Even after scraping the S100 layer away from the MAPP with a razor blade, the two layers did not delaminate completely as pictured in Figure 6.2c. The contrast between the complete delamination of the non reactive bilayer versus the pieces of S100 that remain adhered to the MAPP film support the solubility results, suggesting that an interfacial reaction between MAPP and plasticized starch does indeed occur.

Having confirmed that the MAPP can react with starch, and hence that the MAPP domains can act as physical crosslinking agents, we examined the morphology of the blends. The S100 blend (Figure 6.3a) displays a smooth continuous fracture surface under SEM. There are no starch granules visible in the micrograph, suggesting that the granular structure has been completely disrupted and the glycerol has gelatinized the starch. For the S95 blend (Figure 6.3b), the fracture surface appears mostly smooth, but now numerous features (light gray domains) of size smaller than 5μm appear throughout the image. Upon further increasing the MAPP content to 15wt.%, irregular gray domains are much more clearly evident (Figure 6.3c); in S85, they occupy a larger fraction of the cross sectional area, and also appear to be significantly larger, with some being more than ten μm in size. These domains, which we believe are polypropylene domains, indicate that in both S95 and S85 samples, (1) the morphology is two-phase with MAPP being the dispersed phase, and (2) the MAPP domain size increases significantly with increasing MAPP content. DSC data support the conclusion that the

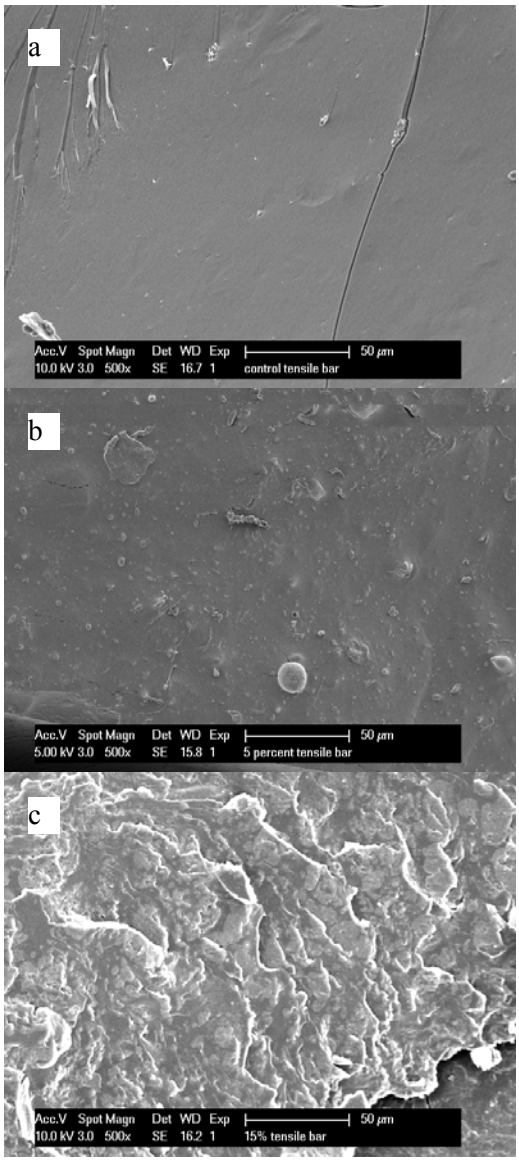


Figure 6.3. SEM micrographs of (a) S100, (b) S95 and (c) S85 blends.

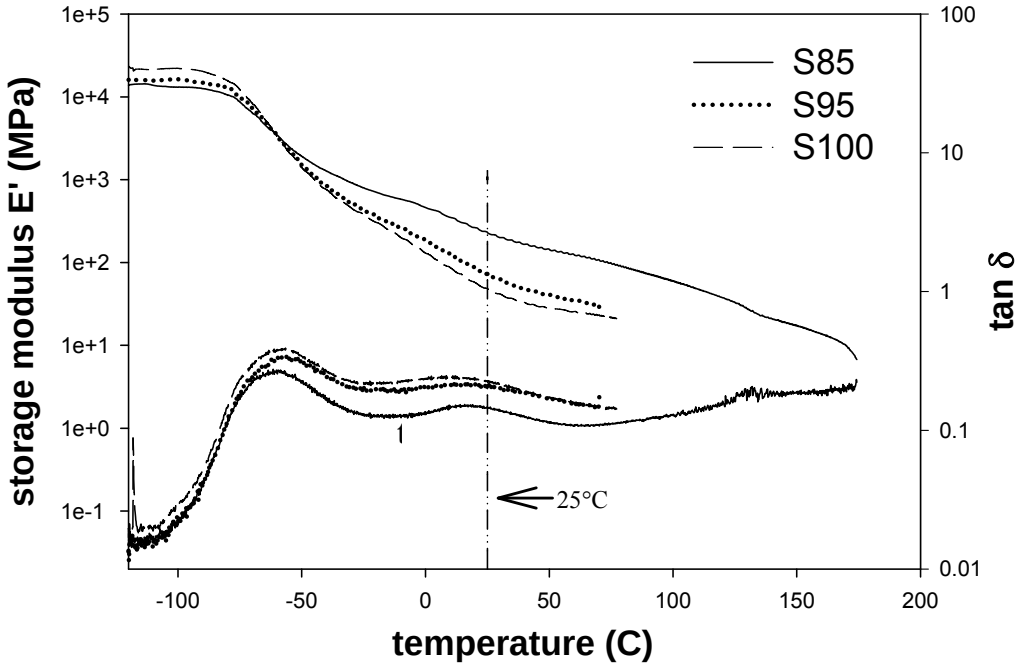


Figure 6.4. DMA results. The vertical line is drawn at 25°C (room temperature).

samples have a two phase morphology, specifically, a polypropylene melting endotherm is clearly evident (see Figure 6.6 below). As mentioned in the Section 6.1, the goal is to show that MAPP/PLS blends have properties that make them potentially-useful as elastomers. In order to test this, DMA experiments were performed to probe the thermomechanical behavior (Figure 6.4). All three samples appear glassy at -100°C with a modulus on the order of $10^4$ MPa. Between about -70°C and -40°C, the S100 sample shows a significant relaxation process, which is indicated by the maximum in tan δ and a decrease in the storage modulus by more than one order of magnitude. This temperature agrees well with the glass transition temperature of PLS measured by DSC [48, 88, 141] and the corresponding relaxation process has been identified as

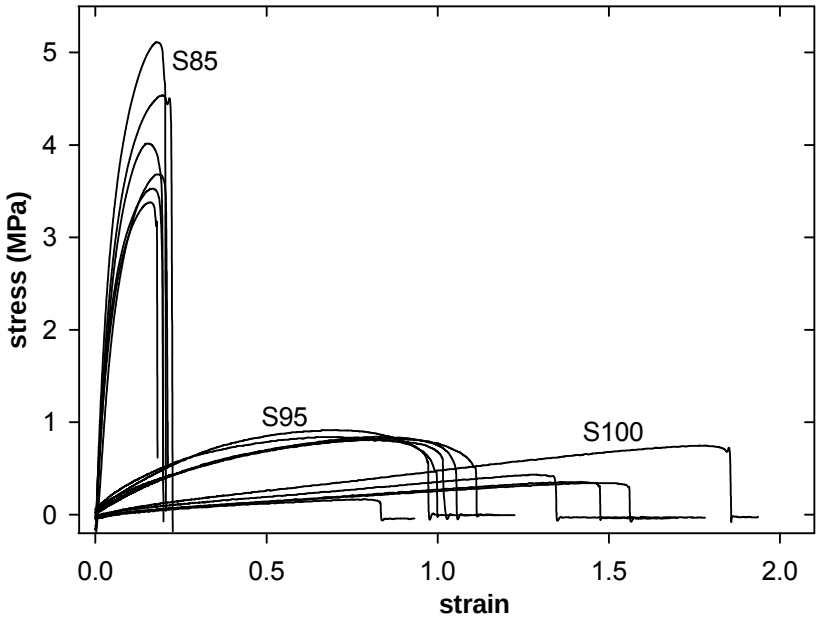


Figure 6.5. Tensile properties of PLS/MAPP blends.

the α relaxation of the glycerol plasticizer [54]. At higher temperatures, a second broad relaxation centered around 10°C is evident in the tan δ curve, but the E' is nearly a plateau until the sample breaks at about 70°C. The DMA data for the S95 sample are virtually identical to that of the S100. However, S85 shows a much wider rubbery plateau that extends far above room temperature; this sample did not break until 170°C, which is close to the melting temperature of the MAPP. It is also noteworthy that the low-temperature relaxation occurs at about -50°C regardless of the MAPP content. These DMA data – specifically the low $T_g$ and the wide rubbery plateau – are the best indicator of the elastomeric nature of PLS/MAPP blends.

The results of the tensile tests for all three samples are presented in Figure 6.5, and the tensile strength, Young's modulus and ultimate elongation obtained from these data are presented in Table 6.II. The ultimate elongation of the S100 blends is about 150%, which is

Table 6.II. Summary of tensile data, presented as the arithmetic average of several specimens of each sample.

| Sample | Tensile Strength (MPa) | Tensile Modulus (MPa) | Ultimate Elongation |
|---|---|---|---|
| S100 | 0.38 | 0.77 | 154% |
| S95 | 0.84 | 2.53 | 111% |
| S85 | 4.04 | 43.64 | 20% |

comparable to that measured previously at comparable glycerol contents [45, 141]. With increasing MAPP content, the ultimate elongation decreases, whereas the ultimate strength and modulus increases. These effects are likely attributable to both the filler effect of the rigid MAPP domains, as well as their physical crosslinking effect. The moduli of the blends range from about 0.75 MPa to about 40 MPa, i.e. MAPP/PLS blends can cover the modulus range of typical elastomers. The ultimate elongation of S85, about 20%, is somewhat low from an elastomeric viewpoint, but ultimate elongation is highly sensitive to glycerol content [149, 150] and hence can be increased.

Finally, it is important to note two challenges that must be overcome before PLS/MAPP blends become viable elastomers. The first is the susceptibility of such materials to water since the glycerol plasticizer can be extracted by water. For example, upon immersion in water, the S85 blend remained physically, however, upon recovering this sample from water and drying it, a weight loss corresponding to the weight of glycerol was noted, and the sample was found to be brittle due to lack of plasticizer. This water susceptibility must be addressed for most potential applications as elastomers.

The second challenge is slow aging of the materials at room temperature. After three weeks of storage, the modulus of all three samples increased, and their ultimate elongation decreased. We believe that such aging is attributable to slow recrystallization of starch, as has

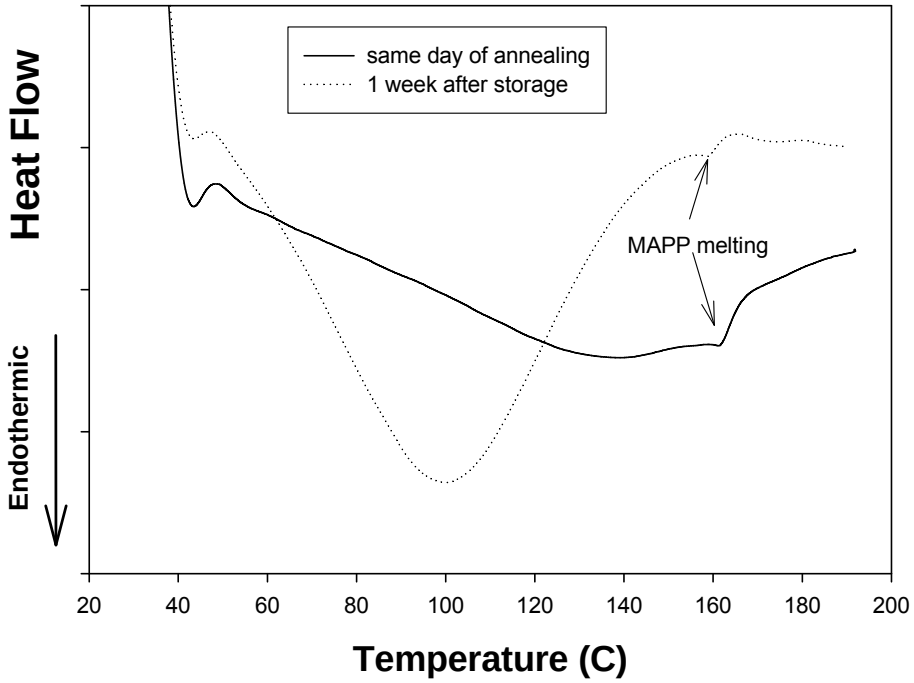


Figure 6.6. DSC data to illustrate effect of room-temperature aging.

also been noted previously [53]. To test whether such recrystallization had indeed occurred in our samples, we conducted DSC experiments: a sample of S95 was annealed at 200 ºF (~93ºC), allowed to cool to room temperature, and a DSC scan was conducted the same day. The sample was then stored at room temperature for one week, and another scan was conducted. Results are presented in Figure 6.6. Both samples show a small endotherm at about 160°C that corresponds to melting of polypropylene; this is consistent with the two-phase morphology suggested by SEM. However, the scan after storage for one week also shows a large and broad endotherm at lower temperatures suggesting crystallization of starch at room temperature. This same trend of slow recrystallization, also known as retrogradation, has been observed by previous researchers [49, 53, 54, 141]. Slow aging is a complication that must be addressed before starch-based elastomers can be used in practical applications.

## 6.3 SUMMARY

We have evaluated the potential for physically crosslinking glycerol-plasticized starch with maleated polypropylene so as to make renewable elastomers. PLS/MAPP blends were prepared by single-screw extrusion and injection-molded specimens were tested. Solubility and adhesion tests show that the MAPP is successful in physically crosslinking the starch, and DSC, DMA and SEM indicate a two-phase morphology consisting of MAPP domains surrounded by the PLS continuous phase. The MAPP/PLS blends have potential for elastomeric applications, as judged by the low $T_g$ of about -50°C, a rubbery plateau extending from room temperature up to as much as 170°C, and tensile properties within the range of many elastomers. Water-susceptibility and slow aging due to starch recrystallization are significant challenges that must be overcome before viable elastomers can be realized.

# 7.0 ENVIRONMENTAL IMPACTS OF PLASTICIZED STARCH AND POLYPROPYLENE BLENDS

Improvements to the processing and properties of plasticized starch (PLS), such as reactive blending with polyolefins and reinforcement of PLS with nanoclay, may lead to an increase of starch based plastics available commercially. This creates the possibility of starch based plastics competing with petroleum based plastics on a mass market level [151] and begs the question: Are starch-based plastics more environmentally friendly than their petroleum based counterparts? At first glance, degradable, starch based plastics may have more favorable environmental impacts than petroleum based plastics. However, without evaluating the materials in a systematic manner, no fair comparison can be made [89, 91-95, 152, 153]. The life cycle assessment (LCA) presented in this chapter is an evaluation of PLS/polypropylene (PP) blends comprised of varying PLS content. We also present the environmental impacts of the addition of nanoclay to PLS/PP blends.

## 7.1 SYSTEM BOUNDARIES AND METHODOLOGY

The goal of this LCA is to investigate the environmental impacts of varying starch content in PLS/PP blends. The LCA will examine the life cycle of a polymer pellet from cradle to factory gate, where the cradle is defined as the raw materials extraction for all processes and the gate is the completion of production of the polymer pellet or resin. The functional unit, or basis on which the environmental impact is analyzed, is defined as the weight of each material. All environmental impacts of the raw material extraction and transportation will be included. No end of life scenarios will be considered and the materials are assessed on a pellet to pellet comparison.

The system boundaries of the PP pellet are shown by the dotted line in Figure 7.1. To evaluate the environmental impacts of the PP portion of the polymer blends, we employ the use of the U.S. Life cycle inventory database [154] developed by the National Renewable Energy Laboratory (NREL) in association with Franklin Associates, which combines data from US companies, related literature and statistical sources.

Throughout the thesis, we discussed PLS made from both cassava and potato starches. Here, we focus on potato starch, rather than cassava starch, since the aim of this work is to model the impacts of PLS production in the United States, which generally implies the use of corn, potato, or wheat starch. Moreover, the U.S. LCI database includes data on potato agricultural practices, including energy use, emissions and transportation data, whereas such data are not readily available for cassava starch. For the PLS component of the polymer blends, potato agriculture is included in the life cycle (Figure 7.1). The system boundaries of the agriculture unit process begin at the production of raw materials. Carbon dioxide and sunlight are used from

the environment. Water is obtained through irrigation. Fertilizer is assumed to be NPK, or a nitrogen, phosphate and potassium mixture. Nitrogen, phosphate and potassium are the raw materials for the fertilizer and are derived from the air, phosphate rock and potash, respectively [155]. Pesticide production data is available from the U.S. EPA and tabulated by the U.S. LCI. It includes raw materials, formulation, packaging and labeling [156]. Irrigation and the energy and emissions associated with it will also be included in the agriculture process. Potatoes are harvested and then transported to be converted to dry starch. During the plasticization, glycerol is added to the dry starch to make PLS pellets. Glycerol was chosen as a plasticizer for starch, in part, for its life cycle benefits. Glycerol is a waste product of biodiesel production from soybeans. In general, using a waste or by product of an existing process is environmentally favorable. The dry PP pellets, the dry starch, and glycerol will all be extruded in one processing step. Since different ratios of starch and PP can result in different blend properties, the environmental trade-offs that arise in balancing petroleum based materials and starch based materials will be evaluated.

### 7.1.1 Inventory analysis and impact assessment

SimaPro 7 [157] is a software tool which uses industrial data to quantify the environmental impacts of a product or process. SimaPro 7 contains inventory databases that include energy uses and emission from many materials, fuels and processes. The U.S. LCI database and Franklin LCI database are built into the SimaPro 7 software and were used for all polypropylene components. Environmental data that are not included in SimaPro 7 were found in the literature [158]. Data for potato starch and PP were obtained from databases within Sima Pro7.

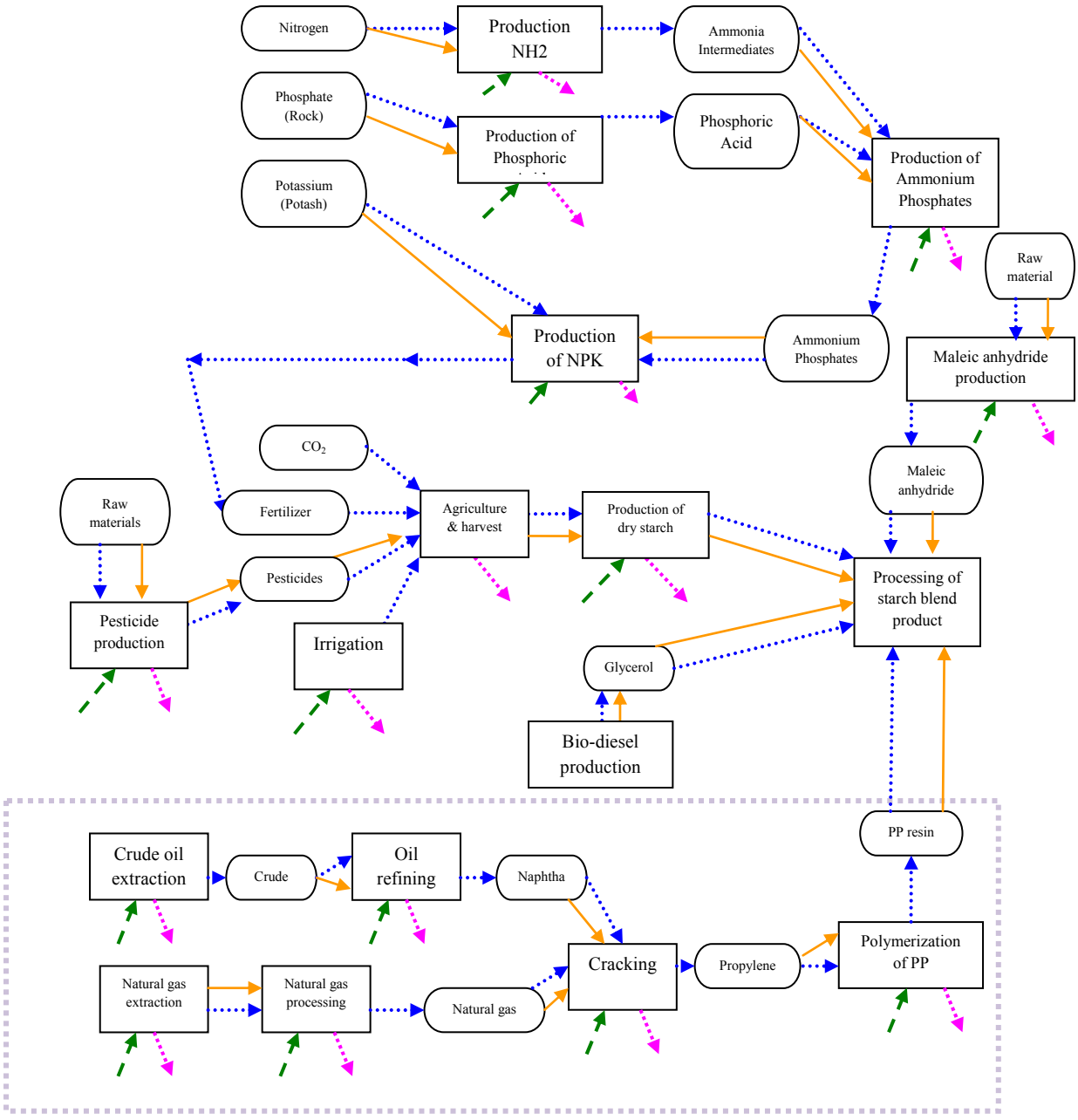


Figure 7.1. Flow chart of PLS/PP pellet production. The dotted line represents the flow process for production of PP pellet. The blue small-dotted arrows correspond to process flow. Orange solid arrows correspond to transportation of a material from one process to the next. Pink dotted and green dashed arrows correspond to the output of emissions and input of energy, respectively.

Maleic anhydride life cycle data were also obtained from SimaPro 7, and is based on direct oxidation on n-butane. Glycerol is modeled in SimaPro 7 as a by-product of biodiesel production from soybeans, which is suitable due to the glycerol surplus that has grown with increasing biodiesel production in the US [159]. The energy and material input and output for each unit process (see Figure 7.1 for flow chart) as well as all of the emissions are tabulated and analyzed using the Tools for the Reduction and Assessment of Chemical and other environmental Iimpacts (TRACI) [160]. TRACI is an assessment method designed by the U.S. EPA and built into SimaPro 7 that evaluates the inventory data by characterizing each substance's impact potential and classifying each substance into a midpoint impact category, rather than an endpoint category. Using this "midpoint" characterization approach, the impact assessment models reflect the relative potential of the environmental stressor at a common mid-point within the cause-effect chain (see Table 7.I). For example, the release of halogenated compounds into the atmosphere destroys ozone, which leads to an increase of UVB radiation. Endpoint effects of increased UVB radiation include skin cancer, crop damage, cataracts and many more [160]. The ability to be able to quantitatively correlate the release of an ozone depleting substance to an endpoint is difficult and varied. By using the midpoint approach, (in this case the midpoint is defined as the ozone depletion potential based on a substances reactivity) forecasting and effect modeling is minimized. Furthermore, the midpoint impact modeling approach allows for the use of more reliable data, eliminating some uncertainty in the model. Environmental categories defined in the TRACI assessment method are:

1. *Ozone depletion*. This impact category accounts for the depletion of the protective ozone layer in the earth's stratosphere due to harmful emissions like

chlorofluorocarbons, halons, etc. The midpoint of this category is selected on the basis of the potential of a chemical to destroy ozone based on its chemical activity and lifetime. The contribution in this impact category indicates the potential contribution to ozone depletion using

$$Ozone\ depletion\ index = \sum_i e_i \cdot ODP_i$$

where $e_i$ is the emission (in kilograms) of substance *i* and $ODP_i$ is the ozone depletion potential of substance *i*. This contribution is measured in terms of CFC-11 equivalents per kilogram of emission.

2. *Climate change*. This impact category refers to the change in earth's climate due to the build-up of chemicals that trap heat from the sun in the atmosphere. The global warming index is defined as

$$Global\ warming\ index = \sum_i e_i \cdot GWP_i$$

where $e_i$ is the emission (in kilograms) of substance *i* and $GWP_i$ is the global warming potential of substance *i*. The unit of contribution for this impact category is kilogram equivalents of $CO_2$.

3. *Acidification*. Acidification includes the processes that increase the acidity of water and soil systems by releasing the expected $[H^+]$ equivalents into the atmosphere from $SO_x$ and $NO_x$ emissions. The unit of contribution for this impact category is expressed in $[H^+]$ moles equivalent per kilogram of emission.

4. *Eutrophication*. Eutrophication potential is estimated based on the release of chemicals containing nitrogen or phosphorous into air or water. They are derived from a particular chemical's influence on algae growth in aquatic ecosystems and the probability that such a

chemical release arrives in an aquatic ecosystem. The contribution for this impact category is measured in terms of nitrogen equivalents released per kilogram of emission.

5. *Photochemical smog*. Photochemical smog is measured by incorporating three factors concerning $NO_x$ and Volatile Organic Chemicals (VOCs). They are: 1) the relative influence of individual VOCs on smog formation, 2) the relative influence of $NO_x$ and VOC mixtures on smog formation and 3) the geographical area upon which the emissions are released. The contribution in this impact category is measured in grams of $NO_x$ or equivalent.

6. *Human health: cancer and non-cancer*. The toxic effects of an emission on human health are calculated based on a human toxicity potential (HTP). HTPs are derived using a closed system, steady-state, multimedia model called CalTOX, a fate and exposure assessment tool for toxic chemicals [161]. The characterization factors are benzene and toluene equivalents per kilogram of emission for human health cancer and human health non-cancer, respectively.

7. *Human health criteria: respiratory effects*. This category accounts for the ambient concentrations of particulate matter which are strongly correlated with increases in the rates of chronic and acute respiratory symptoms. DALY's (Disability Adjusted Life Years) are used here to measure the overall burden of respiratory diseases. The contribution to this impact category is given in terms of DALYs per tonne of emission.

8. *Eco-toxicity*. Ecological toxicity potential is used to quantitatively measure the ecological harm of a given quantity of a chemical released in the environment. The contribution to this impact category is measured in terms of 2,4-dichloro-phenoxyacetic acid equivalents released per kilogram of emission.

Table 7.I. The cause and effect chain selection from Bare, et. al. [160].

| *Impact category and unit of measurement* | *Midpoint level selected* | *Level of site specificity selected* | *Possible endpoints or effects* |
|---|---|---|---|
| **Ozone depletion** *CFC-11 equivalents* | Potential to destroy ozone based on chemical's reactivity and lifetime | Global | Skin cancer, cataracts, material damage, immune-system suppression, crop damage, other plant and animal effects |
| **Global warming** *$CO_2$ equivalents* | Potential global warming based on chemical's radiative forcing and lifetime | Global | Malaria, coastal area damage, agricultural effects, forest damage, plant and animal effects |
| **Acidification** *[H+] moles equivalents* | Potential to cause wet or dry acid deposition | U.S., east or west of the Mississippi River, U.S. census regions, states | Plant, animal, and ecosystem effects, damage to buildings |
| **Eutrophication** *nitrogen equivalents* | Potential to cause eutrophication | U.S., east or west of the Mississippi River, U.S. census regions, states | Plant, animal and ecosystem effects, odors and recreational effects, human health impacts |
| **Photochemical smog** *$NO_x$ equivalents* | Potential to cause photochemical smog | U.S., east or west of the Mississippi River, U.S. census regions, states | Human mortality, asthma effects, plant effects |
| **Ecotoxicity** *2,4-DPA equivalents* | Potential of a chemical released into an evaluative environment to cause ecological harm | U.S. | Plant, animal and ecosystem effects |
| **Human health: air pollutants** *DALYs per tonne emission* | Exposure to elevated particulate matter less than 2.5 micron | U.S., east or west of the Mississippi River, U.S. census regions, states | Disability-adjusted life-years (DALYs), toxicological human health effects |
| **Human health: cancer** *benzene equivalents* | Potential of a chemical released into an evaluative environment to cause human cancer effects | U.S. | Variety of specific human cancer effects |
| **Human health: non-cancer** *toluene equivalents* | Potential of a chemical released into an evaluative environment to cause non-cancer effects | U.S. | Variety of specific human toxicological non-cancer effects |
| **Fossil fuel** *MJ surplus energy/MJ extracted energy* | Potential to lead to the reduction of the availability of low cost/energy fossil fuel supplies | Global | Fossil fuel shortages leading to use of other energy sources, which may lead to other environmental or economic effects |
| **Land use** *human and animal use, scarcity* | Proxy indication expressing potential damage to threatened and endangered species | U.S., east or west of the Mississippi River, U.S. census regions, states | Effects on threatened and endangered species ( as defined by proxy indicator) |
| **Water use** *gallon of water* | Potential for significant water use in areas of low availability | U.S. | Water shortages leading to agricultural, human, plant, and animal effects |

9. *Fossil fuel use*. The contribution in this impact category is calculated using

$$Fossil\ Fuel\ index = \sum_i N_i \cdot F_i$$

where $N_i$ is the increase in energy input requirements per unit of consumption of fuel *i*, and $F_i$ is the consumption of fuel *i* per unit of product. The contribution in this impact category is measured in MJ of surplus energy per MJ of extracted energy in the process.

10. *Land use*. TRACI uses the density of threatened and endangered (T&E) species in a specific area as measurement of the environmental importance of land. The contribution in this category is calculated using

$$Land\ Use\ index = \sum_i A_i \cdot (T\&E_i)/CA_i$$

where $A_i$ is the human activity per functional unit of the product, $T\&E_i$ is the T&E species count for the county and $CA_i$ is the area of the country under consideration.

11. *Water use*. This impact category of TRACI analysis is designed to capture the significant use of water, in mass or volume, in areas of low availability. The contribution unit for this impact category is the gallon.

## 7.2 RESULTS AND DISCUSSION

### 7.2.1 Impacts of polypropylene and plasticized starch polymer blends

We first present the life cycle impacts that result from the production of PLS100 and PP resins, comparing them on a weight to weight basis within the system boundaries. The results of the assessment are presented in Figure 7.2 and, for comparison purposes, are normalized to the material having the largest magnitude of impact value. For example, in the category of global warming impact, PLS100 has less impact potential than PP, but the figure is normalized to negative 1 since the global warming impact magnitude of PLS100 is larger. PLS100 has less environmental impact in all categories except eutrophication, ozone depletion and smog formation potentials and we first discuss these three categories.

Eutrophication results from the release of nitrogen or phosphorus into aquatic ecosystems. Not surprisingly, the fertilizer use associated with the agricultural processes of starch production is the cause of the high eutrophication potential. In the case of PP, the small eutrophication impact is attributable to the use of natural gas and crude oil during the production and processing stages.

Halogenated compounds are primarily responsible for ozone depletion. The process of starch extraction from potatoes includes the heating and compression of potatoes as well as the drying of the extracted starch. The starch extraction process, as modeled in the LCA, employs its heat from diesel sources, which emit bromotrifluoromethane, also known as Halon 1301, into the air and contribute to ozone depletion. The emissions that result from the transportation of PP are the main contributors to its ozone depletion potential.

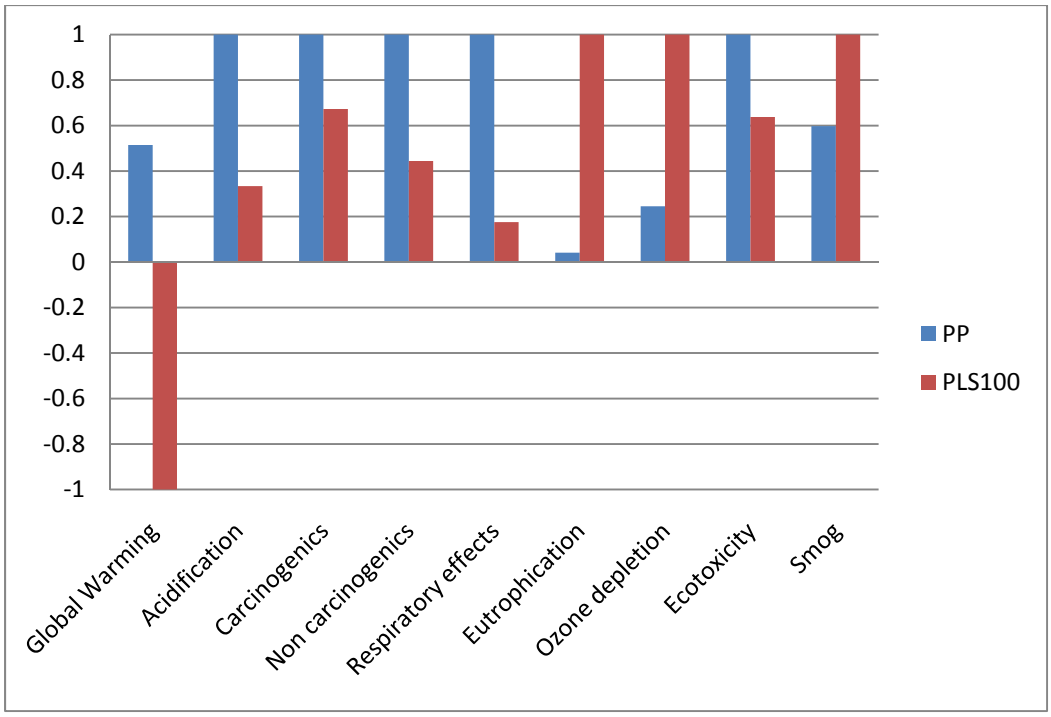


Figure 7.2. The comparative life cycle assessment results of plasticized starch vs. maleated polypropylene on a weight basis.

Smog formation potential, measured in kg of $NO_x$ equivalents, is greater for PLS100 than PP. The primary contributor for both polymers is emission of nitrogen oxides, while emissions from potato plant production also include dinitrogen oxides and ammonia.

Turning to the categories in which PP has a greater impact than PLS, the global warming potential is greater than that of PLS100 due to the use of natural gas during the production process. In fact, there is a negative impact in global warming potential for PLS100 since the potato plant itself is able to take $CO_2$ out of the environment during the its growth.

PP production also has an acidification potential of nearly 4 times that of PLS100. The acidification potential of PLS100 is attributable to the production of potatoes which emits ammonia and nitrogen oxides into the air, both of which significantly contribute to acidification. The emission of sulfur oxides from the natural gas used to produce PP are the cause for its

acidification potential, and are emitted is high quantities compared with that the emissions from PLS100 production.

In the categories of the carcinogens, non-carcinogens and respiratory effects, the main contributors for the both PLS100 and PP are the emissions from the energy use throughout the production processes. The use of natural gas and crude oil in the production of PP accounts for 83% of the effects in the three said categories. The energy use in the production of PLS100 is also the main contributor to these categories, but the overall energy expense of the process is less than of PP.

The differences in ecotoxicity impact potentials of PLS100 and PP are attributable to glycerol. The major contributions to ecotoxicity arise from the crude oil extraction and natural gas use during extraction for PP production and the overall emissions from potato plant production. However, PLS100 is plasticized using glycerol, which comprises 40% by weight of PLS100. Here, glycerol is modeled as a by-product of biodiesel production from soybeans. The cultivation of soybeans results in the uptake of many elemental substances from the soil into the plant, including cadmium, chromium, copper and nickel [162], creating an "eco-toxicity negative" impact potential for glycerol and decreasing the overall impact of PLS100.

Thus far, the context of this LCA has been on a pellet to pellet, or weight to weight, basis. Although polymers resins are often sold on a weight basis, they are molded and sold as products on a volume basis. Taking this into consideration and assuming that one kilogram of PLS can replace one kilogram of PP for a given application, a volume comparison of PLS and PP is presented in Figure 7.3. One kilogram of PLS100 (calculated as the weighted average of potato starch and glycerol) and PP correspond to ~1.4 L and 0.9 L, respectively. From Figure 7.3, it is

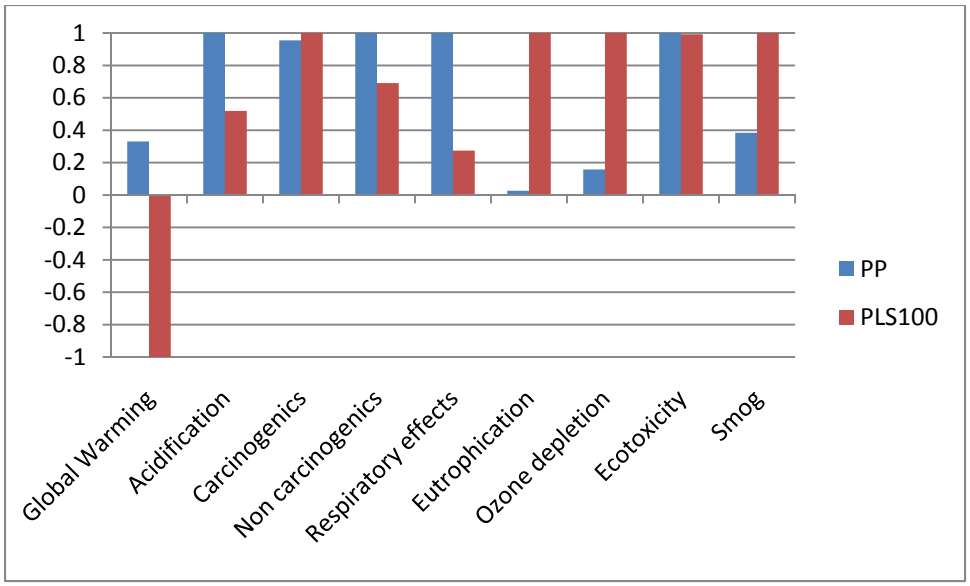


Figure 7.3. The comparative life cycle assessment results of plasticized starch vs. maleated polypropylene on a volume basis.

clear that PP still has a greater impact in most of the categories. However, the environmental benefits that PLS100 had compared with PP in the weight to weight comparison have waned. In fact, PLS100 now has a greater impact in the carcinogenics category. From a volumetric point of view, PLS100 is still environmentally advantageous to PP, but not by such a clear margin. In any case, we do not propose that PLS100, alone, is an apt substitute for PP. In fact, as discussed throughout much of this thesis, modifications, such as blending PLS with PP or reinforcing PLS with clay, can be made to PLS100 to improve its mechanical properties and make it a more viable alternative to commodity plastics. The environmental impacts of these modifications will be discussed in following sections.

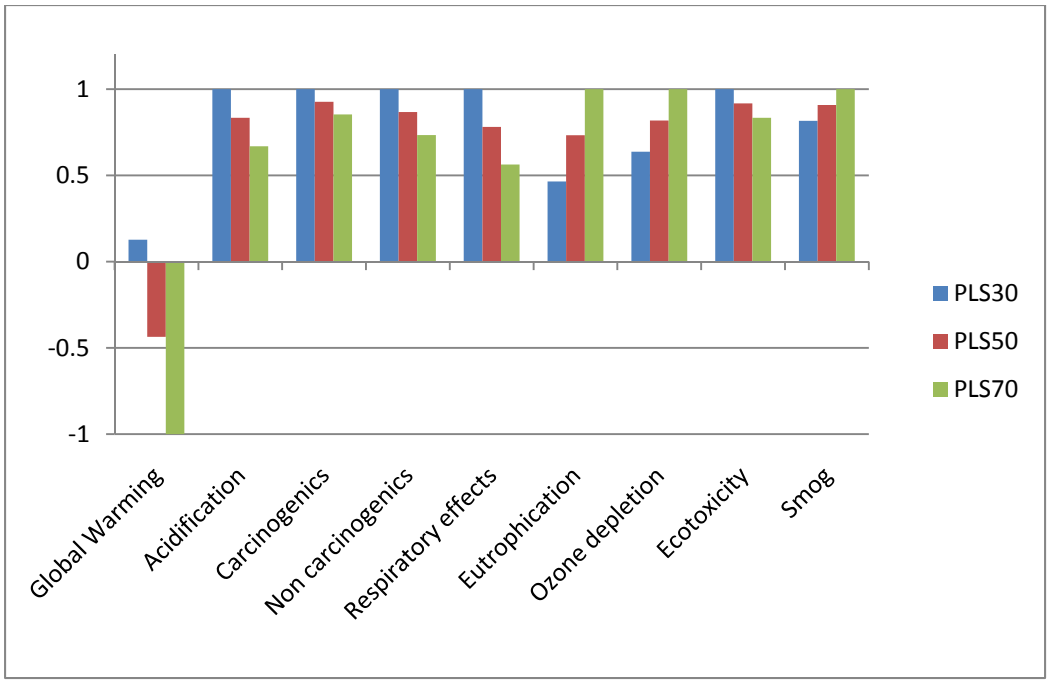


Figure 7.4. The environmental impacts of PLS/PP blends.

Finally, it is noteworthy that in most of the impact categories, the energy use during the life cycle of the material was found to be most detrimental to many of the impact categories. From the LCA, we calculated that non-renewable energy costs for PP are approximately 87 MJ/kg while those for PLS100 are 17.5 MJ/kg. This elucidated an important point: non-renewable energy sources are used to create both renewable and non-renewable materials. The overall impact would likely be significantly different if some portion of the energy sources were renewable and had less environmental impact.

### 7.2.2 Environmental impacts of PLS/PP blends

We next discuss the environmental impact of PLS/PP/MAPP blends, where the maleated polypropylene is added to compatibilize the polymer blends as discussed in Chapters 5.0 and 6.0.

The LCA results for three different blend compositions PLS30, PLS50 and PLS70 are presented in Figure 7.4. The graph displays a weight comparison of the three blends. Following directly from our analysis of the pure components, eutrophication, smog formation and ozone depletion increase in PLS/PP blends as PLS content increases, while all the remaining impact categories are favored by increasing PLS loadings.

### 7.2.3 Effect of the addition of clay to PLS/PP blends

Since researchers at Toyota first began adding layered silicate clays to nylon in the 1990s [130], clay based nanocomposites have been extensively researched [74, 78, 163, 164]. Nanoclays have been shown to greatly improve the mechanical properties of polymer due to their high aspect ratio, without greatly increasing the overall weight of the material. The addition of nanoclay to any polymer may adversely affect the environmental impacts, but an increase in the mechanical properties may be worth the environmental compromises. In effect, smaller quantities of polymer would be needed if the properties are improved. We present the environmental impacts of the addition of 5% by weight of unmodified clay, sodium montmorillonite (MMT), and 5% of a generic organically modified (OMMT) clay to glycerol plasticized starch, corresponding to the environmental impacts of PLS100, PLS100-MMT and PLS100-30B presented in Chapter 5.0 (Recall that 30B is organically modified layered silicate

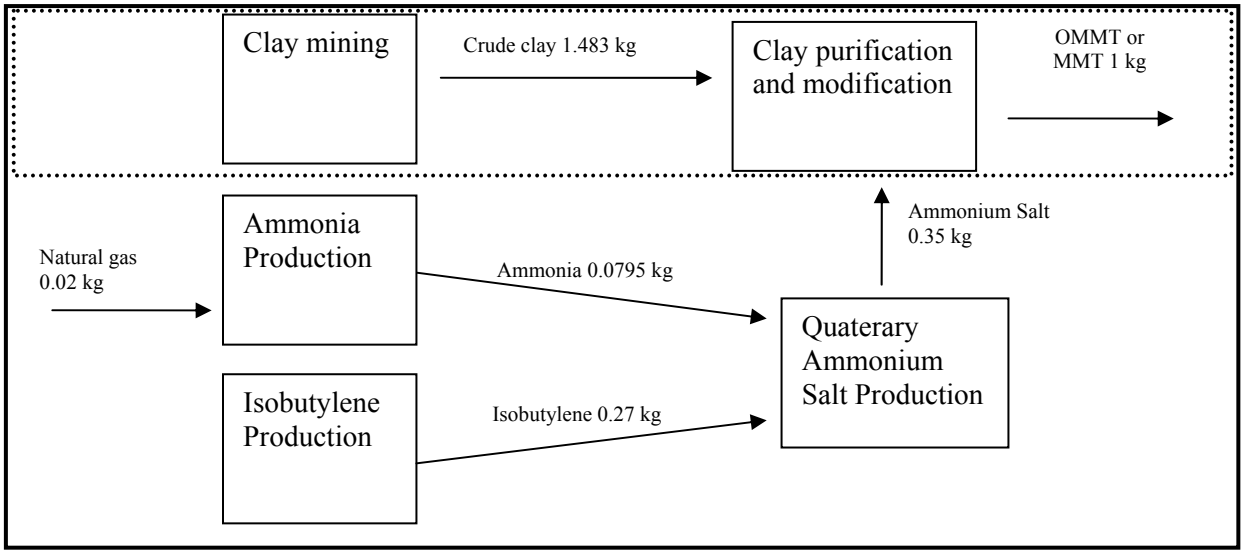


Figure 7.5. The life cycle system boundaries for the production of unmodified clay (boundary shown by the dotted line) and organically modified clay (boundary shown by the solid line).

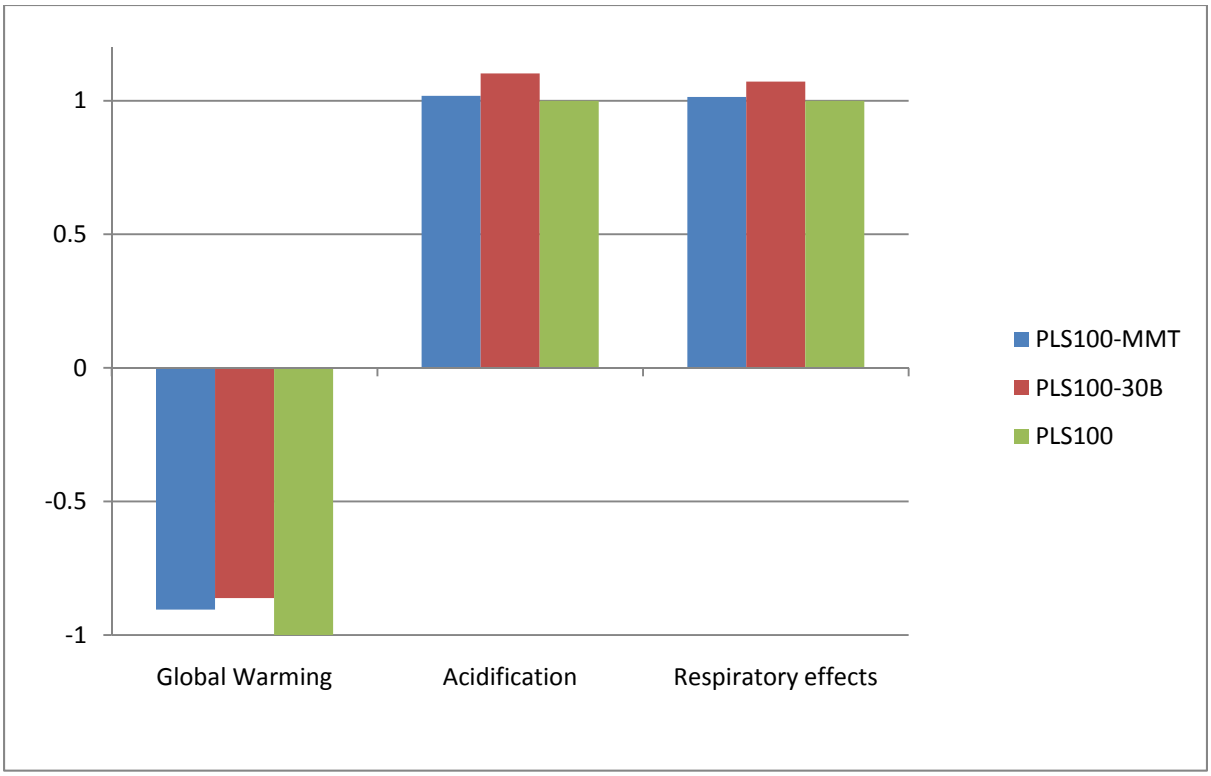


Figure 7.6. The environmental effects of the addition of nanoclay to PLS100.

clay from Chapter 5.0 and is analogous to the OMMT modeled here). Information on the production processes, fuel, and other input requirements for producing nanoclays is mostly proprietary and not generally available. However, Joshi et. al. [158] have taken data from Southern clay, a layered silicate producer and combined it with energy and fuel data from personal communication with Franklin Associates to estimate the cradle to gate impacts of the production of 1 kg of OMMT. The system boundary, including raw materials and processing for clay production is drawn in Figure 7.5, where the solid box denotes the boundary for OMMT and the dashed box denotes the boundary for MMT. According to Joshi, clay production includes separation, purification, delamination, reaction with organic modifiers (for OMMT), homogenization, dewatering, and size reduction. For production of OMMT, counter ion techniques are used for delamination and 35% of organic modifier is added. This percentage is based on average amounts in various modified Cloistie ® clays produced by Southern Clay Products [165]. All material and energy inputs as well as the emissions for clay production were taken from Joshi's work and used in SimaPro7 without modification. The addition of clay replaces the polymer on a weight basis.

Overall, the addition of either clay to PLS had little effect on the environmental impact of the materials. In fact, upon the addition of either MMT or 30B to PLS100, less than a five percent change (positive or negative) was observed in the categories of carcinogenics, non-carcinogenics, ecotoxicity and ozone depletion, eutrophication and smog. Therefore, the remainder of the discussion will focus on the categories affected most by the addition of clay. The global warming potential, acidification and respiratory effects presented in Figure 7.6 and *normalized to the PLS100 data*.

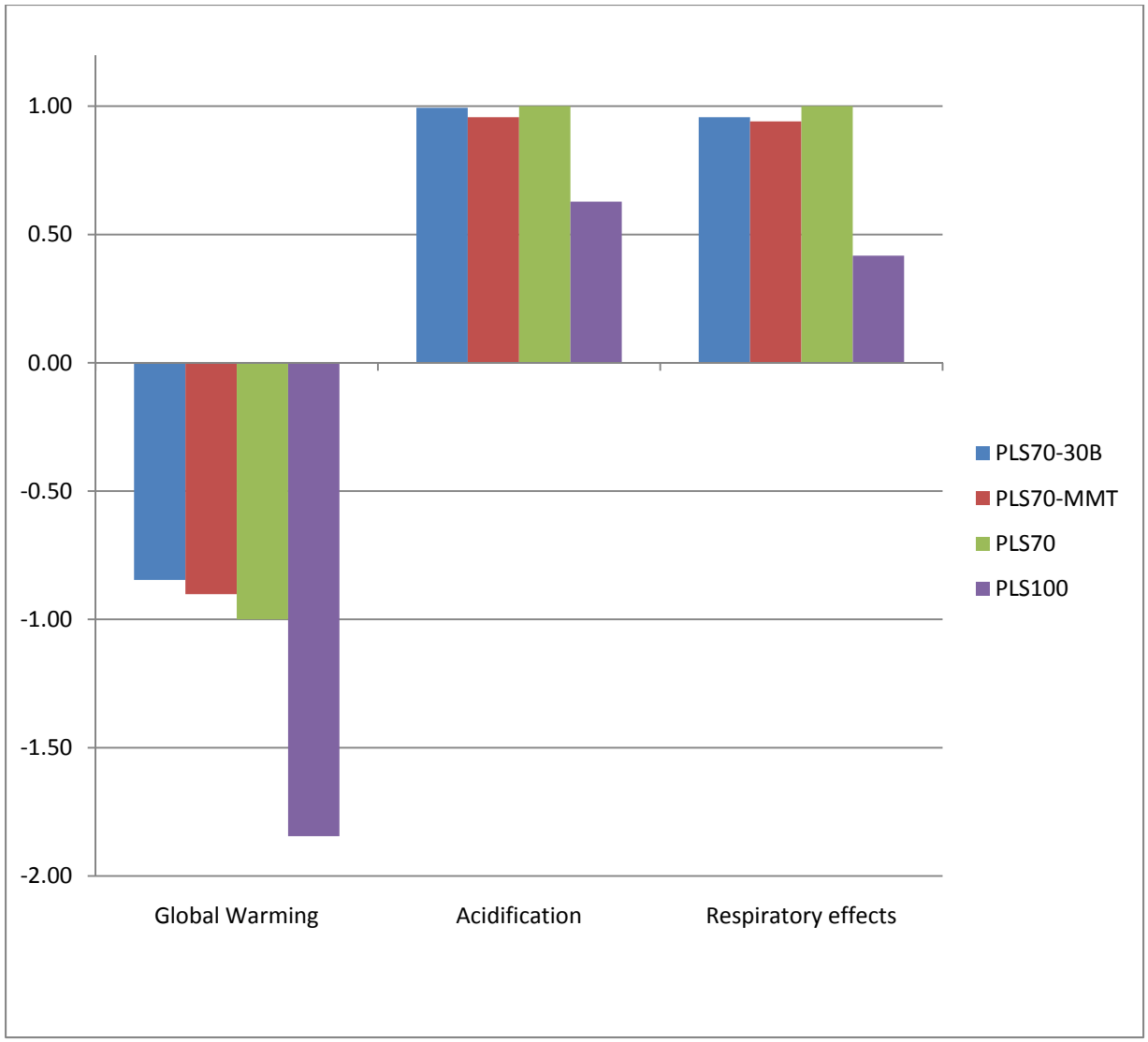


Figure 7.7. The environmental impact of nanoclay to PLS70.

The addition of MMT does not have a significant impact on acidification or respiratory effects (<3%), but increases global warming potential by more 10%. The OMMT clay has a greater impact than MMT in all three categories, especially global warming potential. Recall from Section 5.2.5, that the mechanical properties of PLS100 were so poor that the samples would fail while being loaded into the tensile testing apparatus. The addition of 5% by weight of either clay to PLS100 improved the properties such that they were able to be handled easily and characterized. Aside from global warming potential, the improvement in mechanical properties as a result of the addition of clay is nearly without environmental compromise, i.e. the addition of clay does not adversely affect the environmental properties of PLS100.

Finally, Figure 7.7 presents the environmental impacts of PLS70, with and without the addition of clay and all data are normalized to PLS70 (shown in green). The increase in impact potential of PLS70 from the addition of PP, in the categories shown in Figure 7.7 was discussed in Section 7.2.1 and PLS100 is included here as a frame of reference. We observe only a small increase in global warming potential with the addition of MMT or OMMT. Remarkably, the acidification and respiratory effects potentials *decrease* with the addition of nanoclay to PLS70. Our mechanical characterization of the PLS70 samples with clay showed great increases in the tensile strength and modulus from the addition of either clay. Here, the addition of PP and nanoclay to PLS100 results in a material with both improved mechanical properties as well as minimal increase in environmental impact.

## 7.3 CONCLUSIONS

A comparative life cycle assessment of a petroleum-based polypropylene and plasticized starch was conducted on a weight and volume basis using TRACI as the assessment tool. The categories in which PLS had greater environmental impact than PP were eutrophication potential, ozone depletion potential and smog formation, attributable to fertilizer use, the extraction of starch from potatoes and emissions from potato production, respectively. The impacts of PLS/PP blends were also investigated and revealed tradeoffs that must be considered when combining non-renewable materials with renewable materials. The results suggest that PLS is not a definitively "greener" material than PP.

The impacts of the addition of layered silicate clays to PLS were also investigated. The environmental impacts of PLS nanocomposite materials decreased in the categories of acidification potential and respiratory effects potential. Overall, the small increase in the environmental impact was outweighed by the improvement in mechanical properties resulting from the clay.

# 8.0 FUTURE DIRECTIONS

## 8.1 MORPHOLOGY CONTROL USING CROSSLINKED COMPATIBILIZERS

In Chapter 3.0, we presented a comparison of compatibilization using diblock copolymers vs. using reactive compatibilization. The morphological effects of reactive blending are non-spherical droplets which fuse together forming an interfacial "skin". This can be attributed to the mechanically robust interface that results from interfacial crosslinking. Such interfacial robustness may lead to increased stability in polymer blends with crosslinkable compatibilizers compared to diblock compatibilizers. We believed that such a crosslinked interface offers opportunities for realizing unusual anisotropic morphologies in polymer blends. Anisotropic morphologies are generally difficult to achieve because the interfacial relaxation process drives the system towards isotropic morphologies. Simple mixing won't overcome the interfacial relaxation. To achieve an anisotropic microstructure, the interfacial relaxation process must be overcome by the interfacial compatibilization reaction occurring as quickly as the deformation of the dispersed phase. One way in which this may be examined is by extruding a reactively compatibilized blend through a capillary tube to achieve long fibular structures that do not break up.

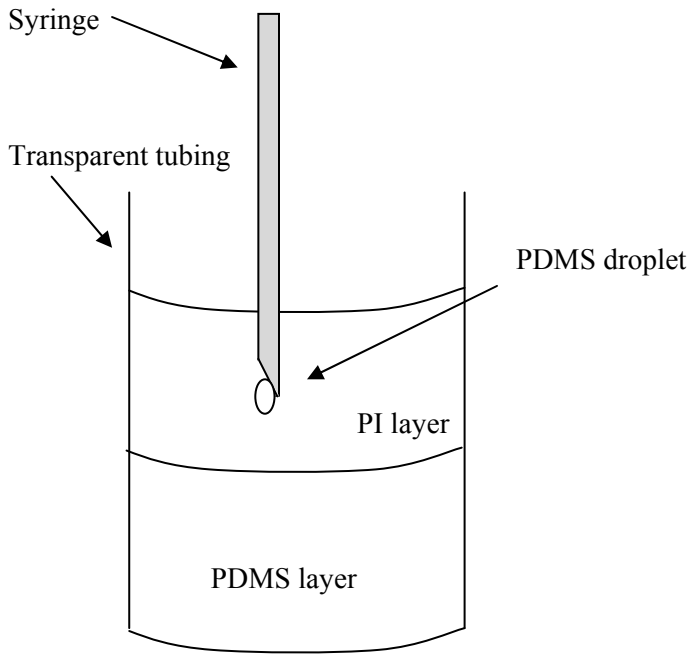


Figure 8.1. Schematic of proposed experimental procedure.

To reiterate, the speed of the reaction, with respect to the rate of deformation, is crucial and the anhydride/amine reaction used in Chapters 3.0 and 4.0 may prove to be too slow to achieve anisotropic morphologies. In that case, another immiscible polymer blend may be used. For example, one well known rapidly occurring reaction is a urethane linkage, which can be accomplished using blend components with isocyanate and hydroxyl functionality.

The asymmetric interaction between droplets in both PI and PDMS continuous blends also needs to be further investigated. As discussed in Chapter 4.0, the asymmetric behavior was attributable to the fact that in PI continuous blends, PDMS droplets appear to stick together, while in the opposite situation, PI droplets do not. We speculated that the differences in droplet interactions were a result of the compatibilizer architecture and the homopolymer chain length. We propose conducting further experiments with the PI/PDMS model system to explore this behavior using the following procedure. A several millimeter thick layer of PI can be placed on

top of an equally thick layer of PDMS as shown by the schematic in Figure 8.1. By injecting a droplet of PDMS into the PI phase of the "bilayer", the interaction of the droplet with the PDMS phase can give insight on the coalescence and sticking behavior of the droplet phase of the blends discussed throughout Chapters 3.0 and 4.0.

## 8.2 CONTROLLING RETROGRADATION IN PLASTICIZED STARCH

As noted in Chapter 6.0, one challenge that is faced when processing glycerol plasticized starch is slow aging, known as retrogradation, attributable to recrystallization of starch. Such aging causes the starch material to become brittle over time and is detrimental to the practical use of starch as an elastomer or plastic.

In general, crystallization is highly sensitive to molecular mobility and the effect of nucleating agents. Clays may restrict chain mobility but may also act as nucleating agents. One research goal is to explore the effects of the addition of nanoclay to PLS on starch retrogradation. It is our hypothesis that the addition of nanoclay will affect aging and we seek to examine the retrogradation behavior of PLS/MAPP blends with added layered silicates. To test this hypothesis, we conducted preliminary experiments on annealed samples stored under controlled temperature and humidity and measured changes in thermal behavior over time using DSC. The samples used here were the same samples used previously and contained 5% clay by weight (preparation procedure from Chapter 5.0). DSC experiments were conducted on PLS100 and PLS100-MMT and we were able to identify the recrystallization endotherm in both samples to be at ~150°C. The recrystallization occurred in the PLS100 over 6-10 days. Due to technical difficulty with the DSC, we were unable to establish a clear baseline surrounding the endotherm

observed in the DSC data, which adversely affected accurate calculation of the heat associated with the transition.

We also compared the difference in aging over a 6 day period for PLS100 and PLS100-MMT using DSC experiments. Upon the addition of an unmodified sodium montmorillonite (MMT, also used in Chapter 5.0), a decrease in the recrystallization peak was observed, but the lack of a clear baseline prohibited a quantitative comparison.

While promising, the preliminary research was hampered by a lack of confidence is the calorimeter. Therefore, further DSC experiments are necessary. The greatest challenge is that in order to DSC as a quantitative tool, it is desirable to plot the data in heat capacity units, which affords the luxury of proper integration limits for measurement of polymer crystallinity. Identifying such a baseline is often difficult and requires precise data acquisition and reliable equipment.

Other methods may also be employed to address PLS retrogradation. For example, increasing the hydrogen bonding between the starch chains and the plasticizer is one approach to starch chain immobilization. The use of different plasticizers, such as those containing amine groups may be used to accomplish this, as amines can more readily form hydrogen bonds with starch as compared to polyols [51], but this may adversely affect the environmental properties of the resulting material.

## 8.3 SMALL MOLECULE CROSSLINKING AGENTS

In Chapter 6.0, we presented novel renewable elastomers based on starch. To complete the characterization of any elastomeric material, recovery after large deformation must be

considered. The ability of rubber compounds to retain elastic properties after prolonged action of compressive stresses is generally given by compression set measurements. Compression set is defined as the residual deformation of a slab material after removal of an applied compressive stress. Resistance to compression set is the ability of the slab of an elastomeric material to recover to its original thickness after having been compressed for an extended period. Low set values mean that the material has recovered nearly to its original thickness, and there is very little residual deformation, indicative of a good rubber.

Preliminary compression set measurements were performed on the samples described in Chapter 6.0 (PLS100, PLS95 and PLS85) using a Wykeham-Farrance 5-ton compression device, fitted with a displacement gauge to measure sample thickness during the experiment. Three millimeter thick samples were placed in the compression apparatus and compressed by 25% of the original thickness to about 2.25 mm for time intervals ranging from 1 minute to 24 hours. The obtained compression set data are plotted in Figure 8.2. At short compression times (less than one minute), the samples displayed nearly full recovery. As the set time increased to 24 hours, PLS100 had the lowest compression set and therefore best elastic recovery, but PLS85, which more highly physically crosslinked, recovered little of its deformation. The results contradict a conclusion Chapter 6.0: a higher degree of crosslinking does not result in better elastic recovery. Therefore, there is a need to explore small molecule crosslinking agents to replace the large molecule maleated polypropylene.

We had previously proposed the use of diisocyantes or dianhydrides as alternative, small molecule crosslinking agents. Both have sufficient functionality to ensure crosslinking and no leaving group results from either reaction. We explored the use of pyromellitic dianhydride (PMDA) as an alternative crosslinking agent. Potato starch was plasticized with glycerol (40%

by weight) and mixed in a Haake Batch mixer with either 0% PMDA, 1% PMDA in DMSO, 5% PMDA in DMSO or 5% dry PMDA. After processing the samples were put under vacuum conditions for 24 hours to eliminate any DMSO that had not evaporated during the processing procedure. Similar to our characterization in Chapter 6.0, we first attempted to confirm the crosslinking reaction using solubility testing in DMSO. Upon, immersion in DMSO for 24 hours, all four samples dissolved completely, suggesting a lack of any reaction between the hydroxyl groups of the starch and the dianhydride.

The attempt to crosslink PLS using PMDA discussed in this section constitutes very preliminary work and, even though a crosslinked material was not realized, creating a renewable, degradable crosslinked material suited for elastomeric applications is worthy of further investigation. Changes to the preparation and processing procedure, such as pre-mixing PMDA with PLS or using more distributive processing equipment, can be used to progress the research.

Finally, diisocyanates are known to readily react with hydroxyl groups to form a urethane linkage. In light of the failure of the PMDA experiments, future research conducted in starch elastomers can take advantage of the well studied isocyanate-hydroxyl reaction. However, the main theme throughout this thesis has been sustainable engineering and the toxicity of isocyanates discouraged us from proceeding further with their use to crosslink starch.

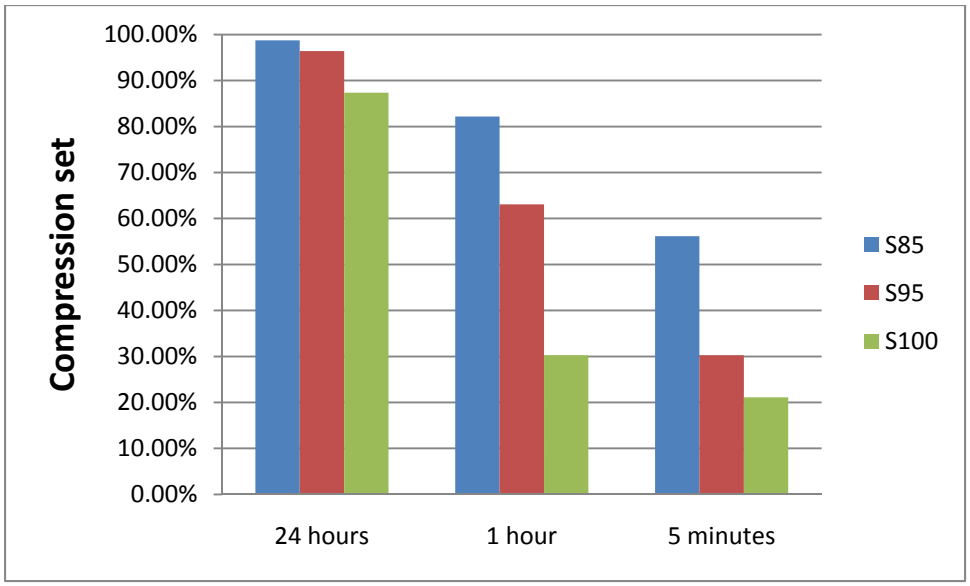


Figure 8.2. Compression set data for the samples discussed in Chapter 6.0. Lower compression set values are indicative of better elastic recovery.

## 8.4 END OF LIFE ANALYSIS OF BIOPLASTICS

### 8.4.1 Degradation of biopolymers

Chapters 5.0 and 6.0 discuss the preparation, processing and characterization of starch based materials as sustainable substitutes for commodity plastics or elastomers. While the LCA methodology is well-developed for cradle-to-gate evaluations, the end of life scenarios of products after being discarded is very poorly characterized. The means of disposal is critical. For example, a plastic grocery bag may be incinerated to generate energy, thrown in a landfill or discarded outside the waste stream. The differences in the environmental impact of these

scenarios are likely large and must be considered when comparing the life cycles of products. Therefore, a future research direction would be to shift the focus to the end of life of biomaterials by conducting soil degradation tests which monitor the degradation rates by measuring both sample weight loss and $CO_2$ emission. Such data is useful for appropriately assessing impact of bioplastics in any end of life scenario.

### 8.4.2 Life cycle assessment

The results of our comparative cradle-to-gate life cycle assessment (Chapter 7.0) of starch based materials vs. commodity plastics showed many environmental tradeoffs and no clear winner between the two types of materials. Using life cycle assessment in combination with resulting data from the degradation experiments described above, the end of life scenario of biopolymers can be compared with typical end of life scenarios, such as landfills or recycling, for polyolefins such as polystyrene and polypropylene. Moreover, landfill gas recovery of carbon dioxide and methane is being increasingly implemented throughout the United States, Canada and Europe. Understanding the byproducts of landfill gas recovery, such as $CO_2$ emissions resulting from the degradation or composting of biopolymers in landfill conditions, is crucial in being able to have a thorough understanding of the production of landfill gas.

## BIBLIOGRAPHY


1. Averous, L., *Biodegradable Multiphase Systems Based on Plasticized Starch: A Review.* Journal of Macromolecular Science-Polymer Reviews, 2004. **C44**(3): p. 231-274.

2. Griffin, G.J.L., *British Patent 1,586,344*, in *British Patent*. 1973.

3. Bikiaris, D. and C. Panayiotou, *LDPE/starch blends compatibilized with PE-g-MA copolymers.* Journal of Applied Polymer Science, 1998. **70**(8): p. 1503-1521.

4. Shogren, R.L., et al., *Structure and morphology of baked starch foams.* Polymer, 1998. **39**(25): p. 6649-6655.

5. Fang, Q. and M.A. Hanna, *Characteristics of biodegradable Mater-Bi®-starch based foams as affected by ingredient formulations.* Industrial Crops and Products, 2001. **13**(3): p. 219-227.

6. Macosko, C.W., et al., *Compatibilizers for Melt Blending: Premade Block Copolymersâ€* Macromolecules, 1996. **29**(17): p. 5590-5598.

7. Lyu, S., Jones, T.D., Bates, F.S., Macoskso, C.W., *Role of Block Copolymers on Suppression of Droplet Coalescence.* Macromolecules, 2002. **35**: p. 7845-7855.

8. Hu, Y.T., D.J. Pine, and L.G. Leal, *Drop deformation, breakup, and coalescence with compatibilizer.* Physics of Fluids, 2000. **12**(3): p. 484-489.

9. Milner, S., T. and H. Xi, *How copolymers promote mixing of immiscible homopolymers.* Journal of Rheology, 1996. **40**(4): p. 663-687.

10. Van Hemelrijck, E., et al., *Interfacial elasticity and coalescence suppression in compatibilized polymer blends.* Journal of Rheology, 2004. **48**(1): p. 143-158.

11. Graebling, D., R. Muller, and J.F. Palierne, *Linear Viscoelastic Behavior of Some Incompatible Polymer Blends in the Melt - Interpretation of Data with a Model of Emulsion of Viscoelastic Liquids.* Macromolecules, 1993. **26**(2): p. 320-329.

12. Martin, J., Velankar, S., *Effects of Compatibilizer on Immisicible Polymer Blends Near Phase Inversion.* Journal of Rheology, 2007. **51**(4): p. 669-692.

13. Tucker, C.L. and P. Moldenaers, *Microstructural evolution in polymer blends.* Annual Review of Fluid Mechanics, 2002. **34**: p. 177-210.

14. Velankar, S., et al., *Steady-shear rheological properties of model compatibilized blends.* Journal of Rheology, 2004. **48**(4): p. 725-744.

15. Wang, J. and S. Velankar, *Strain recovery of model immiscible blends: effects of added compatibilizer.* Rheologica Acta, 2006. **45**(5): p. 741-753.

16. Baker, W.E., C.E. Scott, and G.-H. Hu, *Reactive Polymer Blending*, ed. K.S. Hyun. 2001, Munich.

17. Jeon, H.K., et al., *Coupling reactions of end- vs mid-functional polymers.* Macromolecules, 2004. **37**(7): p. 2563-2571.

18. Schulze, J.S., et al., *Reaction kinetics of end-functionalized chains at a polystyrene/poly(methyl methacrylate) interface.* Macromolecules, 2000. **33**(4): p. 1191-1198.

19. Cernohous, J.J., C.W. Macosko, and T.R. Hoye, *Anionic synthesis of polymers functionalized with a terminal anhydride group.* Macromolecules, 1997. **30**(18): p. 5213-5219.

20. Kim, H.Y., et al., *The effect of chain architecture of in situ formed copolymers on interfacial morphology of reactive polymer blends.* Macromolecular Rapid Communications, 2005. **26**(17): p. 1428-1433.

21. Yin, Z., et al., *Probing of the reaction progress at a PMMA/PS interface by using anthracene-labeled reactive PS chains.* Langmuir, 2003. **19**(2): p. 453-457.

22. Koning, C., et al., *Strategies for compatibilization of polymer blends.* Progress in Polymer Science, 1998. **23**(4): p. 707-757.

23. Brown, S.B., et al., *Solvent-resistant, compatible blends of polyphenylene ethers and thermoplastic polyesters*. 1992, General Electric Company: US.

24. Aycock, D.F. and S.-P. Ting, *Acyl modified polyphenylene ether composition*. 1987, General Electric Company: US.

25. Aycock, D.F. and S.-P. Ting, *Polyphenylene ether-polyamide blends*. 1986, General Electric Company: US.

26. Datta, S. and D.J. Lohse, *Polymeric compatibilizers*. 1996, Munich: Hanser Publishers.

27. Lee, P.C., W.F. Kuo, and F.C. Chang, *In-situ compatibilization of PBT/ABS blends through reactive copolymers.* Polymer, 1994. **35**(26): p. 5641-5650.

28. Martin, P., et al., *Competitive reactions during compatibilization of blends of polybutyleneterephthalate with epoxide-containing rubber.* Polymer, 2001. **42**(6): p. 2463-2478.

29. Hale, W., H. Keskkula, and D.R. Paul, *Compatibilization of PBT/ABS blends by methyl methacrylate glycidyl methacrylate ethyl acrylate terpolymers.* Polymer, 1999. **40**(2): p. 365-377.

30. Wildes, G.S., et al., *Synthesis and characterization of an amine-functional SAN for the compatibilization of PC/ABS blends.* Polymer, 1999. **40**(11): p. 3069-3082.

31. Zhang, H., et al., *Reactive compatibilization of blends containing liquid crystalline polymers.* Polymer, 2000. **41**(8): p. 3069-3082.

32. Lin, B., et al., *Effect of premade compatibilizer and reactive polymers on polystyrene drop deformation and breakup in simple shear.* Macromolecules, 2005. **38**(13): p. 5609-5616.

33. Sundararaj, U. and C.W. Macosko, *Drop breakup and coalescence in polymer blends: The effects of concentration and compatibilization.* Macromolecules, 1995. **28**(8): p. 2647-2657.

34. Beck Tan, N.C., D.G. Peiffer, and R.M. Briber, *Reactive reinforcement of polystyrene/poly(2-vinylpyridine) interfaces.* Macromolecules, 1996. **29**(14): p. 4969-4975.

35. Beretta, C. and R.A. Weiss, *Miscibility enhancement of polymer blends by interacting functional groups.* Polymeric Materials Science and Engineering, 1987. **56**: p. 556-9.

36. Sun, Y.J., et al., *In situ compatibilization of polyolefin and polystyrene using Friedel-Crafts alkylation through reactive extrusion.* Polymer, 1998. **39**(11): p. 2201-2208.

37. Kim, S., J.K. Kim, and C.E. Park, *Effect of molecular architecture of in situ reactive compatibilizer on the morphology and interfacial activity of an immiscible polyolefin/polystyrene blend.* Polymer, 1997. **38**(8): p. 1809-1815.

38. Tselios, C., et al., *In situ compatibilization of polypropylene-polyethylene blends: a thermomechanical and spectroscopic study.* Polymer, 1998. **39**(26): p. 6807-6817.

39. Liu, N.C., H.Q. Xie, and W.E. Baker, *Comparison of the effectiveness of different basic functional-group for the reactive compatibilization of polymer blends.* Polymer, 1993. **34**(22): p. 4680-4687.

40. Chen, L.F., B. Wong, and W.E. Baker, *Melt grafting of glycidyl methacrylate onto polypropylene and reactive compatibilization of rubber toughened polypropylene.* Polymer Engineering and Science, 1996. **36**(12): p. 1594-1607.

41. Baker, W., C. Scott, and G.H. Hu, *Reactive polymer blending, Chapters 4 and 5*. Progress in Polymer Processing, ed. K.S. Hyun. 2001, Cincinnati: Hanser Gardner.

42. Eliasson, A.-C., ed. *Starch in food: Structure, function and applications*. 2004, Woodhead Publishing. 384.

43. Shogren, R.L., *Effect of moisture and various plasticizers on teh mechanical properties of extruded starch*, in *Biodegradable Polymers and Packaging*, C. Ching, D.L. Kaplan, and E.L. Thomas, Editors. 1993, Technomic Publication. p. 141-150.

44. vanSoest, J.J.G., et al., *Crystallinity in starch bioplastics.* Industrial Crops and Products, 1996. **5**(1): p. 11-22.

45. Myllarinen, P., et al., *Effect of glycerol on behaviour of amylose and amylopectin films.* Carbohydrate Polymers, 2002. **50**(4): p. 355-361.

46. Talja, R.A., et al., *Effect of type and content of binary polyol mixtures on physical and mechanical properties of starch-based edible films.* Carbohydrate Polymers, 2008. **71**(2): p. 269-276.

47. Rodriguez-Gonzalez, F.J., Ramsay, B.A., Favis, B.D., *Rheological and thermal properties of thermoplastic starch with high glycerol content.* Carbohydrate Polymer, 2004. **58**: p. 139-147.

48. Teixeira, E.M., et al., *The effect of glycerol/sugar/water and sugar/water mixtures on the plasticization of thermoplastic cassava starch.* Carbohydrate Polymers, 2007. **69**(4): p. 619-624.

49. Forssell, P.M., et al., *Phase and glass transition behaviour of concentrated barley starch-glycerol-water mixtures, a model for thermoplastic starch.* Carbohydrate Polymers, 1997. **34**(4): p. 275-282.

50. Cordoba, A., et al., *The plasticizing effect of alginate on the thermoplastic starch/glycerin blends.* Carbohydrate Polymers, 2008. **73**(3): p. 409-416.

51. Ma, X.F. and J.G. Yu, *The plastcizers containing amide groups for thermoplastic starch.* Carbohydrate Polymers, 2004. **57**(2): p. 197-203.

52. Yang, J.H., J.G. Yu, and X.F. Ma, *Preparation of a novel thermoplastic starch (TPS) material using ethylenebisformamide as the plasticizer.* Starch-Starke, 2006. **58**(7): p. 330-337.

53. van Soest, J.J.G. and J.F.G. Vliegenthart, *Crystallinity in starch plastics: consequences for material properties.* Trends in Biotechnology, 1997. **15**(6): p. 208-213.

54. Lourdin, D., H. Bizot, and P. Colonna, *"Antiplasticization" in starch-glycerol films?* Journal of Applied Polymer Science, 1997. **63**(8): p. 1047-1053.

55. Lu, Y.S., et al., *Preparation and properties of starch thermoplastics modified with waterborne polyurethane from renewable resources.* Polymer, 2005. **46**(23): p. 9863-9870.

56. Thunwall, M., et al., *Film blowing of thermoplastic starch.* Carbohydrate Polymers, 2008. **71**(4): p. 583-590.

57. Park, H.M., et al., *Tensile properties, morphology, and biodegradability of blends of starch with various thermoplastics.* Journal of Applied Polymer Science, 2002. **86**(11): p. 2907-2915.

58. Park, J.W., Im, S.S., *Biodegradable Polymer Blends of Poly(l-lactic acid) and Gelatinized Starch.* Polymer Engineering and Science, 2000. **40**(12): p. 2539-2550.

59. Rodriguez-Gonzalez, F.J., Ramsay, B.A., Favis, B.D., *High performance LDPE/thermoplastic starch blends: a sustainable alternative to pure polyethylene.* Polymer, 2003. **44**(5): p. 1517-1526.

60. Schwach, E. and L. Averous, *Starch-based biodegradable blends: morphology and interface properties.* Polymer International, 2004. **53**(12): p. 2115-2124.

61. Ma, X.F., J.G. Yu, and J.F. Kennedy, *Studies on the properties of natural fibers-reinforced thermoplastic starch composites.* Carbohydrate Polymers, 2005. **62**(1): p. 19-24.

62. Huang, M.F., J.G. Yu, and X.F. Ma, *Studies on the properties of Montmorillonite-reinforced thermoplastic starch composites.* Polymer, 2004. **45**(20): p. 7017-7023.

63. Angles, M.N. and A. Dufresne, *Plasticized starch/tunicin whiskers nanocomposite materials. 2. Mechanical behavior.* Macromolecules, 2001. **34**(9): p. 2921-2931.

64. Ikeo, Y., et al., *Nano clay reinforced biodegradable plastics of PCL starch blends.* Polymers for Advanced Technologies, 2006. **17**(11-12): p. 940-944.

65. Huneault, M.A. and H.B. Li, *Morphology and properties of compatibilized polylactide/thermoplastic starch blends.* Polymer, 2007. **48**(1): p. 270-280.

66. Jun, C.L., *Reactive Blending of Biodegradable Polymers: PLA and Starch.* Journal Of Polymers and the Environment, 2000. **8**(1): p. 33-37.

67. Kalambur, S. and S.S.H. Rizvi, *An overview of starch-based plastic blends from reactive extrusion.* Journal of Plastic Film & Sheeting, 2006. **22**(1): p. 39-58.

68. Mani, R. and M. Bhattacharya, *Properties of injection moulded blends of starch and modified biodegradable polyesters.* European Polymer Journal, 2001. **37**(3): p. 515-526.

69. Pimentel, T., et al., *Preparation and characterization of blends of recycled polystyrene with cassava starch.* Journal of Materials Science, 2007. **42**(17): p. 7530-7536.

70. Macosko, C.W., H.K. Jeon, and T.R. Hoye, *Reactions at polymer-polymer interfaces for blend compatibilization.* Progress in Polymer Science, 2005. **30**(8-9): p. 939-947.

71. Wang, S., J. Yu, and J. Yu, *Influence of maleic anhydride on the compatibility of thermal plasticized starch and linear low-density polyethylene.* Journal of Applied Polymer Science, 2004. **93**(2): p. 686-695.

72. Wang, S., J. Yu, and J. Yu, *Preparation and characterization of compatible thermoplastic starch/polyethylene blends.* Polymer Degradation and Stability, 2005. **87**(3): p. 395-401.

73. Rosa, D.S., C.G.F. Guedes, and C.L. Carvalho, *Processing and thermal, mechanical and morphological characterization of post-consumer polyolefins/thermoplastic starch blends.* Journal of Materials Science, 2007. **42**(2): p. 551-557.

74. Zhao, R.X., P. Torley, and P.J. Halley, *Emerging biodegradable materials: starch- and protein-based bio-nanocomposites.* Journal of Materials Science, 2008. **43**(9): p. 3058-3071.

75. Zeng, Q.H., et al., *Clay-based polymer nanocomposites: Research and commercial development.* Journal of Nanoscience and Nanotechnology, 2005. **5**(10): p. 1574-1592.

76. Chen, B. and J.R.G. Evans, *Thermoplastic starch-clay nanocomposites and their characteristics.* Carbohydrate Polymers, 2005. **61**(4): p. 455-463.

77. Wilhelm, H.M., et al., *Starch films reinforced with mineral clay.* Carbohydrate Polymers, 2003. **52**(2): p. 101-110.

78. Park, H.M., et al., *Environmentally friendly polymer hybrids - Part I - Mechanical, thermal, and barrier properties of thermoplastic starch/clay nanocomposites.* Journal of Materials Science, 2003. **38**(5): p. 909-915.

79. Kalambur, S. and S.H.S. Rizvi, *Biodegradable and functionally superior starch-polyester nanocomposites from reactive extrusion.* Journal of Applied Polymer Science, 2005. **96**(4): p. 1072-1082.

80. Stewart A McGlashan, P.J.H., *Preparation and characterisation of biodegradable starch-based nanocomposite materials.* Polymer International, 2003. **52**(11): p. 1767-1773.

81. Chen, M., B. Chen, and J. Evans, R. G. , *Novel thermoplastic starch-clay nanocomposite foams* Nanotechnology, 2005(10): p. 2334.

82. Kim, Y.C. and J.C. Kim, *Study on the silicate dispersion and rheological properties of PP/Starch-MB/Silicate composites.* Journal of Industrial and Engineering Chemistry, 2007. **13**(6): p. 1029-1034.

83. Chiou, B.-S., et al., *Effects of Processing Conditions on Nanoclay Dispersion in Starch-Clay Nanocomposites.* Cereal Chemistry, 2006. **83**(3): p. 300-305.

84. Makoto, K., U. Arimitsu, and O. Akane, *Synthesis of polypropylene oligomer - clay intercalation compounds.* Journal of Applied Polymer Science, 1997. **66**(9): p. 1781-1785.

85. Chiou, B.-S., et al., *Rheology of starch-clay nanocomposites.* Carbohydrate Polymers, 2005. **59**(4): p. 467-475.

86. Liao, H.T. and C.S. Wu, *Synthesis and characterization of polyethylene-octene elastomer/clay/biodegradable starch nanocomposites.* Journal of Applied Polymer Science, 2005. **97**(1): p. 397-404.

87. Deeptangshu, S.C., *Understanding amylose crystallinity in starch-clay nanocomposites.* Journal of Polymer Science Part B: Polymer Physics, 2008. **46**(10): p. 979-987.

88. Averous, L. and N. Boquillon, *Biocomposites based on plasticized starch: thermal and mechanical behaviours.* Carbohydrate Polymers, 2004. **56**(2): p. 111-122.

89. ISO, *ISO Environmental management -- Life cycle assessment -- Requirements and guidelines*. 2006, International Organization for Standardization.

90. A. K. Mohanty, M.M.G.H., *Biofibres, biodegradable polymers and biocomposites: An overview.* Macromolecular Materials and Engineering, 2000. **276-277**(1): p. 1-24.

91. Harding, K.G., et al., *Environmental analysis of plastic production processes: Comparing petroleum-based polypropylene and polyethylene with biologically-based poly-beta-hydroxybutyric acid using life cycle analysis.* Journal of Biotechnology, 2007. **130**(1): p. 57-66.

92. Mecking, S., *Nature or petrochemistry? Biologically degradable materials.* Angewandte Chemie-International Edition, 2004. **43**(9): p. 1078-1085.

93. Vidal, R., et al., *Environmental assessment of biodegradable multilayer film derived from carbohydrate polymers.* Journal of Polymers and the Environment, 2007. **15**(3): p. 159-168.

94. Vink, E.T.H., et al., *Applications of life cycle assessment to NatureWorks(TM) polylactide (PLA) production.* Polymer Degradation and Stability, 2003. **80**(3): p. 403-419.

95. Weiss, M., et al., *Applying distance-to-target weighing methodology to evaluate the environmental performance of bio-based energy, fuels, and materials.* Resources, Conservation and Recycling, 2007. **50**(3): p. 260-281.

96. Shelley, S., *A renewable route to propylene glycol.* Chemical Engineering Progress, 2007. **103**: p. 6-9.

97. Vink, E.T.H., et al., *Applications of life cycle assessment to NatureWorks(TM) polylactide (PLA) production.* Polymer Degradation and Stability, 2003. **80**(3): p. 403-419.

98. Miller, S.A., A.E. Landis, and T.L. Theis, *Feature: Environmental Trade-offs of Biobased Production.* Environmental Science & Technology, 2007. **41**(15): p. 5176-5182.

99. Landis, A.E., *Comparative Life Cycle Environmental Impacts of the biopolymer PLA and its petroleum derived counterparts*, in *Civil and Environmental Engineering*. 2007.

100. Landis, A.E., S.A. Miller, and T.L. Theis, *Life cycle of the corn-soybean agroecosystem for biobased production.* Environmental Science & Technology, 2007. **41**(4): p. 1457-1464.

101. Miller, S.A., et al., *A comparative life cycle assessment of petroleum and soybean-based lubricants.* Environmental Science & Technology, 2007. **41**(11): p. 4143-4149.

102. Wang, J. and S. Velankar, *Strain recovery of model immiscible blends: Effects of added compatibilizer.* Rheologica Acta, 2006. **45**(5): p. 741 - 753.

103. Martin, J. and S. Velankar, *Control of phase continuity using compatibilizer.* AIChE Journal, in press., 2008.

104. Van Hemelrijck, E., et al., *The effect of block copolymer architecture on the coalescence and interfacial elasticity in compatibilized polymer blends.* Journal of Rheology, 2005. **49**(3): p. 783-798.

105. Hu, Y.T. and A. Lips, *Estimating surfactant surface coverage and decomposing its effect on drop deformation.* Physical Review Letters, 2003. **91**(4): p. 044501.

106. Yoon, Y., A. Hsu, and L.G. Leal, *Experimental investigation of the effects of copolymer surfactants on flow-induced coalescence of drops.* Physics of Fluids, 2007. **19**(2): p. 023102.

107. Fager, R.S., C.B. Kutina, and E.W. Abrahamson, *Use of NBD chloride (7 chloro-4-nitrobenzo-2-oxa-1,3-diazole) in detecting amino acids and as an N-terminal reagent.* Analytical Biochemistry, 1973. **53**(1): p. 290-294.

108. Velankar, S., et al., *Effect of compatibilization on the breakup of polymeric drops in shear flow.* Journal of Rheology, 2001. **45**(4): p. 1007-1019.

109. Martin, J. and S. Velankar, *Effects of compatibilizer on immiscible polymer blends near phase inversion.* Journal of Rheology, 2007. **51**(4): p. 669-692.

110. Oldroyd, J., *The elastic and viscous properties of emulsions and suspensions.* Proceedings of the Royal Society of London. Series A, Mathematical and Physical Sciences, 1953. **218**(1132): p. 122-132.

111. Palierne, J.F., *Linear rheology of viscoelastic emulsions with interfacial tension.* Rheologica Acta, 1990. **29**: p. 204-214.

112. Oldroyd, J.G., *The effect of interfacial stabilizing films on the elastic and viscous properties of emulsions.* Proceedings of the Royal Society of London, 1955. **A232**: p. 567-577.

113. Jacobs, U., et al., *Analysis of Palierne's emulsion model in the case of viscoelastic interfacial properties.* Journal of Rheology, 1999. **43**(6): p. 1497-1509.

114. Riemann, R.E., H.J. Cantow, and C. Friedrich, *Interpretation of a new interface-governed relaxation process in compatibilized polymer blends.* Macromolecules, 1997. **30**(18): p. 5476-5484.

115. Baker, W., C. Scott, and G.H. Hu, *Reactive polymer blending, Section 4.3*. Progress in Polymer Processing, ed. K.S. Hyun. 2001, Cincinnati: Hanser Gardner.

116. Sailer, C. and U.A. Handge, *Melt viscosity, elasticity, and morphology of reactively compatibilized polyamide 6/styrene-acrylonitrile blends in shear and elongation.* Macromolecules, 2007. **40**(6): p. 2019-2028.

117. DeLeo, C. and S. Velankar, *Morphology and rheology of compatibilized polymer blends: Diblock compatibilizers vs. crosslinked reactive compatibilizers.* Journal of Rheology, 2008. **52**(6): p. 1385-1404.

118. Friedrich, C. and Y.Y. Antonov, *Interfacial Relaxation in Polymer Blends and Gibbs Elasticity.* Macromolecules, 2007. **40**(4): p. 1283-1289.

119. Lipatov, Y.S. and A.E. Nesterov, *Interface in Demixing Solutions and Polymer Mixtures*, in *Thermodynamics of Polymer Blends*. 1997, Technomic Publishing: Lancaster, PA.

120. Jay-lin, J., *Structural Features of Starch Granules II*, in *Starch: Chemistry and Technology*, J. BeMiller and R. Whistler, Editors. 2009, Elsevier: New York.

121. Correa, C.A., C.A. Razzino, and E.J. Hage, *Role of Maleated Coupling Agents on the Interface Adhesion of Polypropylene--Wood Composites.* Journal of Thermoplastic Composite Materials, 2007. **20**(3): p. 323-339.

122. DeLeo, C., et al., *Renewable elastomers based on blends of plasticized starch and maleated polypropylene.* Journal of Applied Polymer Science, 2010. **116**(3): p. 1775-1781.

123. Hambir, S., N. Bulakh, and J.P. Jog, *Polypropylene/Clay nanocomposites: Effect of compatibilizer on the thermal, crystallization and dynamic mechanical behavior.* Polymer Engineering & Science, 2002. **42**(9): p. 1800-1807.

124. Naoki, H., et al., *Preparation and mechanical properties of polypropylene-clay hybrids using a maleic anhydride-modified polypropylene oligomer.* Journal of Applied Polymer Science, 1998. **67**(1): p. 87-92.

125. ASTM, *ASTM D 638 Standard Test Method for Tensile Properties of Plastics*. 2008, American Society of Testing and Materials.

126. Zeppa, C., F. Gouanvé, and E. Espuche, *Effect of a plasticizer on the structure of biodegradable starch/clay nanocomposites: Thermal, water-sorption, and oxygen-barrier properties.* Journal of Applied Polymer Science, 2009. **112**(4): p. 2044-2056.

127. Thareja, P. and S. Velankar, *Interfacial activity of particles at PI/PDMS and PI/PIB interfaces: analysis based on Girifalco–Good theory.* Colloid & Polymer Science, 2008. **286**(11): p. 1257-1264.

128. Fenouillot, F., P. Cassagnau, and J.C. Majesté, *Uneven distribution of nanoparticles in immiscible fluids: Morphology development in polymer blends.* Polymer, 2009. **50**(6): p. 1333-1350.

129. Hong, J.S., et al., *The role of organically modified layered silicate in the breakup and coalescence of droplets in PBT/PE blends.* Polymer, 2006. **47**(11): p. 3967-3975.

130. Sinha Ray, S., et al., *Role of organically modified layered silicate as an active interfacial modifier in immiscible polystyrene/polypropylene blends.* Polymer, 2004. **45**(25): p. 8403-8413.

131. Si, M., et al., *Compatibilizing Bulk Polymer Blends by Using Organoclays.* Macromolecules, 2006. **39**(14): p. 4793-4801.

132. Magalhães, N.F. and C.T. Andrade, *Thermoplastic corn starch/clay hybrids: Effect of clay type and content on physical properties.* Carbohydrate Polymers, 2009. **75**(4): p. 712-718.

133. Avérous, L. and P. Halley, J., *Biocomposites based on plasticized starch.* Biofuels, Bioproducts and Biorefining, 2009. **3**(3): p. 329-343.

134. Nielsen, L.E. and R.F. Landel, *Mechanical Properties of Polymers and Composites*. 1994, New York: Marcel Dekker.

135. Galgali, G., C. Ramesh, and A. Lele, *A Rheological Study on the Kinetics of Hybrid Formation in Polypropylene Nanocomposites.* Macromolecules, 2001. **34**(4): p. 852-858.

136. Mohanty, A.K., M. Misra, and L.T. Drzal, *Sustainable Bio-Composites from Renewable Resources: Opportunities and Challenges in the Green Materials World.* Journal of Polymers and the Environment, 2002. **10**(1): p. 19-26.

137. Saito, Y. and Y. Doi, *Microbial synthesis and properties of poly(3-hydroxybutyrate-co-4-hydroxybutyrate) in Comamonas acidovorans.* International Journal of Biological Macromolecules, 1994. **16**(2): p. 99-104.

138. Freier, T., *Biopolyesters in tissue engineering applications*, in *Polymers for Regenerative Medicine*. 2006, Springer-Verlag Berlin: Berlin. p. 1-61.

139. Nakamura, S., Y. Doi, and M. Scandola, *Microbial synthesis and characterization of poly(3-hydroxybutyrate-co-4-hydroxybutyrate).* Macromolecules, 1992. **25**(17): p. 4237-4241.

140. Martin, D.P. and S.F. Williams, *Medical applications of poly-4-hydroxybutyrate: a strong flexible absorbable biomaterial.* Biochemical Engineering Journal, 2003. **16**(2): p. 97-105.

141. Forssell, P.M., et al., *Ageing of rubbery thermoplastic barley and oat starches.* Carbohydrate Polymers, 1999. **39**(1): p. 43-51.

142. Rodriguez-Gonzalez, F.J., B.A. Ramsay, and B.D. Favis, *Rheological and thermal properties of thermoplastic starch with high glycerol content.* Carbohydrate Polymers, 2004. **58**(2): p. 139-147.

143. de Graaf, R.A., A.P. Karman, and L. Janssen, *Material properties and glass transition temperatures of different thermoplastic starches after extrusion processing.* Starch-Starke, 2003. **55**(2): p. 80-86.

144. Cooreman, F.L., H. van Rensburg, and J.A. Delcour, *Pasting Profiles and Solubility of Native and Cross-Linked Corn Starch inDimethylsulfoxide-Water Mixtures.* Journal of Cereal Science, 1995. **22**(3): p. 251-257.

145. Seker, M. and M.A. Hanna, *Cross-linking starch at various moisture contents by phosphate substitution in an extruder.* Carbohydrate Polymers, 2005. **59**(4): p. 541-544.

146. Holden, G. and D.R. Hansen, *Styrenic thermoplastic elastomers, Chapter 3*, in *Thermoplastic Elastomers, 3rd Edition*, G. Holden, H.R. Kircheldorf, and R.P. Quirk, Editors. 2004, Hanser: Munich.

147. Brown, H.R., *Strengthening polymer-polymer interfaces, Chapter 23*, in *Polymer blends, Volume 2: Performance*, D.R. Paul and C.B. Bucknall, Editors. 2000, Wiley Interscience: New York.

148. Cole, P.J. and C.W. Macosko, *Polymer-Polymer Adhesion in Melt-Processed Layered Structures.* Journal of Plastic Film and Sheeting, 2000. **16**(3): p. 213-222.

149. van Soest, J.J.G., et al., *Influence of glycerol on the melting of potato starch.* Industrial Crops and Products, 1996. **5**(1): p. 1-9.

150. van Soest, J.J.G. and N. Knooren, *Influence of glycerol and water content on the structure and properties of extruded starch plastic sheets during aging.* Journal of Applied Polymer Science, 1997. **64**(7): p. 1411-1422.

151. Bastioli, C., *Global status of the production of biobased packaging materials.* Starch-Starke, 2001. **53**(8): p. 351-355.

152. Heyde, M., *Ecological considerations on the use and production of biosynthetic and synthetic biodegradable polymers.* Polymer Degradation and Stability, 1998. **59**(1-3): p. 3-6.

153. Pietrini, M., et al., *Comparative Life Cycle Studies on Poly(3-hydroxybutyrate)-Based Composites as Potential Replacement for Conventional Petrochemical Plastics.* Biomacromolecules, 2007. **8**(7): p. 2210-2218.

154. NREL, *U.S. Life cycle inventory*. 2004, National Renewable Energy Laboratory.

155. Sharbaugh, J. The Fertilizer Institute 2010 [cited 2010 June].

156. EPA, U.S. *Pesticide Establishment Registration and Reporting*. [cited; Available from: http://www.epa.gov/enforcement/monitoring/programs/fifra/establishments.html.

157. *PRe SimaPro 7*. 2006, PRe Consultants: Amersfoort, Netherlands.

158. Joshi, S., *Can Nanotechnology Improve the Sustainability of Biobased Products?* Journal of Industrial Ecology, 2008. **12**(3): p. 474-489.

159. Engelhaupt, E., *Technology Solutions: Biodiesel boom creates glut of glycerin.* Environmental Science & Technology, 2007. **41**(15): p. 5175-5175.

160. Bare, J., C., *TRACI The Tool for the Reduction and Assessment of Chemical and Other Environmental Impacts.* Journal of Industrial Ecology, 2002. **6**(3-4): p. 49-78.

161. *CalTOX Version 2.3*, Lawrence Berkeley National Laboratory, U.S. Department of Energy.

162. Guo, Y., E. George, and H. Marschner, *Contribution of an arbuscular mycorrhizal fungus to the uptake of cadmium and nickel in bean and maize plants.* Plant and Soil, 1996. **184**(2): p. 195-205.

163. Akane Okada, A.U., *Twenty Years of Polymer-Clay Nanocomposites.* Macromolecular Materials and Engineering, 2006. **291**(12): p. 1449-1476.

164. Pinnavaia, T.J. and G.W. Beall, *Polymer-Clay Nanocomposites*. 2001, New York: John Wiley.

165. *Southern Clay. 2007.* http://www.nanoclay.com/. [cited April 2010].